

**Effect of Different Synthesis Conditions on the Physical and Chemical Properties of
MXenes (Two-dimensional Transitional Metal Carbides/Nitrides)**

by

Emre Kayali

A Doctoral dissertation submitted to the Graduate Faculty of
Auburn University
in partial fulfillment of the
requirements for the Degree of
Doctor of Philosophy

Auburn, Alabama

August 7, 2021

Keywords: Two-dimensional Transition Metal Carbides, MXenes, Electrode Design, Atomic
Force Microscopy, Electrochemistry, Supercapacitors

Copyright 2021 by Emre Kayali

Approved by

Majid Beidaghi, Chair, Assistant Professor of Materials Engineering

Dong-Joo Kim, Professor of Materials Engineering

Pengyu Chen, Professor of Materials Engineering

Siyuan Dai, Professor of Materials Engineering

Abstract

Transition metal carbides and nitrides (MXenes) are a new family of two-dimensional (2D) materials first discovered in 2011. They have gained huge interest over the last decade due to their excellent physical and chemical properties. Owing to their fascinating properties, widespread experimental and theoretical research effort has been shown to demonstrate MXenes' capabilities in several research fields such as energy storage, sensors, electronics, catalysis and water purification. $Ti_3C_2T_x$, first and most studied member of the MXene family, has been proven to have exceptional electronic, electrochemical and mechanical properties. Many other MXenes, including V_2CT_x , Ti_2CT_x , Nb_2CT_x , $Mo_{1.33}CT_x$, $Mo_2TiC_2T_x$ etc. showed interesting characteristics due to their unique structure, morphology and surface chemistries. Most members of the MXene family have been extensively studied for electrochemical applications due to their high surface area to volume ratio, metallic conductivity and metal oxide/hydroxide surface functionalities, making them ideal materials for such applications. To fully utilize such properties, controlled synthesis of MXenes plays a crucial role. Synthesis parameters and post-synthesis treatments can alter the physical and chemical properties of the MXene electrodes dramatically. This study aims to discover the effects of the synthesis procedures on the physical and chemical properties of MXenes and furthermore offer an alternative synthesis method to broaden its application and improve its properties.

Acknowledgement

The study presented here would not be possible without the help and guidance of many individuals. I would like to extend my dearest gratitude to those who have helped me during my time here in Auburn.

Firstly, I would like to express my appreciation for my advisor Dr. Majid Beidaghi for all the help and guidance. I learned so much from him and I would like to think I have become a much better researcher thanks to him. I am grateful for the chance he took on me and all the opportunities he provided me during my time here.

I am also thankful to the committee members Dr. Dong-Joo Kim, Dr. Pengyu Chen and Dr. Siyuan Dai, and the University Reader Dr. Tae-Sik Oh, for their time and efforts spent on me and this work. Their guidance helped me go through the most important part of my studies. I would also like to thank the faculty members at the Auburn University Materials Engineering program.

As the longest standing member of our research group, I have worked with many intelligent individuals in our laboratory. I think my work improved thanks to our discussions and in this manner, I am thankful to Dr. Jafar 'Kia' Orangi, Dr. Armin Vahidmohammadi, Andrew Tormanen, Kittichai 'Eddie' Kerdongsang, Hengze 'Kane' Chen, Yeonjin Baek, Shahrouz Zamani and Elnaz Jamshidi. I would like to extend this thank to Mr. Steve Moore and Mrs. Cheryl Rhodes, for not only helping with scientific and departmental work but also accepting and treating me as a friend.

As much as the academic support, emotional and social support from my fellow peers and friends helped me complete this study. Firstly, I am thankful for the former and the current members of Wilmore Labs Office 114, which includes Kai Robbecke, Ralf Fischer, Jan Lieben, Alana MacLachlan, Dr. Kia Orangi, Shane Williams, and Ricardo Gomes. Perfect combination of academic and social support presented in this office made my everyday better, made my Ph.D. life as good as it gets. Also, I would like to extend this appreciation to my dearest friends, Dr. Baris Kopruluoglu, Asia MacKenzie, Anil Bayrakci and Cagdas Orhan for being there for me. Lastly, I am grateful for Michelle and Mara Mayhall, as they made me a better person with some amazing memories along the way.

Finally, I would like to thank my family for their constant support. I would not be where I am today without them. Members of the Kayali Family, Selma, Ercumend, Ersel, Cevriye and Feraye, made me feel confident with who I am. Knowing that they are always there for me shaped me as a person, gave me the strength that I needed to move across the world and complete a doctorate program.

I also appreciate the support from the The Alabama Established Program to Stimulate Competitive Research (ALEPSCoR), Graduate Research Scholars Program (GRSP) doctoral fellowship round 15, which funded my last year in Auburn.

Table of Contents

Abstract	2
Acknowledgments	3
Table of Contents	5
List of Figures	7
List of Abbreviations	14
Chapter 1: Introduction	16
Chapter 2: Literature Review	19
2.1 Two-dimensional (2D) Materials	20
2.2 MAX Phases and Selective Etching	23
2.3 MXenes and Their Properties	33
2.4 Lack of Knowledge and Unexplored Venues	38
Chapter 3: Effect of synthesis conditions on the electrochemical properties of MXenes	44
3.1 Introduction	44
3.2 Materials and Methods	45
3.3 Effect of LiF:MAX molar ratio on the electrochemical properties of $Ti_3C_2T_x$ electrodes	51
3.4 Effect of lateral size of the sheets on the electrochemical properties of produced MXene electrodes	57

3.5	Conclusion.....	72
Chapter 4: Effect of synthesis conditions on the mechanical properties of MXenes...		
	74
4.1	Introduction.....	74
4.2	Assembly of MXene membranes.....	77
4.3	Effect of LiF:MAX molar ratio on the mechanical properties of single layer Ti ₃ C ₂ T _x MXene sheets.....	82
4.4	Mechanical Properties of Ti ₂ Mo ₂ C ₃	86
4.5	Conclusion.....	88
Chapter 5: Development of a novel electrochemical etching method of MAX Phases using a battery system		
		89
5.1	Introduction.....	89
5.2	Experimental Setup.....	91
5.3	Electrochemical Etching of Ti ₃ AlC ₂ and Cr ₂ AlC MAX Phases.....	93
5.4	Conclusion.....	99
Chapter 6: Outlook		
		100
Chapter 7: References		
		101

List of Figures

Figure 2-1: a) Optical microscope image of single-layer graphene flake b) AFM image of the flake on the edge (2x2 μm) c) AFM image of single layer graphene flake (0.8 nm thickness) d) SEM image of an experimental device e) Schematics of the device (20)	20
Figure 2-2: Different two-dimensional material families	21
Figure 2-3: Different synthesis methods of two-dimensional materials shown with the corresponding lateral sizes (33)	22
Figure 2-4: Photographs of commercially available MAX Phases showing their machinability(38).....	24
Figure 2-5: Illustration of MAX Phase atomic structures and etching(42)	25
Figure 2-6: Story of MXenes: history of different etching methods of MAX phases to produce MXenes(18)	26
Figure 2-7: Processing of $\text{Ti}_3\text{C}_2\text{TX}$ MXene after etching with 'clay' method(12)	29
Figure 2-8: AFM Analysis showing the effect of synthesis parameters on the structure of $\text{Ti}_3\text{C}_2\text{T}_x$ sheets(44)	30
Figure 2-9: Different MXene structures reported to be stable theoretically or experimentally(22).....	34
Figure 2-10: MXene application areas, middle ring shows the first paper published in the corresponding research field(22)	36
Figure 3-1: Schematic illustration of $\text{Ti}_3\text{C}_2\text{T}_x$ MXene synthesis process.	45

Figure 3-2: Effect of synthesis parameters on the flake size distribution of the synthesized $Ti_3C_2T_x$. (a) $Ti_3C_2T_x$ flakes synthesized using the MILD method. (b) The thickness of a single layer $Ti_3C_2T_x$ flake prepared using the MILD method is measured to be 1.3 nm on a folded flake. (c and d) $Ti_3C_2T_x$ flakes obtained after the 'clay' synthesis method showing flakes with different thicknesses and up to 1 μm lateral sizes. 47

Figure 3-3: AFM Images showing large $Ti_3C_2T_x$ sheets produced with MILD-synthesis method (Scale bar is 2 μm). 48

Figure 3-4: Histograms showing size distribution of $Ti_3C_2T_x$ flakes prepared using various sonication times and averages sizes of (a) 3.05 μm , (b) 1.00 μm , (c) 0.68 μm , (d) 0.48 μm , (e) 0.30 μm , and (f) 0.18 μm 49

Figure 3-5: Schematic modeled to show the effect of LiF concentration on the structure of $Ti_3C_2T_x$ sheets 52

Figure 3-6: AFM analysis showing nano-holes on the 30 M LiF:MAX molar ratio sample, a-b) AFM images of 30M- $Ti_3C_2T_x$ sheets, c) height profiles of black and red lines shown in the AFM image. 52

Figure 3-7: Cyclic voltametry graphs obtained at increasing charge and discharge rates with different electrodes produced with LiF concentrations, a) 7.5 M, b) 15 M, c) 22.5 M, d) 30 M. 53

Figure 3-8: Comparison of gravimetric and volumetric capacitance values of different $Ti_3C_2T_x$ electrodes produced with 7.5 M, 15 M, 22.5 M and 30 M LiF concentrations by a) volumetric capacitance values at different scan rates, b) gravimetric capacitance values at different scan rates, c) gravimetric capacitance values at different LiF concentrations. 55

Figure 3-9: Comparison of CV graphs at a) 2 mV/s and b) 1000 mV/s scan rates and c) EIS graph obtained with the different $Ti_3C_2T_x$ electrodes produced with 7.5 M, 15 M, 22.5 M and 30 M LiF concentrations 56

Figure 3-10: a) Schematic drawing of the $Ti_3C_2T_x$ structure. b) $Ti_3C_2T_x$ sheets dispersed in water showing the Tyndall effect. c) MXene “paper” film after vacuum filtration of the $Ti_3C_2T_x$ solution. d) SEM Image of the cross-section of MXene film. e) Schematic drawings showing possible ion diffusion paths for different electrode structures.(94)..... 58

Figure 3-11: a) Schematic illustration of the effect of high power sonication on a single-layer MXene flake. Representative AFM images of $Ti_3C_2T_x$ solutions (b) before sonication, and after sonication for (c) 2.5, (d) 5, (e) 10, (f) 15, and (g) 30 min (scale bars are 1 μm). (h) Size distribution of $Ti_3C_2T_x$ flakes prepared by various sonication durations. i) Average flake size versus sonication time.(94) 60

Figure 3-12: Cyclic voltammetry curves of a) electrodes made using large flakes (avg. size of $\sim 3 \mu m$) and b) small flakes (avg. size of $\sim 0.18 \mu m$). c) Gravimetric and volumetric capacitance of the electrodes at various scan rates. d) Nyquist plots showing EIS data collected from all electrodes. e) Cyclic voltammeteries of 1:1 mixture electrode. (f) Representative AFM image of the flakes in the 1:1 mixture (scale bar is 1 μm). (94) 61

Figure 3-13: Cyclic voltammetry graphs for electrodes fabricated using $Ti_3C_2T_x$ flakes with average sizes of a) 3.05 μm , (b) 1.00 μm , c) 0.68 μm , d) 0.48 μm , e) 0.30 μm , and f) 0.18 μm 62

Figure 3-14: Electrochemical impedance spectroscopy graphs for electrodes fabricated using $Ti_3C_2T_x$ flakes with average sizes of (a) 3.05 μm , (b) 1.00 μm , (c) 0.68 μm , (d) 0.48 μm , (e) 0.30 μm , and (f) 0.18 μm 63

Figure 3-15: a) Sheet resistance and b) conductivity values of electrodes measured with four-probe measurement system. 65

Figure 3-16: a) Gravimetric and b) volumetric capacitances of various $Ti_3C_2T_x$ electrodes versus CV scan rates. c) X-ray diffraction patterns of different $Ti_3C_2T_x$ electrodes. d) CV graphs of different $Ti_3C_2T_x$ electrodes at 1000 mV s^{-1} scan rate. e) Log (cathodic current peak) versus log (scan rate) used for calculation of b-values (94)..... 66

Figure 3-17: a) Cyclic voltammetry curves of the 1:1 Hydrogel electrodes b) Ragone plot for the 1:1 mixed and 1:1 hydrogel (The energy and power density are calculated for the electrodes from the results of the three-electrode tests and do not represent the energy and power density of a full cell)(94) 67

Figure 3-18: Cyclic performance and Charge–Discharge curves of (a) 1:1 mixture electrode and (b) 1:1 Hydrogel electrode(94)..... 68

Figure 3-19: Capacitive (surface-controlled) charge storage contribution to the total CV current measured at 5 mVs^{-1} for electrodes fabricated using (a) as-prepared large $Ti_3C_2T_x$ flakes before sonication, (b) flakes produced after 30 min of sonication, (c) 1:1 mix of large and small flakes, and (d) hydrogels fabricated using 1:1 mix of small and large flakes.(94)..... 70

Figure 3-20: Capacitive (surface-controlled) charge storage contribution to the total CV current measured at 50 mVs^{-1} for electrodes fabricated using (a) as-prepared large $Ti_3C_2T_x$ flakes before sonication, (b) flakes produced after 30 min of sonication, (c) 1:1 mix of large and small flakes, and (d) hydrogels fabricated using 1:1 mix of small and large flakes.(94)..... 71

Figure 3-21: SEM images of different $Ti_3C_2T_x$ films showing electrodes thicknesses for the electrode fabricated with flakes of (a) $3.05\text{ }\mu\text{m}$ avg. size, (b) $1.00\text{ }\mu\text{m}$ avg. size, (c) $0.18\text{ }\mu\text{m}$ avg. size, (d) 1:1 mixture, (e) 1:1 hydrogel. (scale bar is $1\text{ }\mu\text{m}$) (94)..... 72

Figure 4-1: Experimental setup used in the measurement of mechanical properties of mechanically exfoliated graphene (87)..... 76

Figure 4-2: a) Optical microscope image of produced Si/SiO₂ wafers with holes b) AFM image and c) depth profiles of the produced holes 76

Figure 4-3: Ti₃C₂T_x sheets a) drop casted and b) spin casted over circular holes. c) Optical microscope and d) AFM images of drop casted and transferred Ti₃C₂T_x sheets 78

Figure 4-4: Photographs of optical microscope and micro-manuplators used in the transfer of spesific Ti₃C₂T_x sheets..... 79

Figure 4-5: AFM images of Ti₃C₂T_x sheets on Si/SiO₂ wafers; a) before and b) after transferring over to patterned wafers. 80

Figure 4-6: Schematic of proposed experimental setup for obtaining and transferring self-assembled Ti₃C₂T_x MXene films 81

Figure 4-7: a) Optical microscope image of self-assembled Ti₃C₂T_x films. AFM images of of self-assembled Ti₃C₂T_x films on Si/SiO₂ wafers b) directly picked up by non-patterned wafers, c) picked up with PDMS and transferred onto patterned wafers. 81

Figure 4-8: a) Schematic showing MXene sheet suspended over holes, b) AFM image showing two suspended Ti₃C₂T_x sheets, c) Height profile of the red line marked in b, showing the thickness of the sheets and the depth of suspended sheets. 82

Figure 4-9: a) Force-Distance graph obtained with repeated nanoindentation experiments with increasing force values on suspended Ti₃C₂T_x sheets produced with 7.5 M LiF:MAX molar ratio, b) Histogram graph showing the distrubution of calculated E2D values for the same sample, c) Histogram graph showing the distrubution of the measured Fracture Force values for the same sample. 83

Figure 4-10: Histogram graphs showing the distribution of calculated E^{2D} values for the samples produced with a) 15 M and b) 30 M LiF:MAX molar ratio, c) Histogram graph showing the distribution of the measured Fracture Force values for the c) 15 M and d) 30 M LiF:MAX molar ratio..... 84

Figure 4-11: Histogram graphs comparing the distribution of calculated a) E^{2D} and b) Fracture Force values for 7.5 M, 15 M and 30 M LiF:MAX ratio samples 85

Figure 4-12: a) Schematic showing MXene sheet suspended over holes, b) AFM image showing suspended $Ti_2Mo_2C_3T_x$ sheets, c) Height profile of the red line marked in b, showing the thickness of the sheets and the depth of suspended sheets, d) Force-Distance graph obtained with repeated nanoindentation experiments with increasing force values on suspended $Ti_2Mo_2C_3T_x$ sheets b) Histogram graph showing the distribution of calculated E^{2D} values for the same sample, c) Histogram graph showing the distribution of the measured Fracture Force values for the same sample. 87

Figure 5-1: Raman measurements showing active electrochemical species in $Et_3NHCl/AlCl_3$ electrolytes with different molar ratios (101)..... 91

Figure 5-2: Cyclic Voltammetry graphs showing the interaction of $Et_3NHCl/AlCl_3$ electrolyte with Ta current collector, Ti_3AlC_2 MAX Phase cathode and Al anode; a) When the voltage window is set between -1 V to 3V b) when voltage window is set between 0.1-1.8 V... 92

Figure 5-3: Electrochemical setup and its components used in the electrochemical etching 93

Figure 5-4: a) Digital images showing Ti_3AlC_2 powders obtained after etching at different temperatures. b) SEM image of etched Ti_3AlC_2 powders and c) EDS analysis showing atomic percentages within the etched particles..... 95

Figure 5-5: SEM images of electrochemically etched Cr₂AlC particles and corresponding EDS Analysis 97

Figure 5-6: a) Electrochemical setup using Carbon paper as current collector for MAX phase cathodes b) Aqueous delaminated etched-Cr₂AlC and carbon black (CB) suspension c) Etched-Cr₂AlC-CB film obtained by vacuum-filtration of the solution shown. d) SEM image of the cross-section of obtained films. e) AFM image showing the thickness of Etched-Cr₂AlC sheets on Si/SiO₂ wafer surface. 98

List of Abbreviations

2D	2-dimensional
3D	Three-dimensional
TMOs	Transition metal oxides
TMDs	Transition metal dichalcogenides
GO	Graphene oxide
rGO	Reduced graphene oxide
LiF	Lithium fluoride
HF	Hydrofluoric acid
THF	Tetrahydrofuran
HCl	Hydrochloric acid
MSC	Micro-supercapacitor
CV	Cyclic voltammetry
EIS	Electrochemical impedance spectroscopy
GCD	Galvanostatic charge-discharge
VAE	Vacuum-assisted filtration
XRD	X-ray Diffraction
AFM	Atomic Force Microscope
TEM	Transmission Electron Microscopy
SEM	Scanning Electron Microscopy

Dedication

To my mother Selma,

and to my Father Ercumend,

for the constant support you showed to me.

To my brother Ersel,

for being there for me since my day 1.

Chapter 1: Introduction

The energy storage devices of the future, such as advanced batteries and electrochemical capacitors (ECs, also called supercapacitors), are required to deliver higher energy and power densities for longer periods of time. Improving these properties requires not only finding materials with high storage capacities but also understanding how these materials can be assembled into electrode structures with high ionic and electronic conductivities.(1,2) A family of two-dimensional (2D) materials called MXenes has been recently introduced as exceptional electrode materials for energy storage devices.(3,4) MXenes are transition metal carbides, nitrides, and carbonitrides with a general formula of $M_{n+1}X_nT_x$, where M is an early transition metal, X is carbon or nitrogen, and T_x refers to surface functional groups such as OH, O, and F.(5) Since the discovery of the first MXene ($Ti_3C_2T_x$) in 2011,(6) these materials have been the subject of much research, revealing their promising properties for numerous applications ranging from energy storage and water desalination to catalysis and electromagnetic shielding, to name a few.(7–11) In particular, electrochemical properties of MXenes as supercapacitor electrodes have both fundamental and applied significance.(12) The charge storage mechanism of MXenes is based on pseudocapacitance, which is fundamentally different from electric double layer capacitance (EDLC), which is the charge storage mechanism of carbon materials including graphene. (1,13–15)Therefore, similar to other well-known pseudocapacitive materials such as MnO_2 and RuO_2 , MXenes store charge by fast surface redox reaction and are capable of delivering very high specific capacitances.(4) At the same time, the high electrical conductivity of MXenes and their highly accessible interlayer spacing leads to their high rate capability and high power densities. (16)

The family of 2D MXenes has rapidly expanded in the past few years to include 21 members including $Ti_3C_2T_x$, Ti_2CT_x , V_2CT_x , Mo_2CT_x , etc.(4) All of these materials are synthesized by selective removal of atoms from the structure of MAX phases, layered ternary carbide and/or nitrides with a general formula of $M_{n+1}AX_n$.(17) In the structure of MAX phases, the 2D $M_{n+1}X_n$ layers (MXenes) are separated by layers of A atoms (such as Al, Si, and Ga) and can be separated by a selective removal (etching) of these layers.(4,17) The etching process is usually performed in concentrated aqueous HF solutions, but in some cases, milder etchants that contain metal fluoride salts (e.g.,LiF) and HCl can be used to remove A layer atoms.(18) The capacitive properties of MXenes were first reported by Lukatskaya et al.(3) and Ghidui et al.,(12) where they studied the electrochemical properties of $Ti_3C_2T_x$ in various aqueous electrolytes. Even in these early studies, the very high performance of the fabricated electrodes (e.g., a specific volumetric capacitance of about 900 F cm^{-3}) suggested the discovery of an exceptional electrode material for supercapacitors. Recently, Lukatskaya et al.(14) have shown that even higher capacitances at very high charge–discharge rates can be achieved by engineering the structure of MXene electrodes. Peng et al. recognized that the higher electrical conductivity of larger $Ti_3C_2T_x$ flakes can be utilized to fabricate current collectors for on-chip microsupercapacitors, while the electrode can be fabricated with using smaller flakes with higher capacitance.(19)

The excellent capacitive performance of $Ti_3C_2T_x$ is due to its unique structure which consists of two layers of C atoms sandwiched between three layers of Ti atoms. The high conductivity of $Ti_3C_2T_x$ stems from its conductive carbide core, while its high pseudocapacitive properties arise from its functionalized transition metal surfaces. However, previous studies have largely overlooked the significant effect of the lateral dimensions of 2D MXene on their electrochemical properties. As the synthesis methods and processing conditions immensely impact

the dimensions of the produced MXene flakes, the lack of information on the size-dependent properties of MXenes prevents a comprehensive understanding of their electrochemical properties.

For my Ph.D. research, I am planning to synthesize, fabricate, and engineer superior electrode architectures based on 2D MXenes and investigate the effect of synthesis methods and post synthesis treatments on individual sheets quality and lateral size and therefore their electrochemical performance.

The goal of the proposed research is to understand synthesis mechanism of MXenes and use the information gained to further control the structure, quality and lateral size of the individual sheets. Control of such properties will allow us to study and improve electrochemical performance of MXene electrodes and provide a unique opportunity to characterize their mechanical properties. Furthermore, it is intended to use the gained knowledge to offer an alternate electrochemical selective etching method for synthesis of different MXenes and investigate the effect of this new synthesis method on the electrochemical properties of MXenes. Following chapters will initially provide current status of MXene research in detail. Then, explanation and discussion of the proposed research, followed by the preliminary results will be presented. Lastly, the used experimental methods will be stated, the outlook and possible future impacts of this research will be specified.

Chapter 2: Literature Review

This chapter presents a literature review of two-dimensional materials, MAX phases, MXene synthesis methods and their properties. As synthesis is a big part of the proposed research, literature review will begin with introducing two-dimensional (2D) materials and their synthesis methods. 2D Materials' journey initially took off with the graphene's first experimental proof which is shown in Fig. 2-1.(20) Over 16 years since the first report, scientific community explored the 2D world of materials to its limits. Numerous synthesis methods are reported to produce atomically thin materials, defying previous theoretical predictions claiming 2D materials would not be stable.(21) Although, not all 2D materials were predicted or theoretically studied beforehand. For example, there were no predictions on the existence of MXenes prior to their synthesis in 2011.(22) This chapter will go over different procedures to synthesize 2D materials and examine the current MXene research on its synthesis and properties.

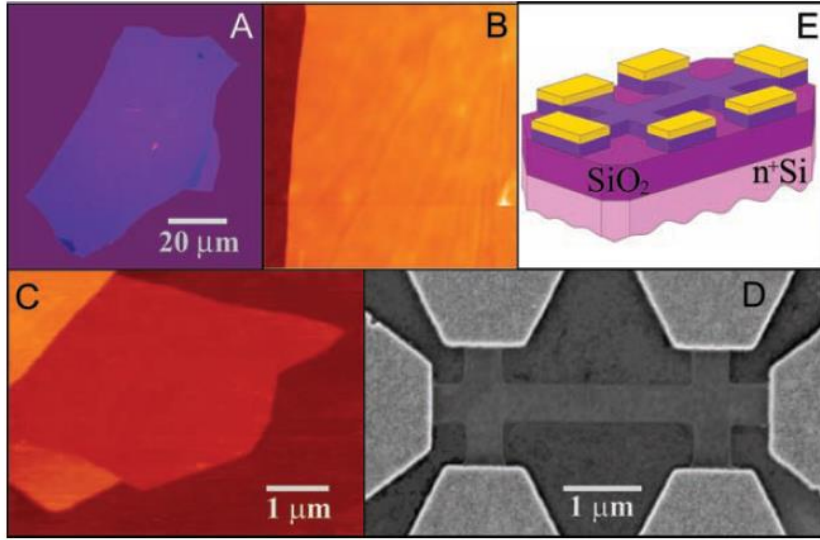


Figure 2-1: a) Optical microscope image of single-layer graphene flake b) AFM image of the flake on the edge ($2 \times 2 \mu\text{m}$) c) AFM image of single layer graphene flake (0.8 nm thickness) d) SEM image of an experimental device e) Schematics of the device (20)

2.1 Two-dimensional (2D) Materials

In the scientific community, the existence and the stability of two-dimensional (2D) materials were a widely discussed topic.(23) Due to thermal lattice fluctuations, 2D materials are thought to be thermodynamically unstable according to classical physics.(24) It was observed that the melting point of the thin films decreased as the thickness of the thin film is decreased.(21) However, a major breakthrough was reported in 2004, when Scotch tape exfoliation of graphite was demonstrated to form the first stable 2D material graphene.(20) Dr. Novoselov and Dr. Geim measured electronic properties of graphene and proved that single-layer graphene flakes are stable at the room temperature (Fig 2-1). They were awarded for a Nobel Prize in 2010, for their study which opened the door for researchers to walk through and explore 2D materials world. Since then, ever-growing number of new 2D material systems and families have been reported. (25)

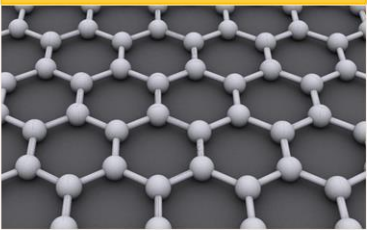
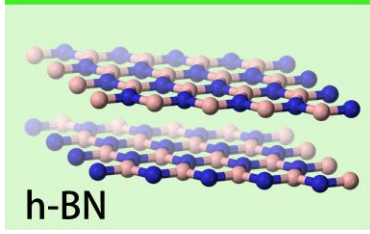
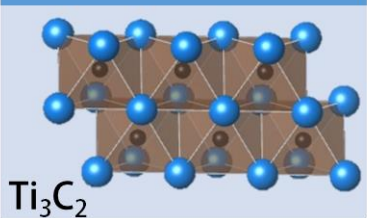
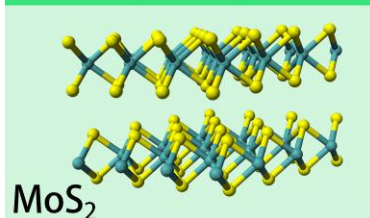
<p style="text-align: center;">Graphene</p>	<p style="text-align: center;">Xenes</p>	<p style="text-align: center;">Hexagonal Boron Nitride</p>
	<ul style="list-style-type: none"> • Borophene • Silicene • Phosphorone • Bismuthene • 	 <p style="text-align: center;">h-BN</p>
<p style="text-align: center;">MXenes</p>	<p style="text-align: center;">Transition metal oxides and hydroxides, clays</p>	<p style="text-align: center;">Transition Metal Dichalcogenides (TMDs)</p>
 <p style="text-align: center;">Ti_3C_2</p>	<ul style="list-style-type: none"> • MoO_3 • WO_3 • Ga_2O_3 • $CsCa_2Nb_3O_{10}$ • 	 <p style="text-align: center;">MoS_2</p>

Figure 2-2: Different two-dimensional material families

History of layered materials goes back as far as we can think, and they have been scientifically researched for over 150 years. However, scientific community is exploring their true potential only recently.(21) It has been showed that each layered material exhibits enhanced properties when it is thinned down to its atomic layers compared to its bulk form.(26) Thickness of produced 2D materials is crucial as it has a huge effect on the electronical, optical and vibrational properties since motion of the electrons in the third dimension is governed by quantum physics at this scale.(27) Also, 2D materials can form gapless contact with each other and the interactions at the interlayer can change properties of this heterostructures. Moreover, when size of a material goes from 3D to 2D, surface to volume ratio increases dramatically, which results in very different interfacial and electrochemical properties compared to their bulk counterparts.(28)

So far, ever-increasing number of 2D materials has been reported to be stable experimentally or theoretically. These materials include but not limited to; graphene, hexagonal boron nitride (h-BN), Xenes (such as Borophene, Silicene, Phosphorene, Bismuthene, etc.), transitional metal oxides, hydroxies and clays, (such as MoO₃, WO₃, Ga₂O₃ etc.), transitional metal dichalcogenides (TMDs, such as MoS₂, WS₂ etc) and transitional metal carbides/nitrides or carbonitrides (MXenes). (29–32)

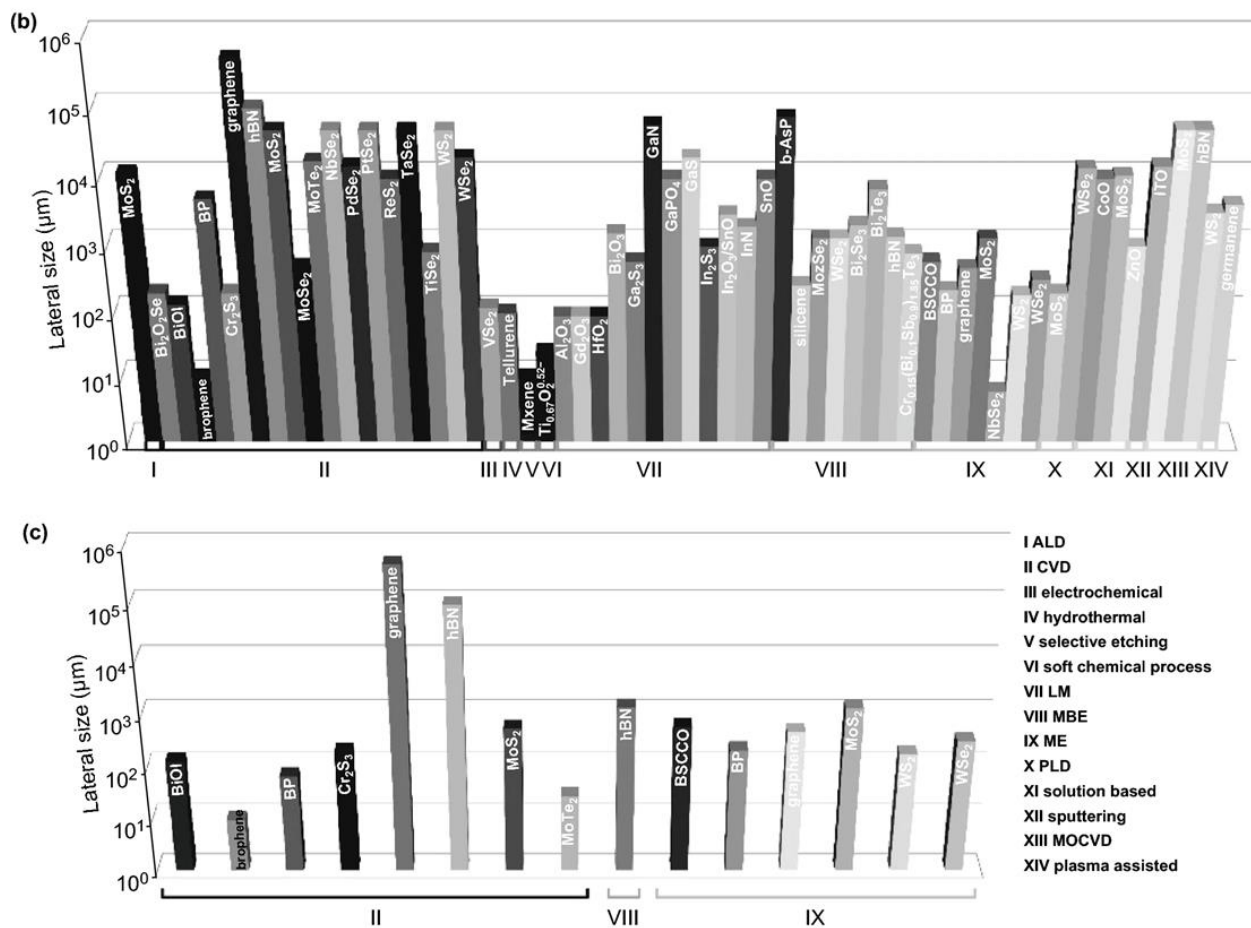


Figure 2-3: Different synthesis methods of two-dimensional materials shown with the corresponding lateral sizes (33)

There has been a widespread global research on producing 2D materials. Early studies with 2D materials used a top-down approach for synthesis such as mechanical cleavage or liquid exfoliation techniques.(34) Soon after bottom-up methods using atomic growth techniques have emerged. It is important to be able to grow 2D materials in a thickness-controlled manner, as it allows engineering of electronic devices with complex mechanisms. CVD method, as the most potent bottom-up method, has been proved to be capable of producing 2D materials with controlled thickness and high large areas over 100 micrometers (Fig. 2-3)(33). Although it is an industry relevant and relatively easy to apply method, there are numerous parameters that needs to be controlled and optimized for the production thus requiring experience and knowledge in the field. On the other hand, liquid exfoliation techniques are widely used to produce large amounts of 2D materials.(35,36) Although it can produce large amounts, several drawbacks of this method including the lower quality of sheets compared and smaller lateral sizes compared to mechanical cleave, have been a focus point for researchers to be improved. Recently, a new family of 2D materials has emerged using a new technique called Selective Etching similar to liquid exfoliation methods. With this method, removal of specific atomic layers from the layered precursor materials called MAX phases is achieved to yield 2D materials called MXenes. (25)

2.2 MAX Phases and Selective Etching

Discovery of MAX phases dates back to 1960s; initially Dr. Nowotny's group in Vienna reports more than 100 new nitrides and carbides including Ti_3SiC_2 .(37) However, number of studies on these materials were very limited until 1990s when Dr. Barsoum and Dr. El-Raghy synthesized more phase-pure samples of first Ti_4AlN_3 and Ti_3SiC_2 .(38) These discovered revealed that these materials share the same atomic structure and thanks to this structure, they exhibited unique properties. This shared structure is later denominated as $M_{n+1}AX_n$ phases where

'M' is a transitional metal, 'A' an A-group element and 'X' could be nitrogen and/or carbon. This led to the name 'MAX phases'.(39) Layered structure and unique combination of metallic and covalent bonding in the structure of MAX phases gave them excellent properties.(40) It was shown that MAX phases exhibit an excellent combination of ceramic and metallic properties; highly electrically and thermally conductive, resistance to thermal shock and oxidation, as well as being mechanically sturdy and easily machinable (Fig.2-4)(38). Thanks to this combination of properties, MAX phases are considered for a variety of applications where high temperature resistance is important and excellent mechanical properties are required.

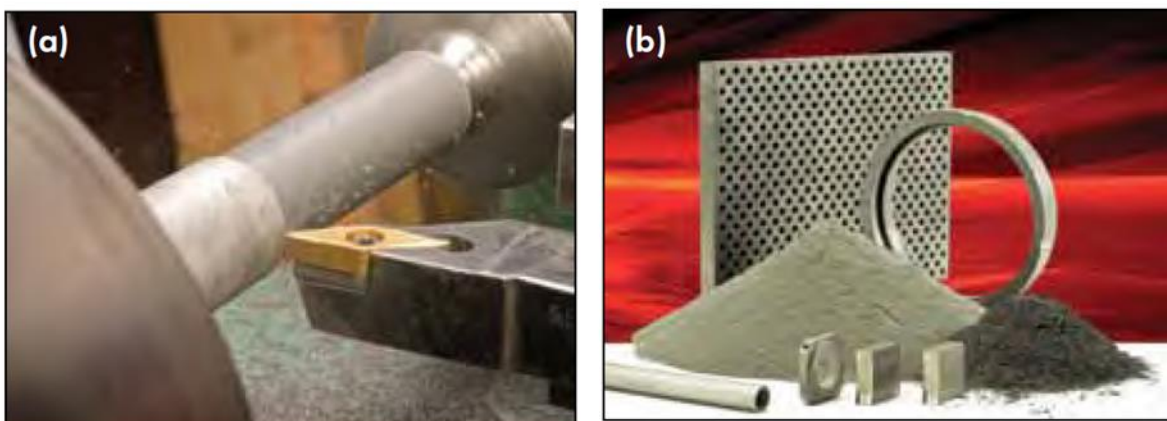


Figure 2-4: Photographs of commercially available MAX Phases showing their machinability(38)

As MAX phases drew more interest with their unique properties, they were initially thought as ideal candidates for Li ion batteries by Dr. Yuri Gogotsi.(41) They were thought as a replacement of graphite being used in Li ion batteries as anodes. However, initial results were not promising and, in an attempt to reduce particle size of Ti_3AlC_2 MAX phases chemically it was discovered that with hydrofluoric acid (HF) treatment, Al layers can be selectively etched from the structure where Ti and C layers are remained untouched keeping that two-dimensional structure.

Since this discovery was published in 2011, selective etching of A-layer from MAX phases generated huge interest as a way of producing a new type two-dimensional material; MXenes.(36)

Current selective etching methods can be categorized under 5 different topics based on the etchant type used; 1) HF containing etchants, 2) HF forming etchants, 3) Alkaline and/or Hydrothermal etching, 4) Molten Salt etchants and 5) Electrochemical etching.

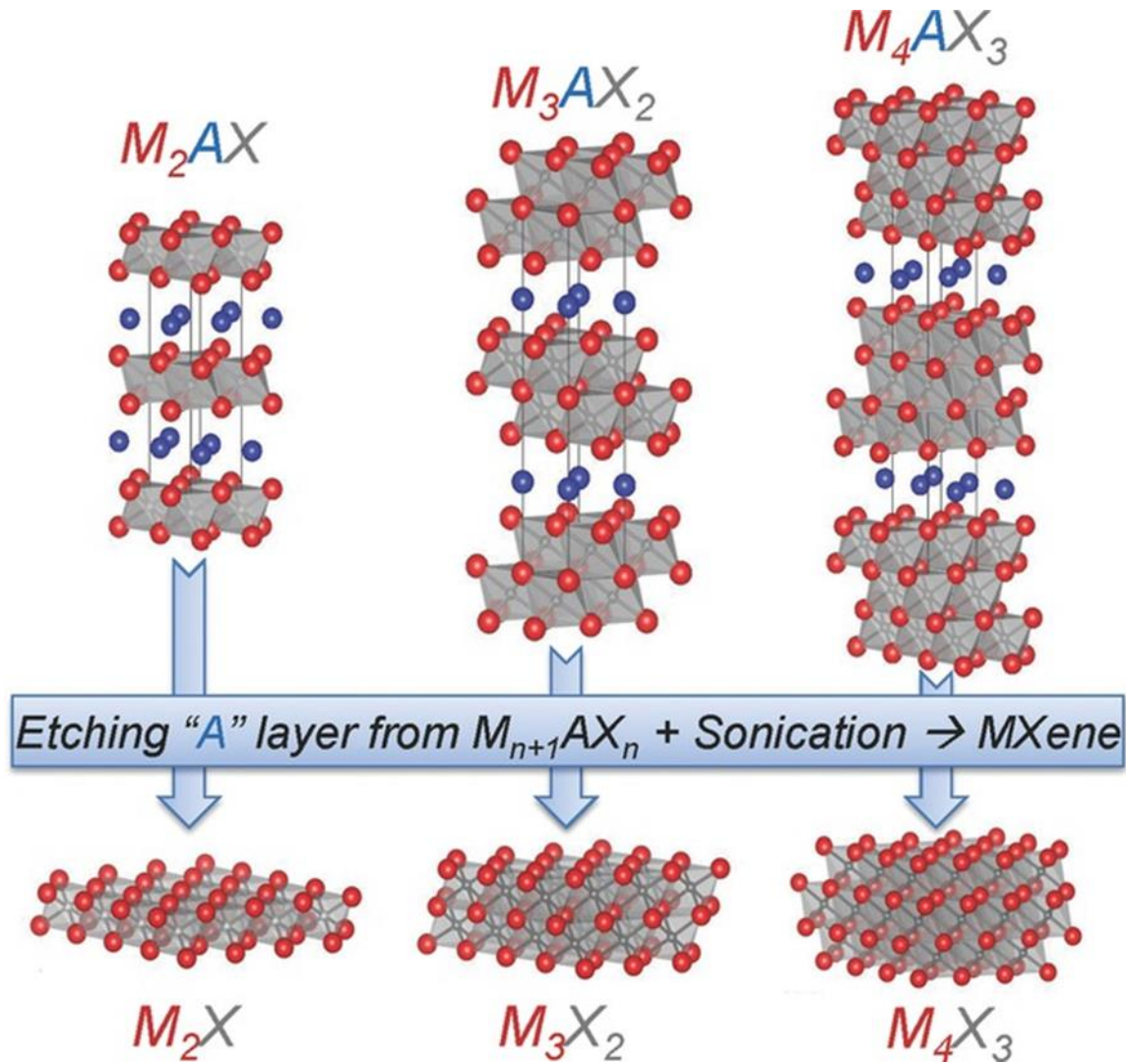
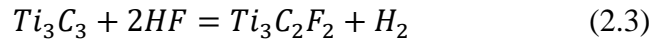
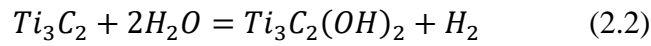
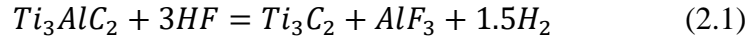


Figure 2-5: Illustration of MAX Phase atomic structures and etching(42)

HF Containing Etchants

It was proposed with the initial study that when Ti_3AlC_2 MAX phase was immersed in HF following reactions occurred;



Reaction (2.1) was followed by Reaction (2.2) and/or Reaction (2.3), meaning that surface is functionalized with OH and F groups.(6) This study used %50 concentrated HF and demonstrated for the first time that Al can be removed from Ti_3AlC_2 MAX phase to produce 2D $Ti_3C_2T_x$, where T_x is used for denominating the surface groups.

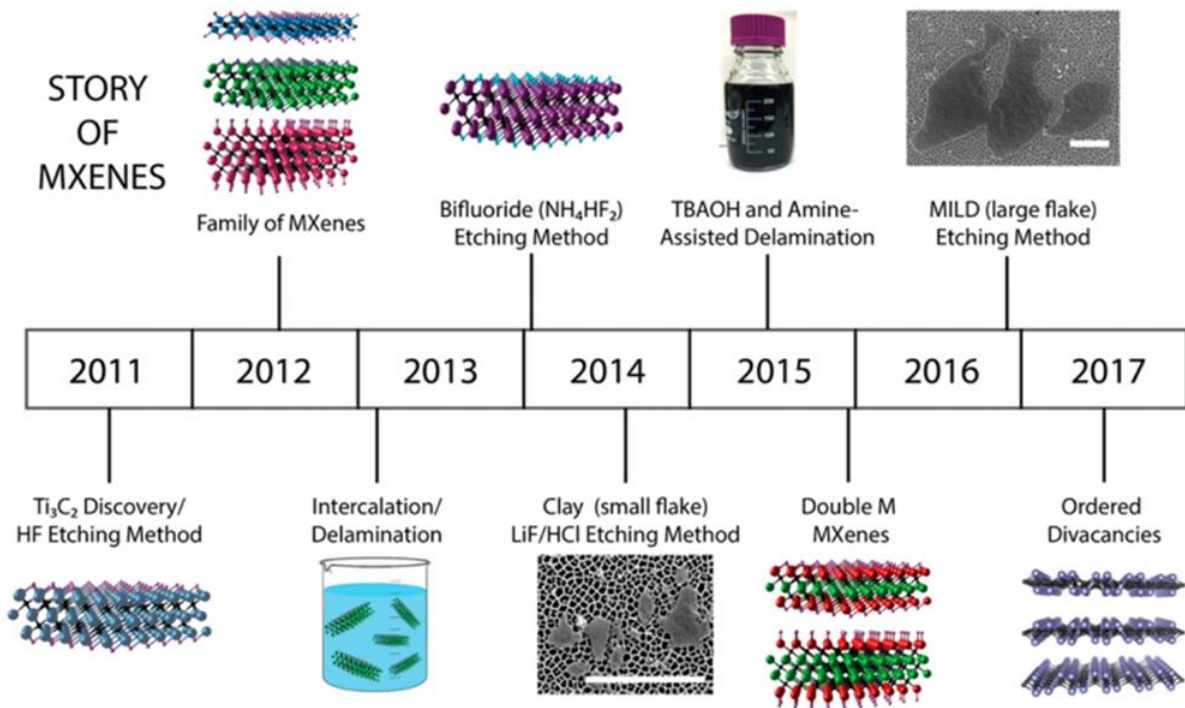
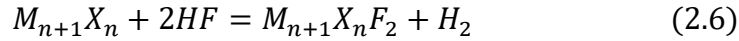
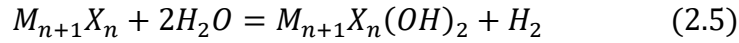
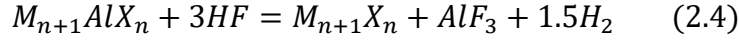


Figure 2-6: Story of MXenes: history of different etching methods of MAX phases to produce MXenes(18)

Soon after this report, HF etching is used for other MAX phases such as Ti_2AlC , Ta_4AlC_3 or Ti_3AlCN and demonstrated that $Ti_3C_2T_x$ is the first member of a larger 2D materials, now called MXenes.(17) Therefore, reactions are also generalized for all MAX phases;



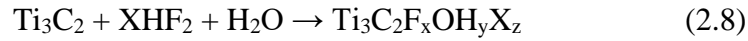
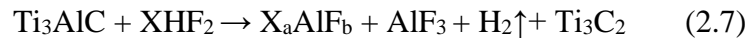
Reaction (2.4) is responsible for the H_2 generation during the etching process. This H_2 generation was also proposed to be the reason for ‘accordion’ shape observed with the etched MAX phase particles. (39)

In 2013, it was proposed that relatively large molecules can be intercalated between the layers of etched MAX phase particles which would result in higher ‘interlayer spacing’, meaning increasing the distance between each layer.(3) Outcome of the increased interlayer spacing is lower interaction between the layers, so that each layer can be delaminated and dispersed in a solvent. As proposed, intercalation of organic molecules such as DMSO and Urea is demonstrated to increase interlayer spacing with the etched MXene particles. Sonication is used as a final step to fully delaminate the layer and achieve dispersion in water. Although HF etching is relatively practical, dangers of handling HF and exothermic nature of the reaction led the researchers to find milder etchants.

HF Forming Etchants

In order to avoid handling of concentrated HF and to provide intercalant ions during the synthesis different methods have been proposed. Firstly, use of Bifluorides such as KHF_2 , NH_4HF_2 and $NaHF_2$ was tested as etchants. (43) It was shown that selective etching of Ti_3AlC_2 can be

achieved through different bifluorides while cations such as K^+ , Na^+ and NH_4^+ intercalate the structure to increase interlayer spacing. Etching reactions are proposed as;



However, these MXenes also needed sonication to delaminate the layers and similar to HF etching surface functionalities of -F, -OH and =O are observed.

Another in situ HF forming etchant is suggested as a combination of a fluoride salt and hydrochloric acid (HCl). Etchant solution is prepared with dissolving lithium fluoride (LiF) in diluted HCl.(12) This etchant is shown to be capable of not only removing Al from Ti_3AlC_2 MAX phase, but also increased c-lattice parameter on the still-hydrated etched powders. Increased c-lattice parameter and the swelling of etched powder indicated that water molecules are able to intercalate between the Ti_3C_2 layers, giving it clay-like properties. After etching is completed water is added to powders to form Ti_3C_2 'clay' where it can be rolled into free-standing films as shown in Fig 2-7.(12) These rolled clay films are shown to be excellent electrodes when used in aqueous supercapacitors with 1M H_2SO_4 electrolyte. Produced clays can also be sonicated in water to produce delamination of layers which results in MXene suspensions in water with high concentration.

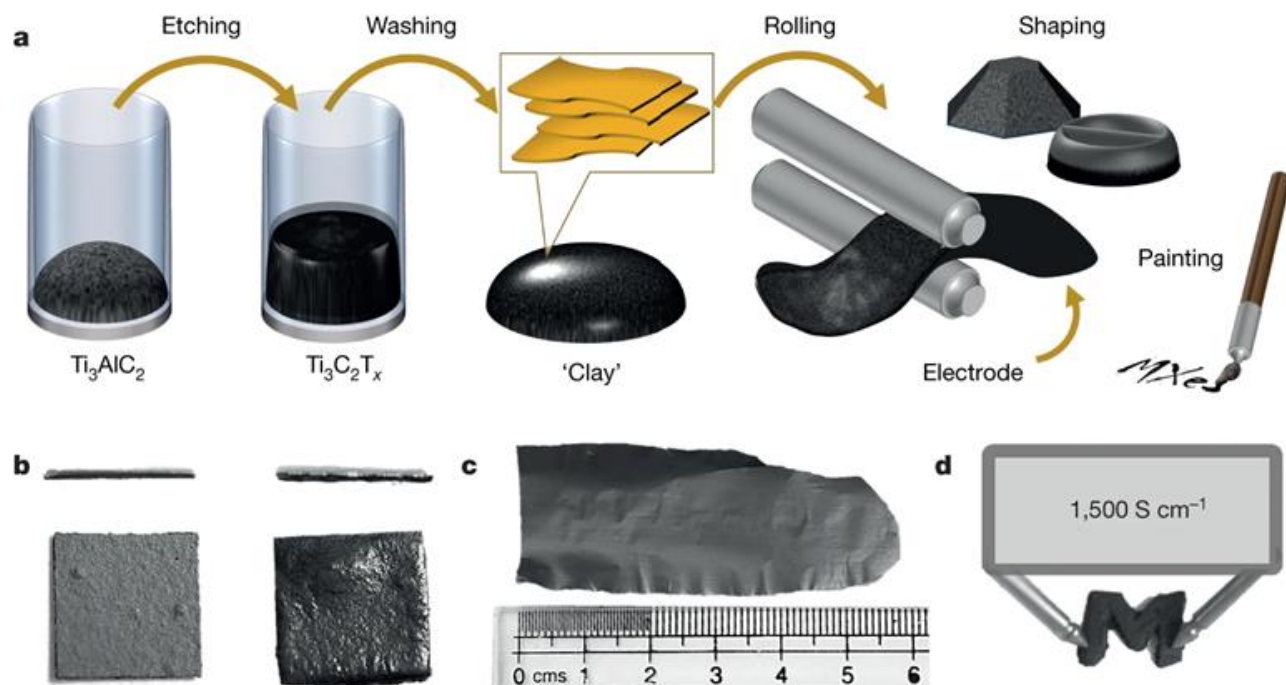


Figure 2-7: Processing of $Ti_3C_2T_x$ MXene after etching with 'clay' method(12)

Easy and scalable synthesis of $Ti_3C_2T_x$ MXene drew attention of researchers from different fields. Detailed scanning tunneling electron microscope (STEM) characterizations showed that concentrated HF etching along with sonication introduces defects to the structure causing vacancy and vacancy cluster formation. Use of sonication also limited the lateral size of produced sheets to only a few hundreds of nanometers which prevented single-flake characterizations. To eliminate the need for sonication, one approach was made through the optimization of etching parameters. Increasing the concentration of intercalant H^+ and Li^+ cations by increasing molar ratios of HCl and LiF to Ti_3AlC_2 , it was shown that etching and delamination can be achieved at the same time.

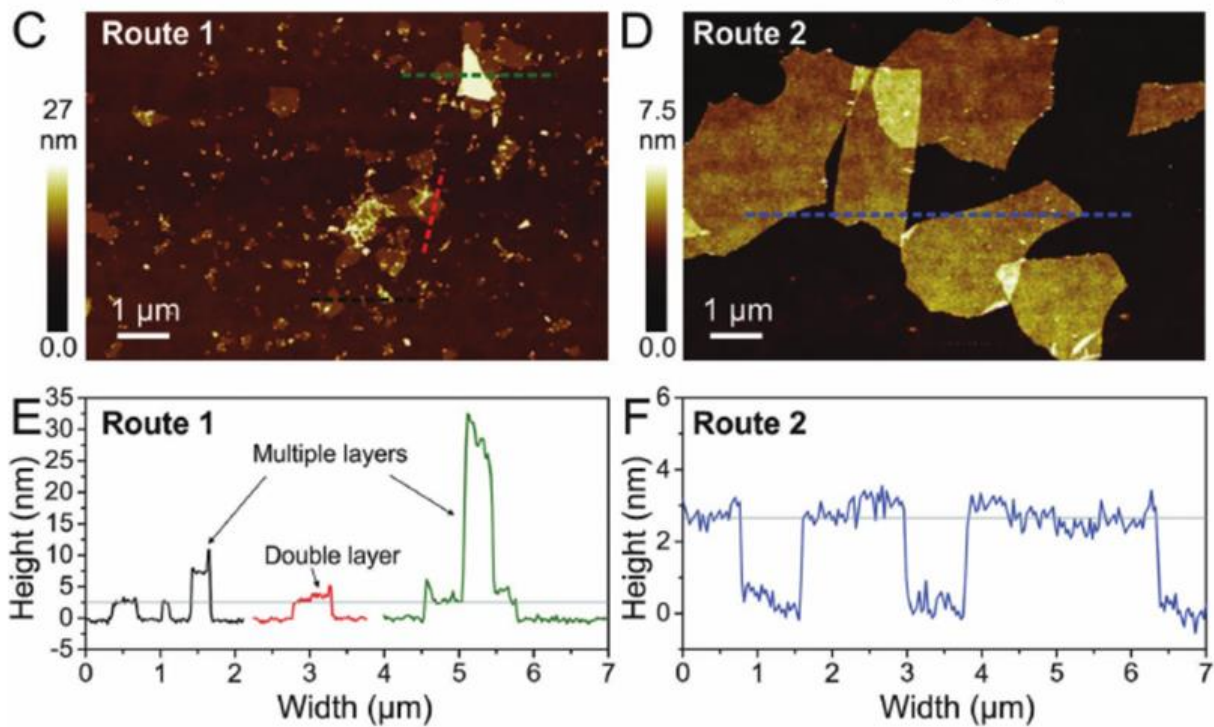


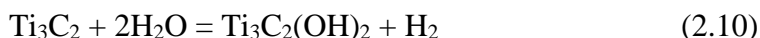
Figure 2-8: AFM Analysis showing the effect of synthesis parameters on the structure of $\text{Ti}_3\text{C}_2\text{T}_x$ sheets(44)

Where the ‘clay’ method used 5M LiF in 6M HCl, this optimized method used 12M LiF in 9M HCl. Moreover, since this method did not need a sonication for delamination of the sheets, produced sheets are reported to have up to 15 microns. This optimized method is named as ‘minimally intensive layer delamination’ method or MILD method for short.(44) Large area single layer and high-quality sheets resulted with this etching method also enabled single-flake characterization, allowing researchers discover more intrinsic properties of MXenes.

Alkaline and/or Hydrothermal Etching

Several attempts have been made for alkali etching of Ti_3AlC_2 MAX phases, considering alkali’s strong binding capability with Al.(45–49) Early attempts required either a pre-etching or post-etching acid treatments. Due to thin layer of protective native oxides present on MAX phases,

HF was utilized for pre-etching before using TMAOH as etchant.(45) Another approach used high temperature NaOH, followed by H₂SO₄ acid treatment, since NaOH was not able to dissolve produced aluminum oxide or hydroxides(49). Since etching was limited to only the surface of MAX phase particles. In 2018, two different studies overcame this problem by using so called Bayer process.(46,47) Through this process, it is possible to dissolve aluminum oxides or hydroxides at elevated temperature and pressure, thus enabling the continuation of the etching through the bulk of MAX phase particles. Both studies used very high concentrations of KOH or NaOH (near saturation) at high temperatures of 150 to 270 °C and proved that Ti₃C₂T_x MXenes can be produced without using any fluoride component, leading to surface groups of only -O and -OH. Etching reactions are proposed as the followings;



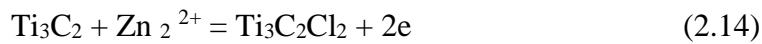
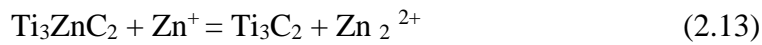
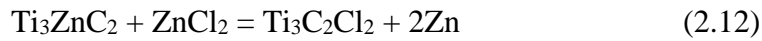
Where X can be Na or K. (45,46)

It must be noted here that theoretical calculations show -O and -OH surface groups perform better compared to -F surface groups at several electrochemical applications, thus making -F surface functionality undesirable.(50–52)

Molten Salt Etching

Although only a limited number of studies showed molten salt etching, the most recent study also showed that it is possible to have different surface groups on MXene surface rather than -O, -OH or -F.(53,54) In this technique, ZnCl₂ salt is used with Ti₃AlC₂ MAX phase with 6:1 molar ratio. Powder mixture is then heat treated at 550 C for 5 hours under inert atmosphere. It was argued that above melting temperature of ZnCl₂, which is 280 C, the salt ionizes to Zn²⁺ and ZnCl₄²⁻ in its molten state and acts as a Lewis acid in which Al atoms Ti₃AlC₂ reduces to Al³⁺ ions.

These Al^{3+} ions react with Cl^- to form AlCl_3 which has a boiling point around $180\text{ }^\circ\text{C}$ and evaporates at $550\text{ }^\circ\text{C}$ which is the reaction temperature. Evaporation of Al enables continuing etching, but initially Zn atoms replace these empty spaces forming a Zn-MAX phase; Ti_3ZnC_2 . Only after forming Zn-MAX phase, in the presence of excess molten salt, reaction continues to form $\text{Ti}_3\text{C}_2\text{Cl}_2$, resulting in further etching of Zn and -Cl terminated MXenes. Etching reactions are proposed as;



This elemental replacement approach is a significant development since for the first time exclusively -Cl surface terminations are reported with MXenes.(53) Recent theoretical studies also showed that Cl-terminated MXenes might have superior electrochemical properties and be more stable when compared with F-terminated MXenes.(55,56) It is also important to note that this method was not able to produce MXenes with different MAX phases of V_2AlC or Ti_2AlN .

Electrochemical Etching

Most recent approach on the selective etching of MAX phases has been electrochemical etching method where MAX phases used as electrodes and etching is carried out under applied voltage between the electrodes.(57–60) Only aqueous electrolytes used so far and only one method where a mixture of $1\text{M NH}_4\text{Cl}$ and 0.2 M TMAOH is used as the electrolyte resulted in delaminated $\text{Ti}_3\text{C}_2\text{T}_x$ ($\text{T}_x = -\text{OH}, -\text{O}$) sheets. Electrochemical etching methods are important as they have the

potential to provide mild etching conditions where MXene sheets can be produced with minimal amounts of defects and large sizes. For example, Yang et al reported $Ti_3C_2T_x$ sheets up to 18.6 micrometers which is the largest sheet size reported.(60) On the other hand, using diluted HCl Peng et al reported electrochemical etching of V_2AlC and Cr_2AlC MAX phases along with Ti_3AlC_2 .(57) Although it must be noted that etching of MAX phase other than Ti_3AlC_2 resulted mostly in transitional metal oxides and low M/Al ratio, indicating etching is not complete.(57)

Nevertheless, etching of different MAX phases signal the capabilities of the method. Studies show that optimization of the electrolyte in such systems might result in a universal etching method that is capable of working with different MAX phases. Although many different approaches are taken in the recent years, HF etching is still the only choice for the majority of the MAX phases as researchers are working towards different selective etching systems.

2.3 MXenes and Their Properties

Since the first synthesis report of $Ti_3C_2T_x$ MXene in 2011, number of published articles on peer-reviewed journals about MXenes raised exponentially. More than 750 institutions from over 50 different country joined this exploration and they have reported more than 30 different compositions of MXenes experimentally and dozens more are predicted theoretically so far (numbers reported in 2019.).(22) Reported MXenes are shown in Fig.2-9.(22) MXenes also drew interest to MAX phase research, where new MAX phases with ordered double-transitional metal elements have been reported within the past few years.(61,62) It was also shown that MXenes can have two different transitional metal elements within their structure, which can be found in and out of plane ordered as well as randomly distributed.(63) These solid solution MXenes are also shown to be capable of having different stoichiometric ratios, raising the number of possible combinations virtually to infinite. There are also recent attempts to include Boron as an X element

to MXene family, to synthesize 2D transitional metal borides, further increasing the number of possible structures in this 2D materials family. (64–66)

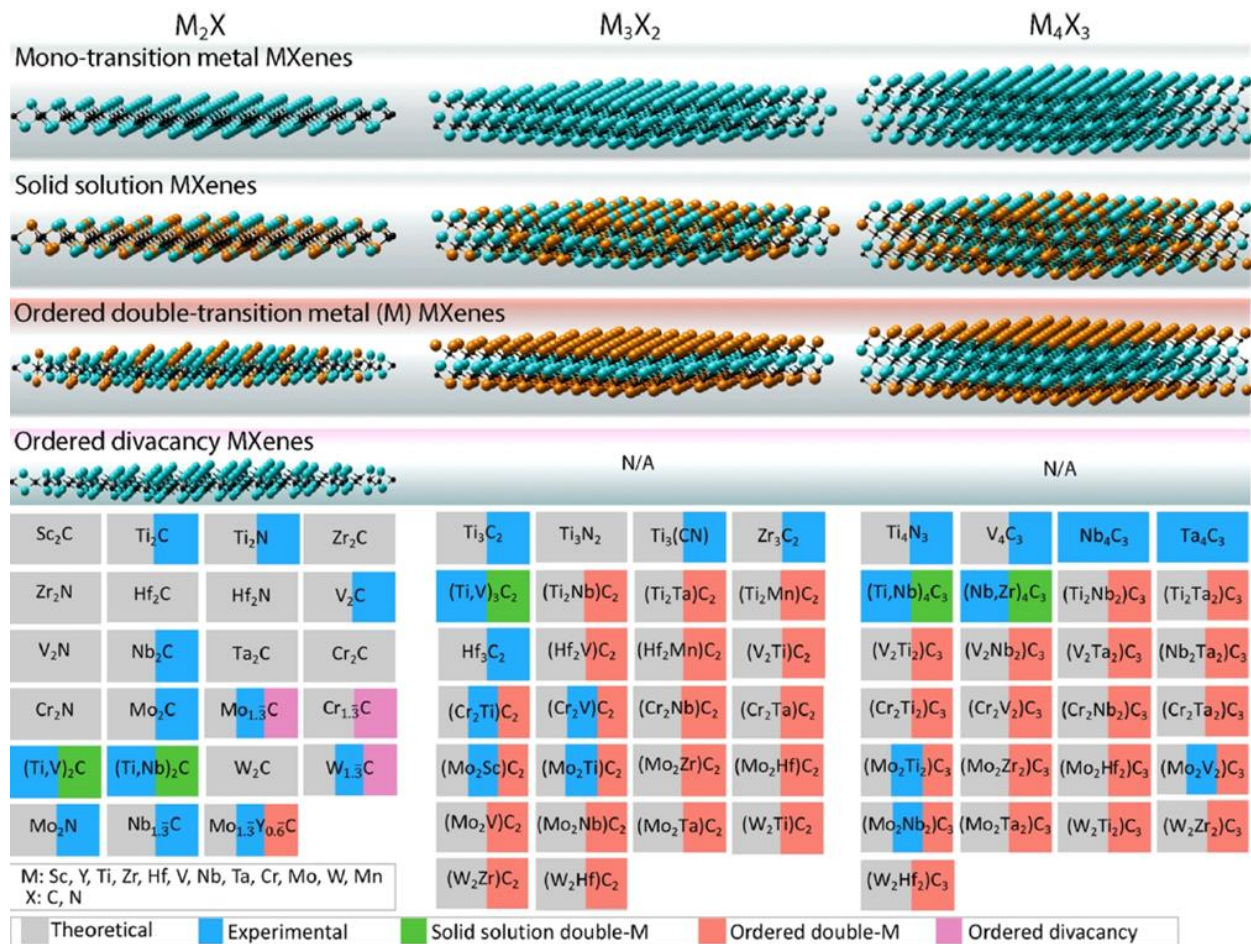


Figure 2-9: Different MXene structures reported to be stable theoretically or experimentally(22)

Above mentioned different etching methods also attributed to this growing interest on MXenes, elimination of HF-containing or HF-forming etchants from the synthesis procedure made it possible for different laboratories to produce MXenes as well.

MXenes, due to this large number of different compositions, are able to present unique combination of properties.(67) Transitional metal carbide or nitride structure offer excellent mechanical properties and high electrical conductivity whereas surface terminations which can be -O, -OH, -F and -Cl or possibly more different elements, determine unique chemical properties such as hydrophilicity or target-specific surfaces.(51) These properties enable MXenes to be used in various applications such as energy storage, catalysis, electronics and more as shown in Fig, 2-10.(22) Second ring in Fig 2-8 indicates the first research article published in the corresponding field. The first reported biomedical, sensor or electromagnetic applications of MXenes are only 3-4 years old; showing that MXene research is still on its early stages. Many theoretically predicted magnetic or insulating properties have not been validated experimentally yet.(68–70)

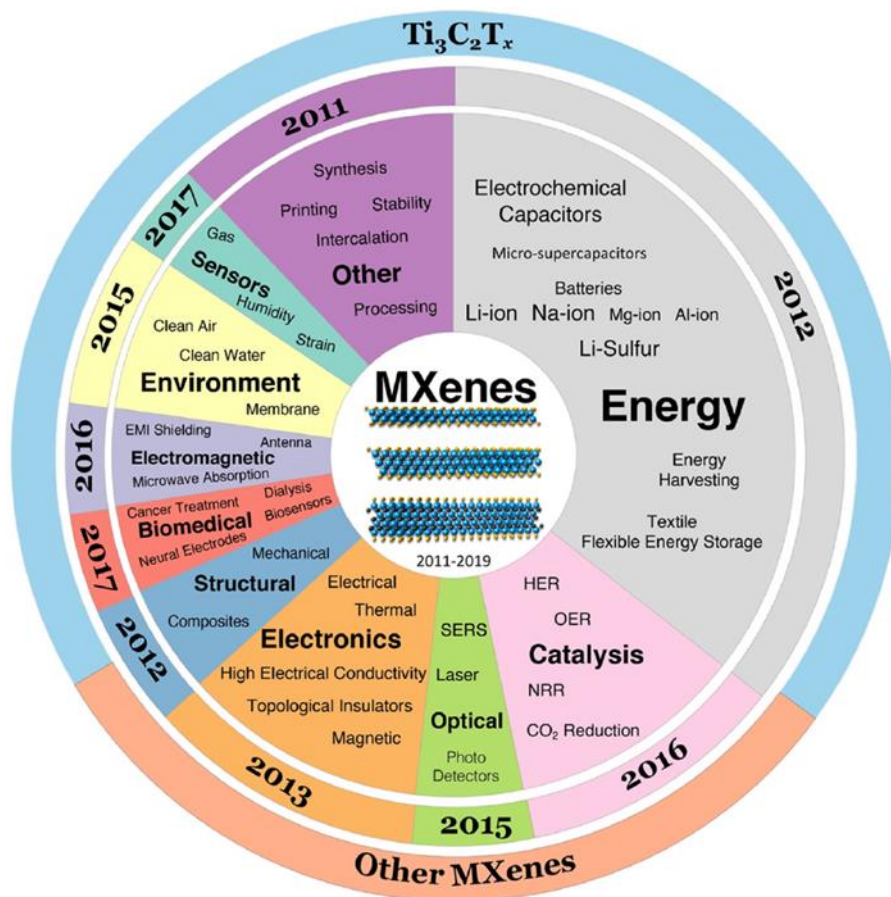


Figure 2-10: MXene application areas, middle ring shows the first paper published in the corresponding research field(22)

Nevertheless, researchers made some great advancements in MXene research, especially in processability of MXenes and in fields such as energy storage or catalysis.(25,71) As mentioned in the section before, most of MXene synthesis ends with a colloidal suspension of produced sheets in deionized water or organic solvents.(72) Vacuum filtration of these suspensions results in horizontally aligned and densely packed sheets which form a flexible film called MXene film or MXene paper.(73,74) These films can be used directly as free-standing electrodes in energy storage application as they exhibit high electrical conductivity. However, these structures also have a disadvantage since dense stacking of 2D sheets due to van der Waals interactions limit the

available surface area for the electrolyte.(75) Various studies have studied original structure designs in order to increase the surface area for electrolyte and to decrease ionic diffusion paths.(61,76,77) It was shown that increasing interlayer spacing in vacuum filtrated MXene films leads to a better performance at higher charge/discharge rates, higher specific capacitance and better cyclability.(78)

In attempts to increase the interlayer spacing, researchers used different additives such as carbon nano tubes or different polymers.(78–80) Use of CNTs have been demonstrated in various energy storage applications, showing that CNTs can act as spacers between the MXene sheets and increase the electrochemical performance of the MXene film electrodes.(81,82) One study showed that not only mixing CNT suspension with MXene suspensions but also filtrating each alternatively to produce sandwich-like structure of $Ti_3C_2T_x$ and CNTs, which resulted in a better electrochemical performance compared to simple mixing of suspensions and filtering. Fabrication of MXene and polymer composites is also proved to be an effective method to improve electrochemical properties of these electrodes. Moreover, these electrodes demonstrated better mechanical properties and flexibility. One study used incorporation of aniline monomers as spacers between the MXene sheets and demonstrated the *in-situ* polymerization using HCl.(78) Increasing the interlayer spacing through the use of polymers enabled electrodes to keep up the performance even with higher thickness. However, it must be noted that use of polymer might affect the electrical conductivity unfavorably, consequently MXene to polymer ratio is presumed to be an important factor in production of composite films. (83,84)

Another interesting approach was reported by Lukatsaya et al, with the use of polymethyl methacrylate (PMMA) microspheres as templates for MXenes.(14) The microspheres are used to shape MXenes into hollow spheres. Resulting structure of the electrodes was less ordered and less

dense compared to vacuum filtered films while upholding the high electrical conductivity. This macroporous $Ti_3C_2T_x$ structure enabled shorter diffusion paths for ions thus demonstrated to have very high capacitance values even at very high scan rates of 100,000 mV/s when used in aqueous supercapacitors. Same study also employed another new strategy of making hydrogels with MXene films. These electrodes are soaked in the electrolyte for up to 3 days right after vacuum filtration which enabled exchange of water with electrolyte. This method is important as it proves to increase the capacitance of MXene electrodes without using any additives.(14)

Based on the summarized recent advances in MXene research, basis of the proposed study will be discussed in the next chapter.

Following the literature review, this chapter will initially address the gaps in the current knowledge of MXene research. Focus points of this study will be highlighted with brief research statements, and our motivation to follow these directions will be discussed. Next, the proposed study will be detailed under four different research tasks. I will also further explain how to achieve these tasks, describe proposed experiments and follow it by presenting preliminary results.

2.4 Lack of Knowledge and Unexplored Venues

Even though MXenes are first reported at 2011, researchers showed huge interest in these two-dimensional materials, making it one of the fastest growing family of 2D materials. Early studies used concentrated hydrofluoric acid for making MXenes which is a highly dangerous method which resulted in low quality sheets. Only about after 5 years, in 2016, a more reliable and relatively safer etching method was reported.(44) This synthesis method allowed production of higher quality $Ti_3C_2T_x$ sheets and enabled more research applications as well as more detailed characterization of $Ti_3C_2T_x$ MXene itself. It was understood that the control over the structure, lateral size and quality of the MXene sheets can be only achieved via the synthesis methods. For

electrochemical applications of MXenes, these characteristics have the utmost importance. To date, precise control of the structure, lateral size and quality of $\text{Ti}_3\text{C}_2\text{T}_x$ MXene through the synthesis conditions and post-synthesis treatments is not reported.

To grasp the significance of this matter clearer, it can be mentioned the method used for making MXene solutions used sonication as a tool to delaminate more etched MAX phases and therefore get higher concentrated solutions. However, although sonication does delaminate more etched powders, it is shown that it also introduces more defects on the already delaminated sheets, and it breaks them down, decreasing the lateral size and the quality of the sheets.(85,86) Without a doubt, these changes over the structure of MXenes can also change their physical and chemical properties. Electrical conductivity, mechanical and chemical stability and electrochemical activity of MXene electrodes can be altered by manipulating the structure of individual sheets.

Designing electrodes for specific electrochemical applications has always been an attention point for researchers. To prepare MXene electrodes, vacuum filtration of the MXene solutions is the most used method due to its ease. With vacuum filtration, MXene films or ‘papers’ can be obtained, where sheets stack on top of each other with a horizontal alignment. Although it is a practical method, these electrodes suffer from the narrow ‘interlayer spacing’ (also called d-spacing) that is the Angstrom scale distance between two individual sheets. In this stack of 2D MXene sheets, how an ion, a charge carrier, moves through the thickness of the electrode determines the electrochemical characteristic of the electrodes and it depends on two things: the interlayer spacing and the number of the paths available to it. To control the interlayer spacing researchers used additive materials, also called ‘spacers’, such as carbon nano tubes or spherical nanoparticles. To increase the number of ion diffusion paths, pores are introduced to MXenes using

different porogen agents. However, control and design of the vacuum filtrated MXene electrodes' through MXene synthesis methods, without using additives, has not been reported.

As mentioned previously, controlling the lateral size of the MXene sheets and therefore isolation of larger flakes enables further characterization. One of the most important intrinsic properties of the 2D materials is their mechanical properties such as their elastic modulus and breaking strength. Determination of mechanical characteristics of 2D materials paves the way for their use in a variety of applications. After the report of graphene's extraordinary structural strength, high elasticity and resistance to break under high loads, graphene material has been used in structural composites and protective coatings where exceptional mechanical properties are a necessity.(87,88) To measure the mechanical properties of individual 2D materials a unique experimental setup is required in which the 2D material is suspended over a hole or a trench. Atomic Force Microscope is then utilized to measure how these atomically thin materials respond to mechanical strain on nanoscale. In the case of MXenes, assembly of the suspended sheets remains a challenge due to several factors; relatively small lateral sizes of sheets and liquid processing makes them harder to suspend over micron scale holes. Although there have been several theoretical studies indicating excellent mechanical properties, experimental proofs have yet to be offered. Measurement of such characteristics will only be possible through synthesis and isolation of large lateral sized MXene sheets. To date, there has not been a study where mechanical properties of different MXenes measured experimentally.

So far, it has been discussed that synthesis parameters have crucial impacts on the properties of MXenes. Literature review shows us that used etching techniques usually involves aqueous solutions. However, at this point of MXene research, these widely used aqueous etchants have several shortcomings that needs to be addressed.

An efficient etching technique is expected to completely remove the A-layer elements from the MAX phases without removing M elements. After removal of A-layer elements, transitional metal atoms on the surface forms surface groups with the available atoms in the etchant solution. These surface groups can have different types and concentrations and moreover, it can be accompanied by intercalation of water or different ions between the MXene layers. These changes in the crystal structure, specifically the c-lattice constant, can be measured with X-ray Diffraction (XRD) method. Therefore, analysis of this constant can expose important characteristics of the structure. Several studies show that wet MXenes after etched with aqueous solutions show higher c-lattice constants than their dried forms, showing that water does intercalate between the layers. Although water molecules increase d-spacing, residual water between the MXene layers is a problem with a variety of water sensitive applications such as energy storage or sensors. Residual water has been demonstrated to react with electrolytes in battery application which results in consumption of the electrolyte and therefore poor cyclability.(89)

Another issue with the use of aqueous etchants is the stability of the MXenes in water. Even $Ti_3C_2T_x$ MXene, which is one of the most chemically stable MXenes, has been shown to be stable in DI water for only 2-3 weeks, which is dependent on several factors such as amount of dissolved oxygen in the water, concentration of the solution or the ambient temperature.(90,91) On the other hand, different MXenes are found to be less stable under water. For example, aqueous Ti_2CT_x suspensions stay stable only several hours before completely oxidization of the structure occurs. Therefore, several MXenes start to oxidize and lose their properties right after the synthesis.

Besides etching the A-layers from MAX phases, used etchants can also react with the transitional metal and carbon atoms and form defects in the structure. Formation of nanopores on

the MXene sheets was reported after using high concentration HF solutions as etchants. It was hypothesized that Ti vacancies and vacancy clusters in Ti_3AlC_2 that can result in pores in the structure is correlated with the concentration of the used etchants. Even when the MILD etching method was used, a scanning transmission electron microscopy (STEM) study showed that defect concentration increases with the formed HF concentration. On the other hand, an electrochemical etching method using aqueous $NH_4Cl + TMAOH$ electrolyte showed that very high quality of $Ti_3C_2T_x$ MXenes can be produced with lateral sizes up to 20 micrometers, indicating that an electrochemical method can be employed for etching MAX phases without creating high concentration of defects.(60)

Recent studies on the etching of MAX phases also focused the effect surface terminations on the properties of produced MXenes. Traditional selective etching methods yields MXene surface functional groups such as $-OH$, $-O$ and $-F$. These functional groups have been shown to have direct impact on the properties of MXenes such as energy storage capacity, band gap or magnetism. Several attempts have been made to eliminate $-F$ surface groups, since theoretical calculations showed that MXenes with $-OH$ and $-O$ surface groups have better electrochemical properties. To achieve this goal, researchers used synthesis methods containing high concentrations of hydroxides such as $NaOH$ or KOH . As molten salt etching methods also emerged, MXenes with exclusively $-Cl$ surface groups are studied and theoretically predicted to have better electrochemical properties rather than $-O$, $-OH$ or $-F$ surface groups. These studies show us that a water-free, fluorine-free electrochemical etching method might have the potential to yield high quality MXenes. It is also important to note here that most of the etching methods are demonstrated with Ti_3AlC_2 MAX phase, where most MAX phases can only still be etched with

HF containing etchants. To date, a water-free, fluorine-free electrochemical etching method of MAX phases to produce MXenes have not been reported.

Chapter 3: Effect of synthesis conditions on the electrochemical properties of MXenes

This chapter will present the used methods to produce MXene sheets with different structure and lateral size and discuss the obtained results regarding the electrochemical properties of MXenes.

3.1 Introduction

In this section, it is shown that synthesis parameters along with controlling the lateral size of the sheets make it possible to control the lateral size of $Ti_3C_2T_x$ flakes with high precision. Sonication is used as a tool to break down MXene sheets controllably. However, studies showed that effect of sonication is not only related to lateral size of the MXene sheets but also defect density of the flakes. In the next section, effects of the changes in synthesis and post-synthesis conditions on the electrochemical performance of MXene electrodes will be discussed. Moreover, isolation of large-area single-layer sheets also enables the characterization of individual MXene sheets. In the section 4.3, above-mentioned isolated large-area MXene sheets will be used to suspend over micron sized holes to investigate mechanical properties of the sheets.

This dissertation shows the successful synthesis of the various precursor MAX Phases, which is essential for preparation of MXenes. The next section further describes the materials and methods used in this study comprehensively. Our lab is currently able to synthesize various MAX phases including but not limited to the following MAX Phases: Ti_3AlC_2 , Ti_2AlC , Nb_2AlC , V_2AlC , Cr_2AlC , $Mo_2Ti_2AlC_3$, Mo_2TiAlC , Cr_2TiAlC . For this step of the proposed research, the Ti_3AlC_2 MAX phase was used since traditional etching methods usually only cover this MAX Phase.

3.2 Materials and Methods

MAX Phases Synthesis: Ti_3AlC_2 powders were synthesized as reported before.(92) Briefly, first Ti_2AlC MAX phase was prepared by the reaction of TiC powder (99.5%, Alfa Aesar), Titanium powder (99.5%, Alfa Aesar) and Aluminum powder (99.5% Alfa Aesar) in 0.85:1.15:1.05 molar ratio. This mixture was heated to 1400 °C for 4 hours with a 5 °C/min heating rate. The resulting block of Ti_2AlC was milled into a powder and mixed with TiC powder (99.5%, Alfa Aesar) in a 1:1 molar ratio. This mixture was also heated to 1400 °C for 2 hours with a 5 °C/min heating rate. Then, the resulted block of Ti_3AlC_2 MAX was milled to form the precursor powder used for the synthesis of MXenes.

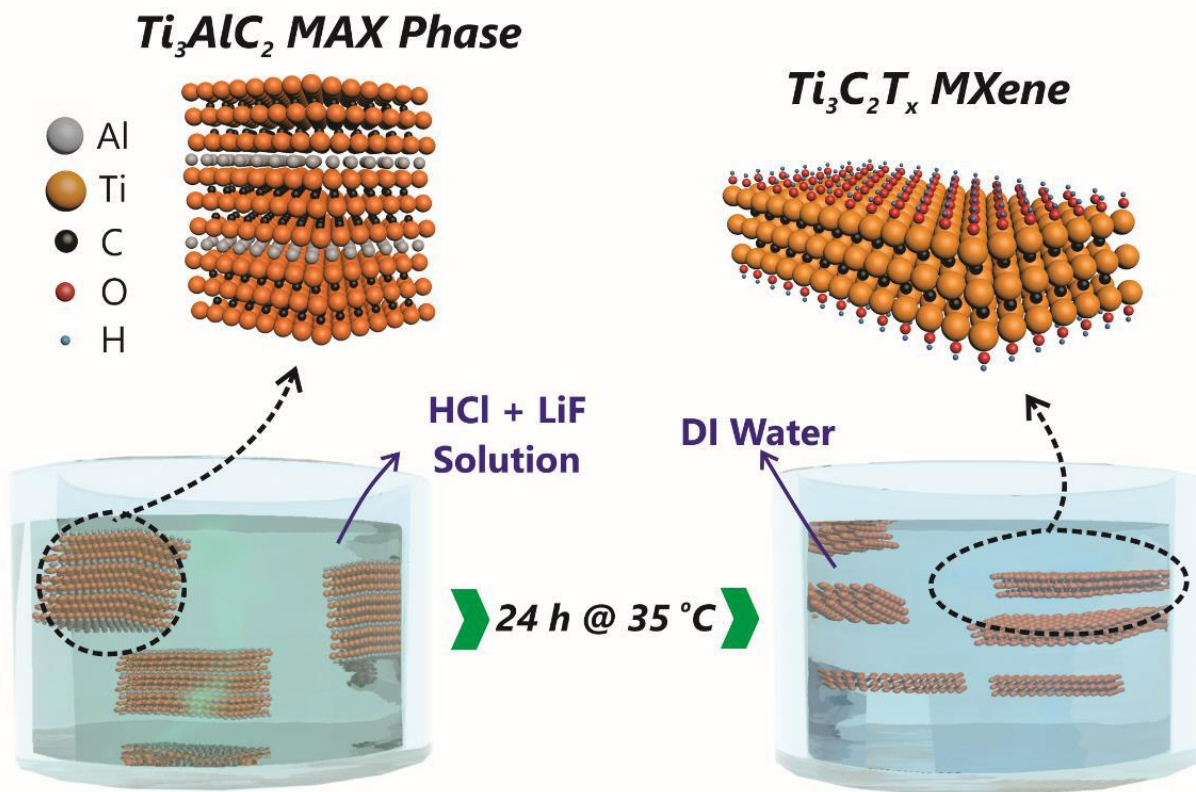


Figure 3-1: Schematic illustration of $Ti_3C_2T_x$ MXene synthesis process.

Preparation of $Ti_3C_2T_x$ Suspension: The dispersions of the $Ti_3C_2T_x$ flakes in water were prepared by a recently introduced method called minimally intensive layer delamination (MILD) synthesis method.(44) To synthesize $Ti_3C_2T_x$ flakes 1g of the precursor Ti_3AlC_2 MAX phase was immersed in 20 ml of a mixture lithium fluoride (LiF, 98.5% Alfa Aesar) and hydrochloric acid (ACS Grade, VWR). The mixture was prepared by adding 1g of LiF to 20 ml of 6M HCl solution. The resulting suspension was stirred in a water bath at 35 °C temperature and for 24 hours. Then, the suspension was added to four centrifuge bottles and diluted with the addition of DI water and centrifuged at 3500 rpm followed by decanting the supernatant to wash the synthesized material. The bottles were only hand shaken between washing cycles (no sonication). The washing cycle was continued until a dark green supernatant was remained after 1-hour centrifuge, showing that $Ti_3C_2T_x$ sheets are completely delaminated in water. For comparison, the ‘clay’ synthesis method was also used. The difference between this method and the one explained above is the different composition of the etching solution as reported before.(12) Figure 4-2 shows a comparison of the MXene flakes produced with these two methods.

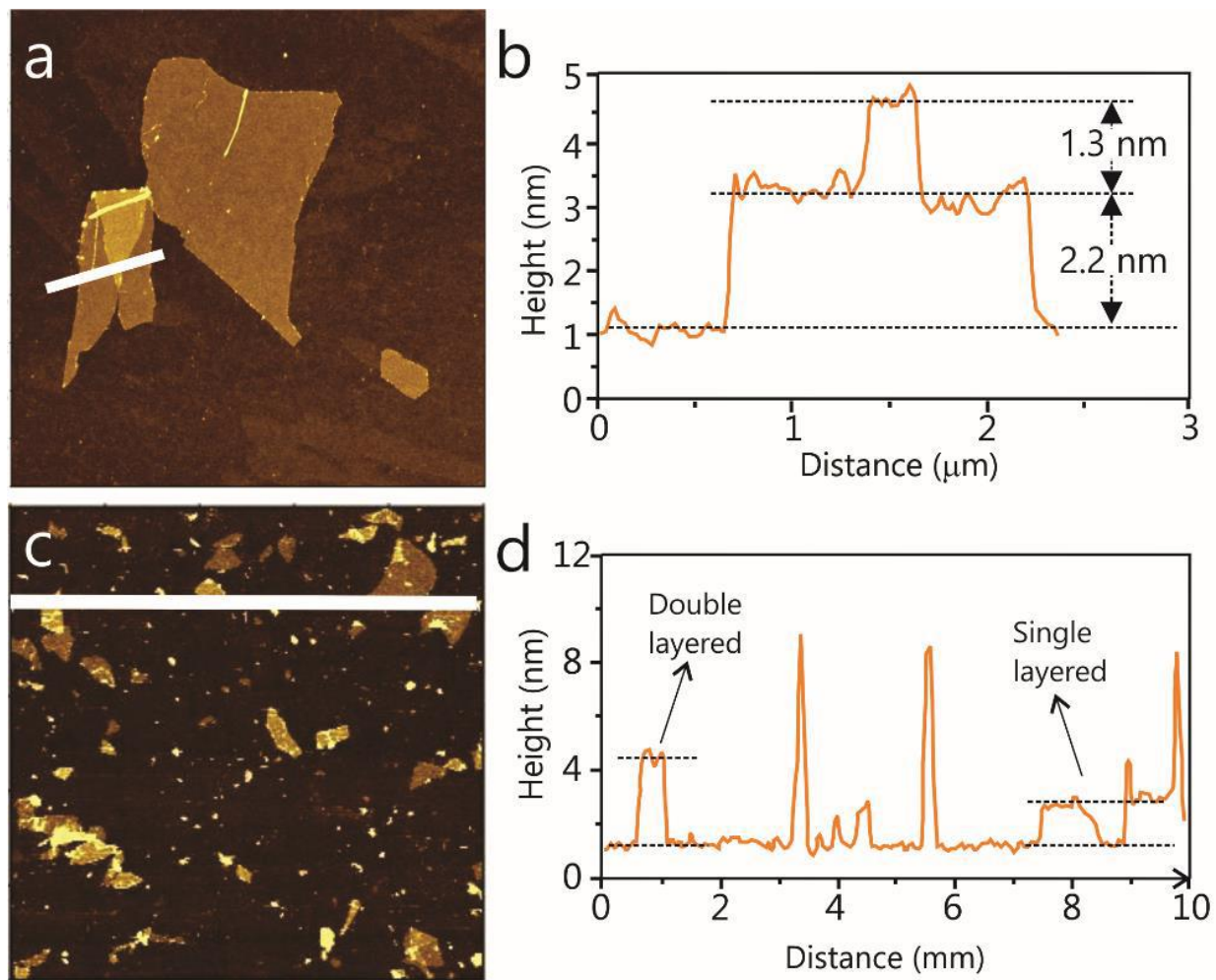


Figure 3-2: Effect of synthesis parameters on the flake size distribution of the synthesized $\text{Ti}_3\text{C}_2\text{T}_x$. (a) $\text{Ti}_3\text{C}_2\text{T}_x$ flakes synthesized using the MILD method. (b) The thickness of a single layer $\text{Ti}_3\text{C}_2\text{T}_x$ flake prepared using the MILD method is measured to be 1.3 nm on a folded flake. (c and d) $\text{Ti}_3\text{C}_2\text{T}_x$ flakes obtained after the 'clay' synthesis method showing flakes with different thicknesses and up to 1 μm lateral sizes.

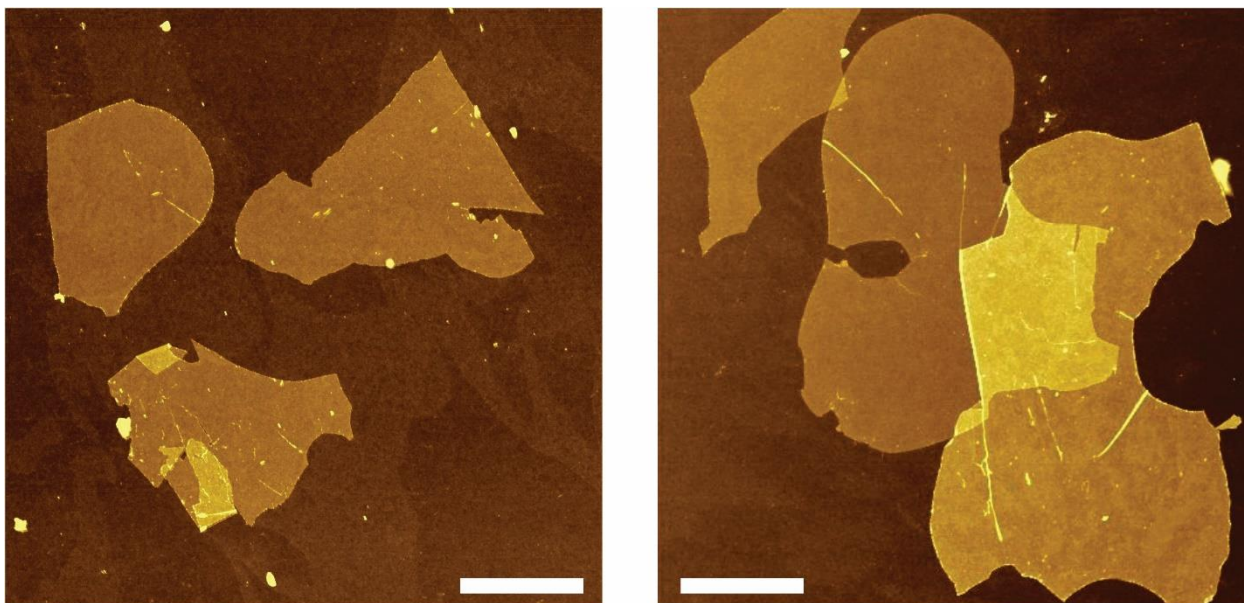


Figure 3-3: AFM Images showing large $\text{Ti}_3\text{C}_2\text{T}_x$ sheets produced with MILD-synthesis method (Scale bar is $2\mu\text{m}$).

The $\text{Ti}_3\text{C}_2\text{T}_x$ flakes synthesized by the MILD method are mostly large flakes, but there are also a lot of small flakes in the prepared dispersions. Therefore, we used an additional centrifuge step to separate the large flakes from the smaller ones. For this, the dispersion was poured into centrifuge bottles and centrifuged at 4500 rpm. The light green colored supernatant was decanted, and the sediment which consisted only large flakes of $\text{Ti}_3\text{C}_2\text{T}_x$ was re-dispersed in water. To produce uniform solutions of smaller flakes, this dispersion was used as the starting dispersion to produce various dispersions sonicated for 2.5, 5, 10, 15 and 30 minutes. Sonication steps were performed using a Qsonica Q700 tip sonicator with a power of 35 W.

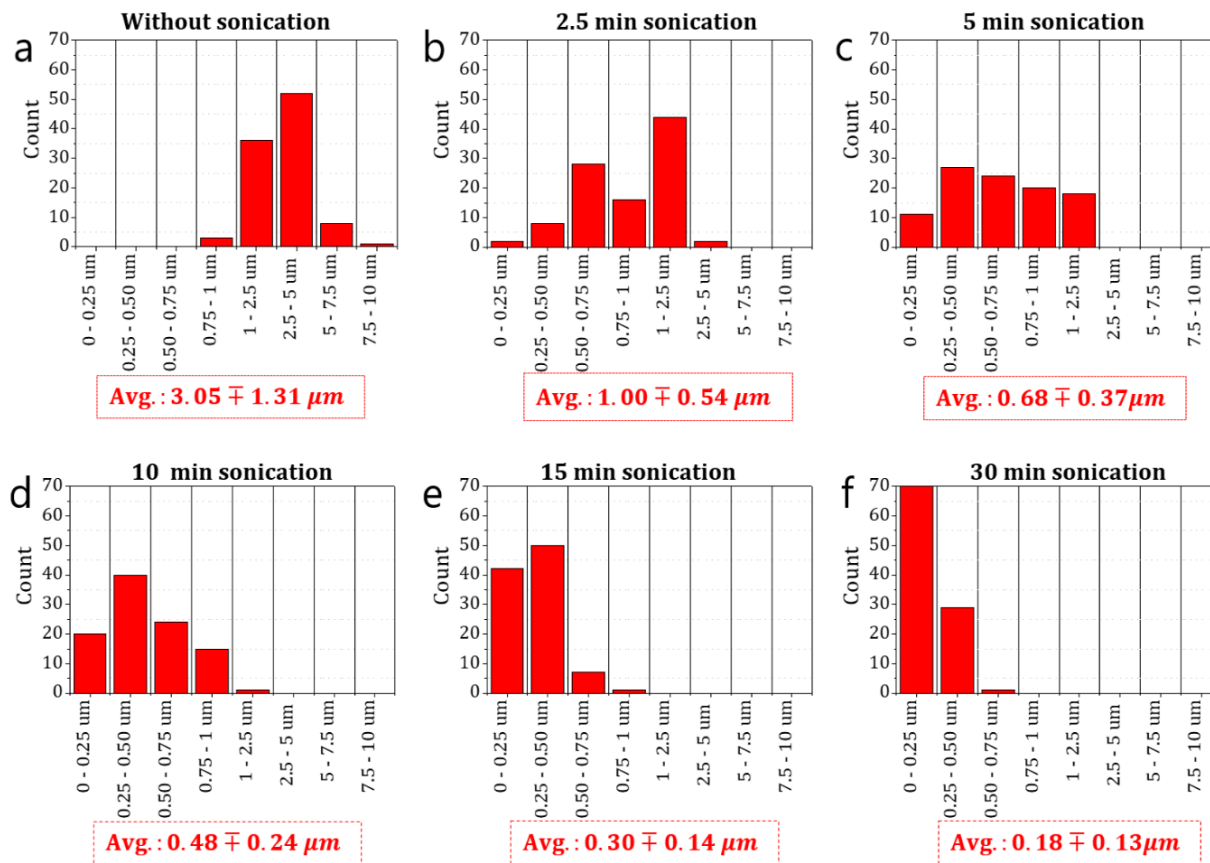


Figure 3-4: Histograms showing size distribution of $Ti_3C_2T_x$ flakes prepared using various sonication times and averages sizes of (a) $3.05 \mu m$, (b) $1.00 \mu m$, (c) $0.68 \mu m$, (d) $0.48 \mu m$, (e) $0.30 \mu m$, and (f) $0.18 \mu m$.

Electrode fabrication: To achieve an equal thickness for all MXene papers (electrodes) the same volumes of each MXene dispersion was filtered for the fabrication of the papers. The electrode thicknesses were measured by a thickness gauge and confirmed by cross-sectional SEM images. All electrodes were about $4 \mu m$ in thickness ($3 \mu m$ for hydrogel sample). Except for the hydrogel samples, all MXene papers were dried in air and punched to the desired size and were used as freestanding electrodes for the electrochemical measurement. To make the hydrogel sample, the films were taken out of the filtration system before drying and were carefully peeled off from the filtration paper in acetone and then soaked in the electrolyte for three days. Wet hydrogel electrodes were then directly

used in a three-electrode setup for the electrochemical tests. The mass and volume of the paper electrodes were measured before the electrochemical tests, but the same measurements of the hydrogel electrodes were performed after the electrochemical test. Before these measurements, the electrodes were first washed with ethanol and water and dried in vacuum oven overnight. The densities of the fabricated electrodes were measured by dividing the mass of each electrode by its volume. Electrode densities were found to be in the range of 3.5-3.6 g/cm³ for all electrodes regardless of the size of the flakes used in their fabrication.

Electrochemical measurements: The electrochemical measurements were carried out in three-electrode setups using plastic Swagelok cells on a multi-channel potentiostat (VMP3, Biologic Science Instruments). Electrochemical performance of different MXene electrodes was characterized by using cyclic voltammetry (CV), galvanostatic charge/discharge, and electrochemical impedance spectroscopy (EIS) techniques in a 3M H₂SO₄ aqueous electrolyte. In each cell, glassy carbon was used the current collector, and a large activated carbon film and Ag/AgCl electrode were used as the counter and reference electrodes, respectively.

The gravimetric capacitance of the electrodes was calculated using equation (1) by considering the whole area under the CV curves.

$$C = \frac{\int IdV}{2mv \Delta V} \quad (1)$$

where I is current (A), V is the potential (V), v is scan rate and m is mass of the electrode.

Volumetric capacitances were calculated using the volume of the electrode instead of their mass in equation (1). The energy density (E, Wh kg⁻¹) and power density (P, W kg⁻¹) electrodes were calculated using equations (2) and (3), respectively.

$$E = \frac{0.5 \times C \times V^2}{3600} \quad (2)$$

$$P = E \times v/V \times 3600 \quad (3)$$

Material Characterization techniques: To analyze the effect of sonication on $\text{Ti}_3\text{C}_2\text{T}_x$ sheets, atomic force microscope (AFM) (Park Systems, NX10) was used to measure the size of the produced flakes. Before filtering each solution, a small amount of the solution was diluted with DI water and drop-casted on the pieces of thermally oxidized silicon wafers. Numerous AFM images were obtained from each solution to measure the size of at least one hundred $\text{Ti}_3\text{C}_2\text{T}_x$ flakes and calculate the average flake size of each dispersion. The size of a $\text{Ti}_3\text{C}_2\text{T}_x$ flake was defined as the length of their longest edge.

The X-Ray analysis of MXene papers was performed by a Bruker D8 X-ray diffractometer with 40 kV and 40 mA Cu $\text{K}\alpha$ radiation. Scanning electron microscope (SEM) images were taken using a JEOL JSM-7000F SEM

3.3 Effect of LiF:MAX molar ratio on the electrochemical properties of $\text{Ti}_3\text{C}_2\text{T}_x$ electrodes

This section initially studies the effect of the effect of LiF:MAX phase molar ratio on the electrochemical properties of produced $\text{Ti}_3\text{C}_2\text{T}_x$ sheets. Previous studies investigated the effect of LiF:MAX phase molar ratio on the produced $\text{Ti}_3\text{C}_2\text{T}_x$ sheets structure. Sang et al. used HAADF-STEM to investigate the effect of increasing LiF concentration on the atomic defects produced on $\text{Ti}_3\text{C}_2\text{T}_x$ sheets. It is clearly shown that increasing the *in-situ* HF concentration results in increasing surface Ti atom vacancies. With further increase of HF concentration, point defects turn into

vacancy clusters. Within the vacancy clusters, exposed metallic Ti and C atoms are predicted to be making bonds with O and H atoms, respectively. A model schematic is shown in Fig. 4.8 to demonstrate increasing Ti vacancies with increasing LiF concentration. Fig.4-9 also shows high resolution AFM images showing that vacancy clusters can grow up to 25 nm holes on the sheets.

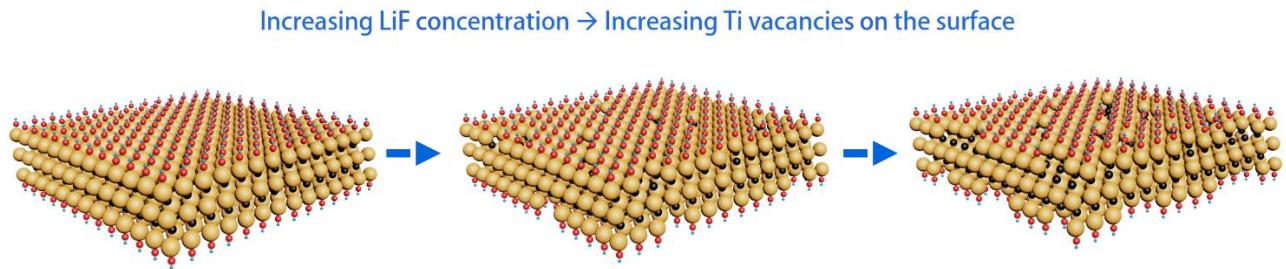


Figure 3-5: Schematic modeled to show the effect of LiF concentration on the structure of $\text{Ti}_3\text{C}_2\text{T}_x$ sheets

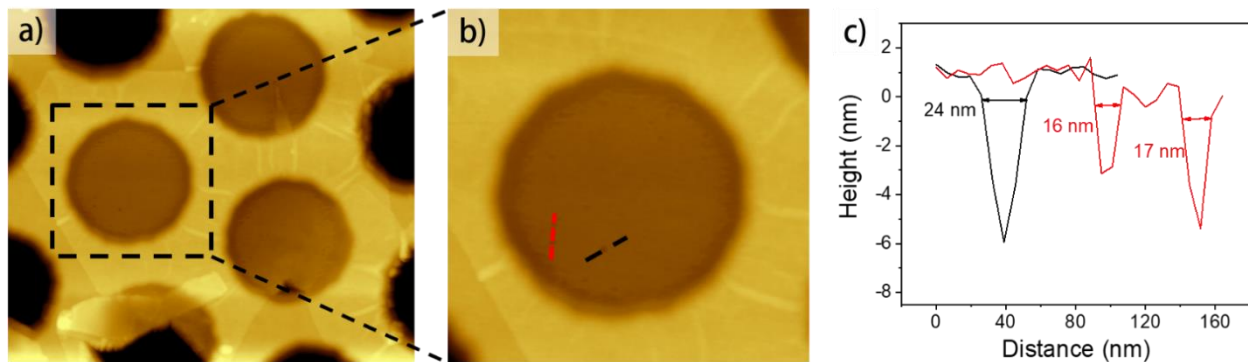


Figure 3-6: AFM analysis showing nano-holes on the 30 M LiF:MAX molar ratio sample, a-b) AFM images of 30M- $\text{Ti}_3\text{C}_2\text{T}_x$ sheets, c) height profiles of black and red lines shown in the AFM image.

To investigate the effect of this structural change on the electrochemical properties of these materials, electrodes are produced by vacuum assisted filtration of $Ti_3C_2T_x$ solutions prepared with different LiF concentrations. 4 different LiF concentrations are used in this study, 7.5 M, 15 M, 22.5 M, and 30 M. After mixing of 30 M LiF and 9 M HCl solution it is observed that solution gets very viscous indicating that it is near its saturation point. Thickness of the prepared electrodes are kept the same at 2 micrometers to neglect the effect of electrode thickness.

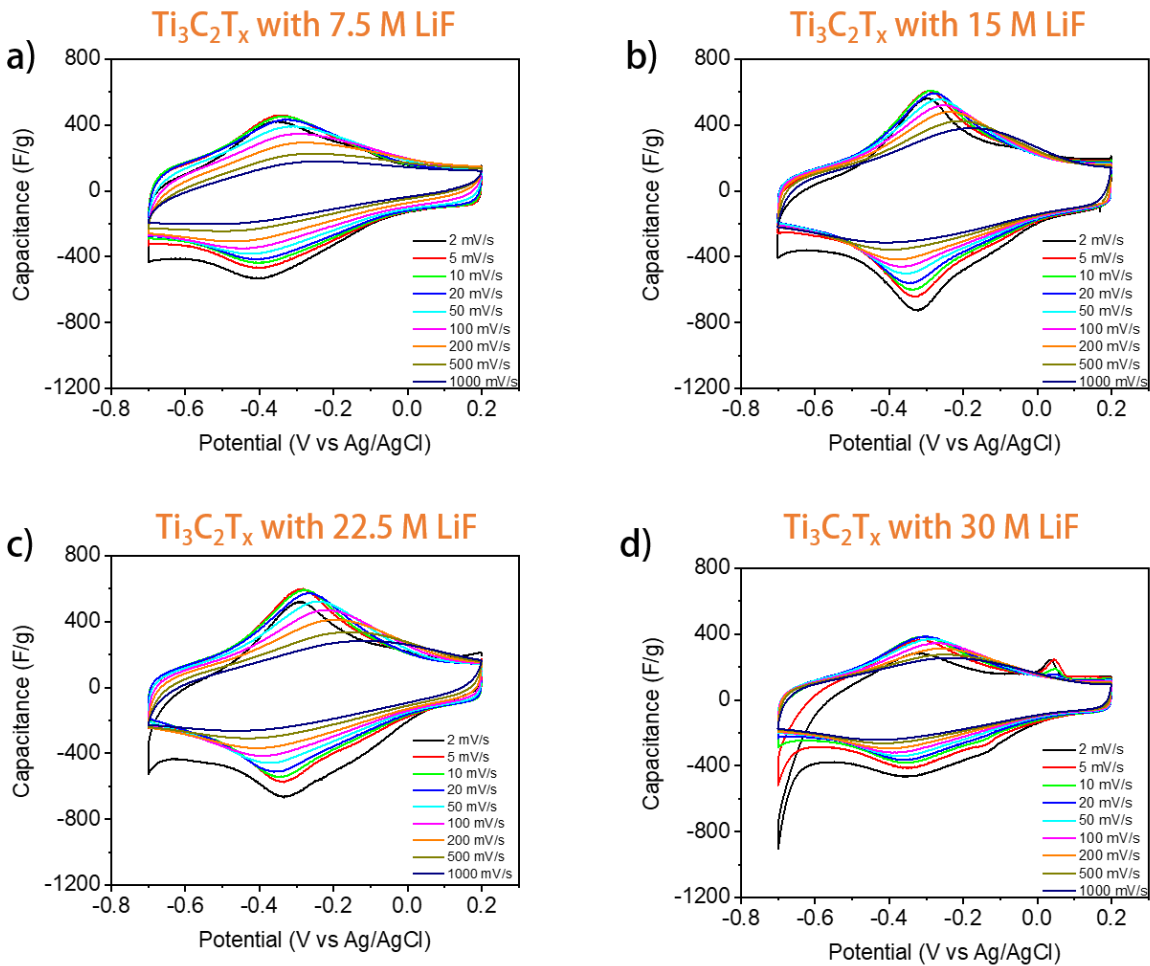


Figure 3-7: Cyclic voltammetry graphs obtained at increasing charge and discharge rates with different electrodes produced with LiF concentrations, a) 7.5 M, b) 15 M, c) 22.5 M, d) 30 M.

To observe electrochemical properties of these materials, 3-electrode supercapacitor systems are used. Electrochemical cells using glassy carbon as current collector and 3 M H₂SO₄ as the electrolyte are prepared and Ti₃C₂T_x electrodes are used as working electrodes against activated carbon counter electrodes, as described in the Materials and Methods section. Fig.3.7 shows the cyclic voltammetry graphs obtained with different electrodes. It is observed that initial increase of LiF concentration increases the electrochemical performance Ti₃C₂ electrodes at both slow and fast scan rates. 7.5M-Ti₃C₂T_x electrodes have a gravimetric capacitance of 271 F.g⁻¹ and volumetric capacitance of 903 F.cm³ at a slow scan rate of 2 mV/s. With 15M-Ti₃C₂T_x electrodes, these values increase to gravimetric capacitance of 332 F.g⁻¹ and volumetric capacitance of 1184 F.cm³ at the same scan rate, a 22% increase in the performance. At the high scan rate of 1000 mV/s, 7.5M-Ti₃C₂T_x electrodes have a gravimetric capacitance of 124 F.g⁻¹ and volumetric capacitance of 413 F.cm³. With 15M-Ti₃C₂T_x electrodes, these values increase to gravimetric capacitance of 224 F.g⁻¹ and volumetric capacitance of 525 F.cm³ at the same scan rate, a huge improvement of 80% increase in the performance. But further increase in the LiF concentration results in lower performances. 22.5M-Ti₃C₂T_x electrodes have gravimetric capacitance of 308 F.g⁻¹ and volumetric capacitance of 993 F.cm³ at 2 mV/s and gravimetric capacitance of 179 F.g⁻¹ and volumetric capacitance of 557 F.cm³ at 1000 mV/s. Decrease in the electrochemical performance continues with the increasing LiF concentration. 30M-Ti₃C₂T_x electrodes have gravimetric capacitance of 250 F.g⁻¹ and volumetric capacitance of 806 F.cm³ at 2 mV/s and gravimetric capacitance of 164 F.g⁻¹ and volumetric capacitance of 529 F.cm³ at 1000 mV/s. Comparison of these performances are also displayed in Fig. 3-8 by capacitance values and in Fig.3-9 by the CV graphs.

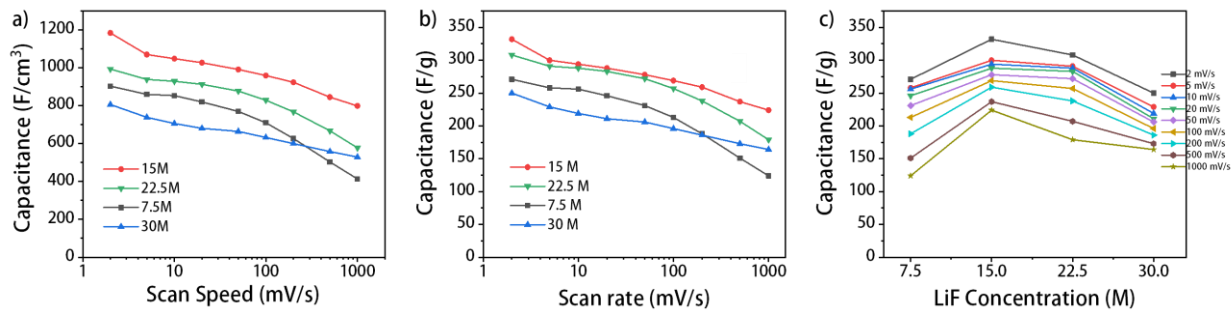


Figure 3-8: Comparison of gravimetric and volumetric capacitance values of different $\text{Ti}_3\text{C}_2\text{T}_x$ electrodes produced with 7.5 M, 15 M, 22.5 M and 30 M LiF concentrations by a) volumetric capacitance values at different scan rates, b) gravimetric capacitance values at different scan rates, c) gravimetric capacitance values at different LiF concentrations.

Based on these results, we observe that Ti vacancy formation on the MXene sheets initially improves the electrochemical performance. However further increase in the defective structure results in an inferior performance. These findings might be explained by the structural change and the effect of that on the electrochemical processes. We can hypothesize that initial increase in the Ti vacancies results in mostly point defects which results in more electrochemically active metal oxide surface areas. However, as the LiF concentration continues to increase, it can be thought that vacancy clusters become more dominant mechanism as proposed in Sang et al.'s work. It is also pointed out in their work that vacancy clusters expose more C and metallic Ti atoms. It is shown that these Carbon atoms bond with available H^+ ions, which is evident with C-H peak in NMR analysis. It is also mentioned that charge differences around the exposed metallic Ti atoms attract and trap water molecules around them. It was noted that partially free Ti atoms on the MXene surfaces might enhance the catalytic activity. Considering this information, the decrease in the

electrochemical performance of MXene sheets can be explained with the ‘trapping’ effect of vacancy clusters.

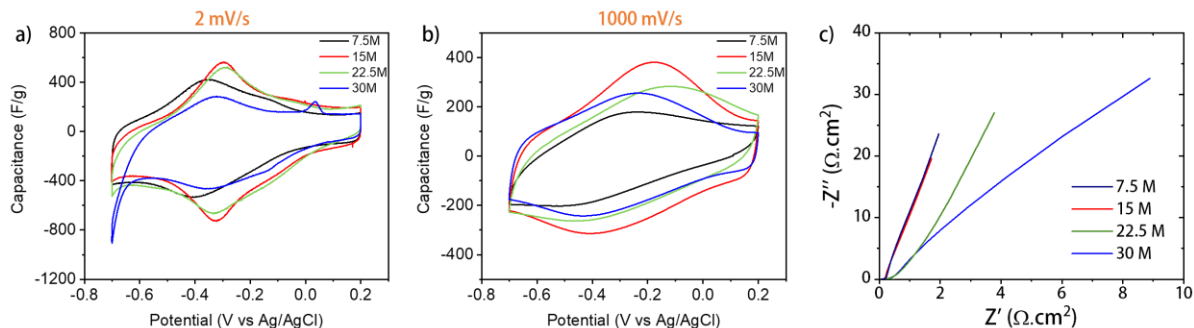


Figure 3-9: Comparison of CV graphs at a) 2 mV/s and b) 1000 mV/s scan rates and c) EIS graph obtained with the different $\text{Ti}_3\text{C}_2\text{T}_x$ electrodes produced with 7.5 M, 15 M, 22.5 M and 30 M LiF concentrations

As protons in aqueous environment are used as charge carriers in this study, it is not surprising that with the increasing amount of vacancy clusters more water molecules and protons are being trapped, resulting in an inferior performance. This is also evident with the EIS graph shown in Fig. 3-9.c. EIS data suggests that as LiF concentration increases, resistivity to ion diffusivity in the system also increases which might be due to the above-mentioned ‘trapping’ effect of vacancy clusters on the MXene surface. Moreover, increased catalytic activity is also evident with the 30M- $\text{Ti}_3\text{C}_2\text{T}_x$ electrodes. As shown in Fig. 3.9.a, CV graphs point out a growing ‘tail’ at the lower potential limit, indicating an increased catalytic activity, further confirming electrochemical activity of the vacancy clusters.

This study shows for the first time that controlling the defect structure have a huge impact on the electrochemical properties of $\text{Ti}_3\text{C}_2\text{T}_x$ electrodes. Findings reported here can be used to produce $\text{Ti}_3\text{C}_2\text{T}_x$ electrodes specifically designed for different applications such as energy storage or catalytic studies.

3.4 Effect of lateral size of the sheets on the electrochemical properties of produced MXene electrodes

In this section, I first shed light on the effects of flake size on the electrochemical performance of the freestanding MXene electrodes. Then, I show that controlling the dimensions of the synthesized 2D $\text{Ti}_3\text{C}_2\text{T}_x$ would allow designing electrodes with high ionic and electric conductivities. The studied electrodes have layered structures and are fabricated by vacuum filtration of the dispersions of MXenes in water (Figure 4-5-b-d). This type of freestanding electrodes (often referred to as paper or membrane electrodes) are widely used to study the electrochemical properties of MXenes, and other 2D material, for supercapacitor applications.(4,17,93)

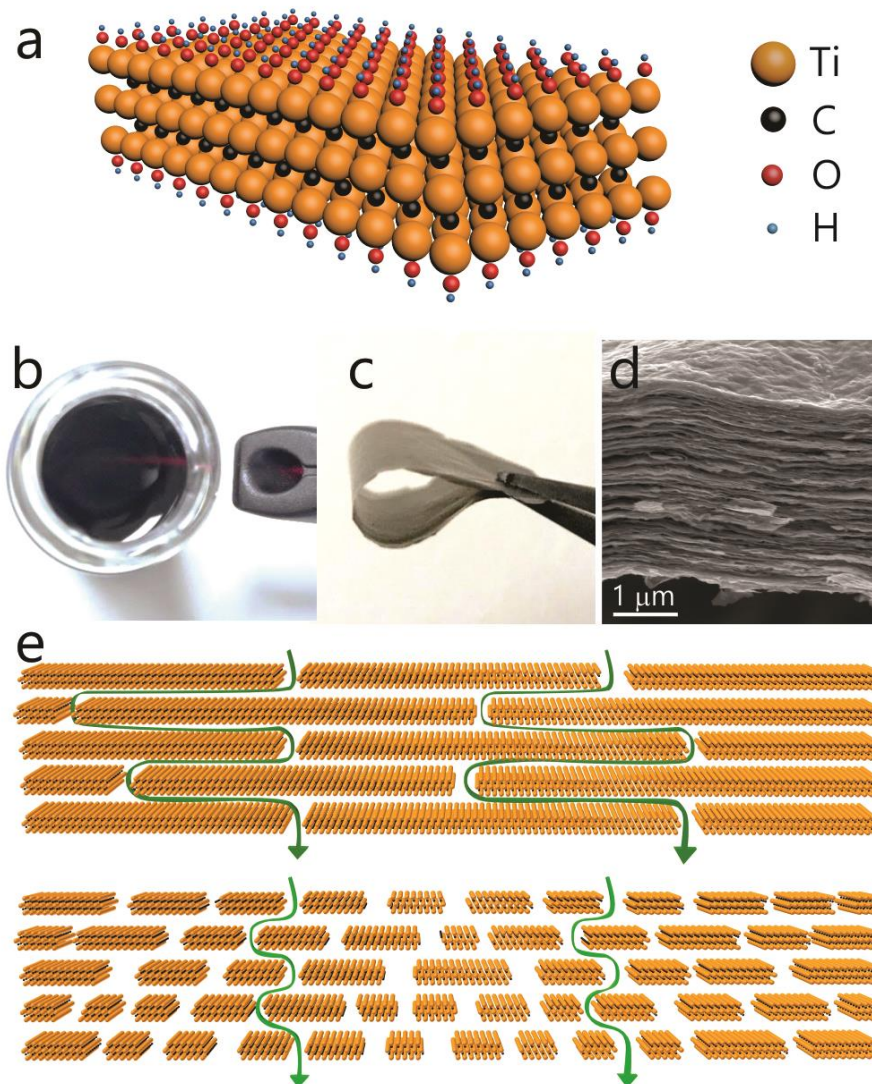


Figure 3-10: a) Schematic drawing of the $Ti_3C_2T_x$ structure. b) $Ti_3C_2T_x$ sheets dispersed in water showing the Tyndall effect. c) MXene “paper” film after vacuum filtration of the $Ti_3C_2T_x$ solution. d) SEM Image of the cross-section of MXene film. e) Schematic drawings showing possible ion diffusion paths for different electrode structures.(94)

As shown previously, there are a few different methods to synthesize $Ti_3C_2T_x$; however, the most frequently used method is based on selective etching of Al atoms from Ti_3AlC_2 in a solution of LiF and HCl and sonication of the produced multilayered materials in water to separate

the individual MXene flakes (schematically shown in Fig. 4-1). However, the MXene flakes produced by this method usually have a wide size distribution and a maximum size of $\sim 1 \mu\text{m}$ (Fig. 4-3). In 2016, Lipatov et al. showed that larger $\text{Ti}_3\text{C}_2\text{T}_x$ flakes could be synthesized by changing the composition of the etchants ($\text{LiF}:\text{HCl}:\text{Ti}_3\text{AlC}_2$ ratio) and eliminating the need for high power sonication to delaminate the 2D flakes.⁽⁴⁴⁾ It was reported that single layer $\text{Ti}_3\text{C}_2\text{T}_x$ flakes as large as about $\sim 15 \mu\text{m}$ could be produced using this method.²⁴ In our studies, we confirmed the synthesis of large flakes using the optimized synthesis method, but we also observed a wide size distribution in the produced flakes and a large number of smaller flakes (below $1\text{--}2 \mu\text{m}$), preventing investigation of the size-dependent properties of the produced MXenes. Both electrical and ionic conductivity of the MXene paper electrodes can be affected by the lateral size of the $\text{Ti}_3\text{C}_2\text{T}_x$ flakes used in their fabrication. As suggested by the schematic drawings of Fig. 4-5e, electrodes fabricated using the large MXene flakes could show higher electrical conductivities compared to those fabricated using the small ones due to less interfacial contact resistance in the electrodes. However, the smaller flakes should, in principle, provide more accessible ion diffusion paths, leading to the higher ionic conductivity of the fabricated electrodes.

To further investigate the effects of lateral dimensions of the flakes on the electrochemical performance of $\text{Ti}_3\text{C}_2\text{T}_x$ electrodes, we first used a modified synthesis method to produce large $\text{Ti}_3\text{C}_2\text{T}_x$ flakes dispersed in DI water. Then, the prepared dispersion was sonicated (using a tip sonicator at a power of 35 W) for various durations to uniformly break the synthesized flakes to smaller sizes (Fig. 4-4 and Fig 4-6a.). Figures 4-6-b–g show representative atomic force microscope (AFM) images of the MXene flakes produced after different sonication times. Evidently, high power sonication is a very effective method to uniformly break the larger flakes into smaller ones. The as-synthesized $\text{Ti}_3\text{C}_2\text{T}_x$ flakes were as large as $\sim 10 \mu\text{m}$ (Figure 4-6b and

Fig. 4-3) and after the highest sonication time (30 min) their size was reduced to tens of nanometers.

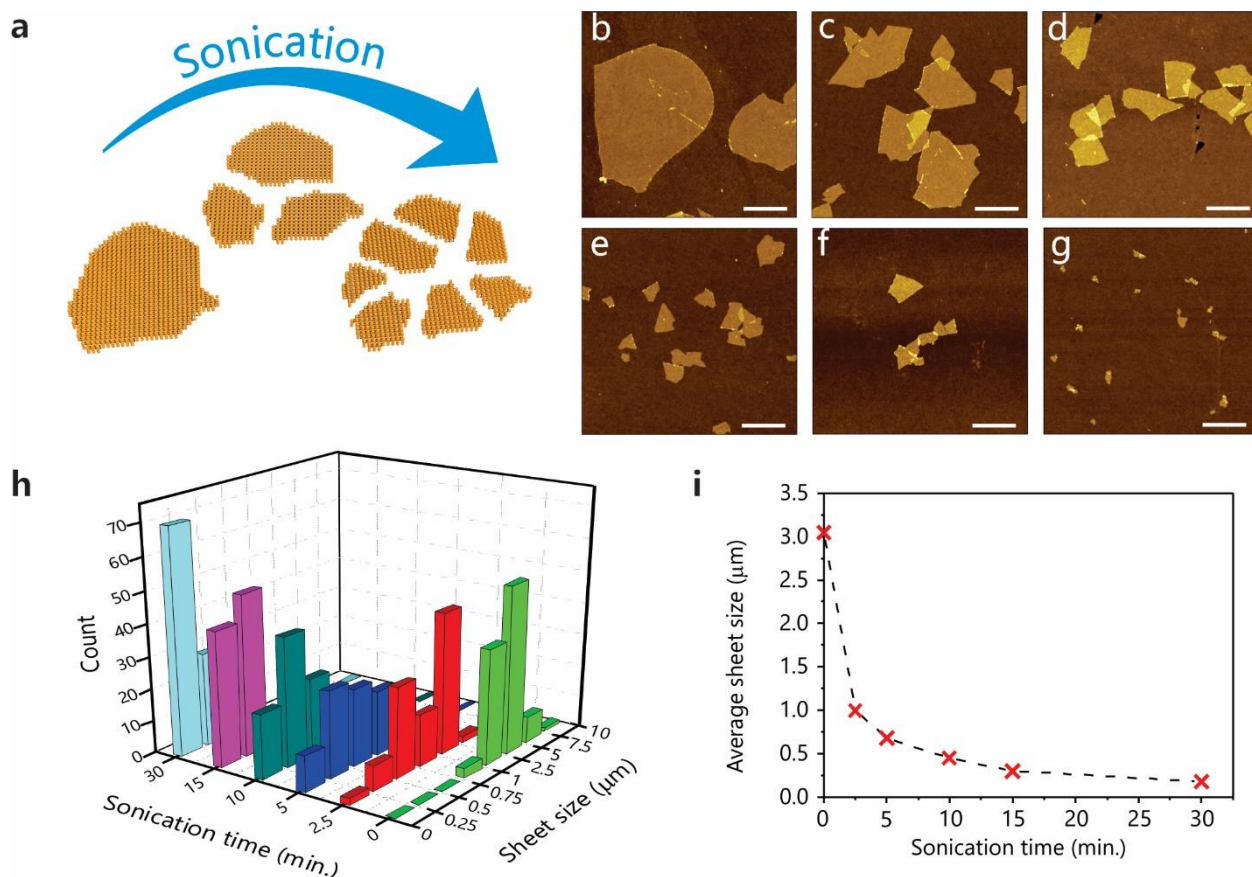


Figure 3-11: a) Schematic illustration of the effect of high power sonication on a single-layer MXene flake. Representative AFM images of $Ti_3C_2T_x$ solutions (b) before sonication, and after sonication for (c) 2.5, (d) 5, (e) 10, (f) 15, and (g) 30 min (scale bars are 1 μm). (h) Size distribution of $Ti_3C_2T_x$ flakes prepared by various sonication durations. (i) Average flake size versus sonication time.(94)

Figure 2h shows the average size and size distribution of the MXene flakes produced using different sonication times. The size of the as-synthesized flakes (without sonication) ranges from 1 to 10 μm with an average size of $\sim 3 \mu m$. The average size gradually decreases with increasing

sonication time to $\sim 0.18 \mu\text{m}$ for the flakes produced by sonication for 30 min. For this sonication time, 70% of the produced MXene flakes are smaller than 250 nm, and the remaining are between 250 and 500 nm. As shown in Figure 4-6i, the average size of the flakes changes almost exponentially with the sonication time, indicating that more energy is required to break smaller flakes.

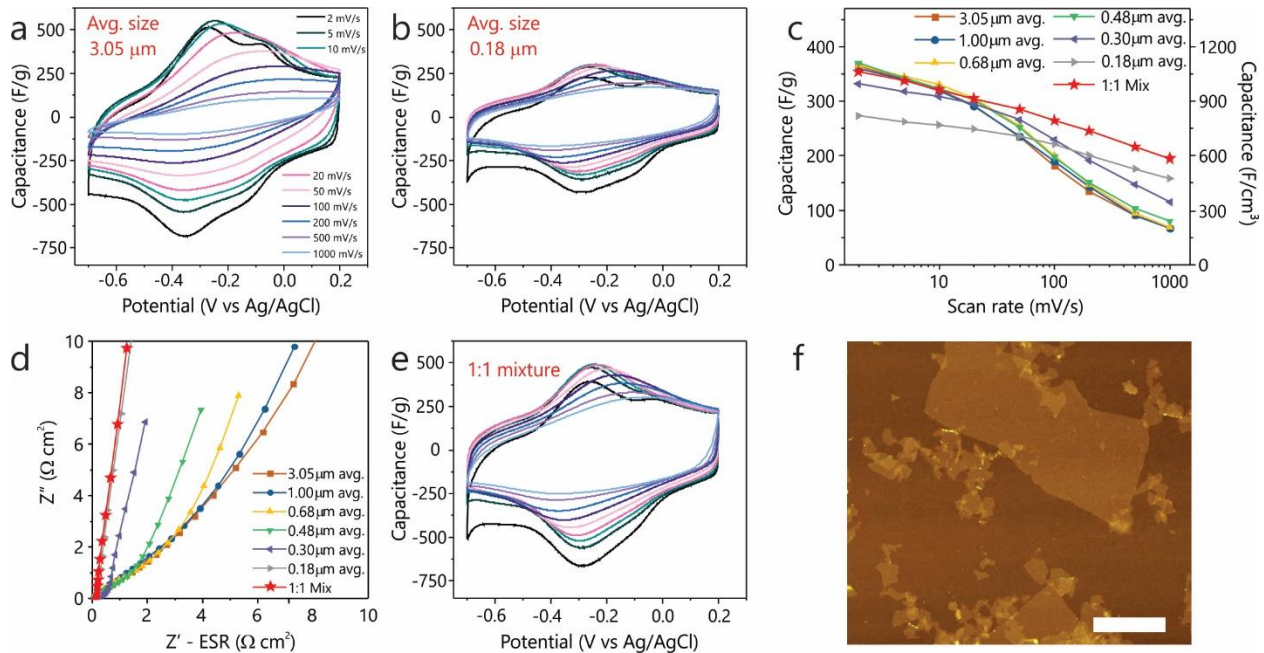


Figure 3-12: Cyclic voltammetry curves of a) electrodes made using large flakes (avg. size of $\sim 3 \mu\text{m}$) and b) small flakes (avg. size of $\sim 0.18 \mu\text{m}$). c) Gravimetric and volumetric capacitance of the electrodes at various scan rates. d) Nyquist plots showing EIS data collected from all electrodes. e) Cyclic voltammeteries of 1:1 mixture electrode. (f) Representative AFM image of the flakes in the 1:1 mixture (scale bar is $1 \mu\text{m}$).⁽⁹⁴⁾

Freestanding paper electrodes were fabricated using MXene flakes with various sizes and were tested as working electrodes in three-electrode cells. Activated carbon and Ag/AgCl electrodes were used as the counter and reference electrodes, respectively. The pseudocapacitive performance of $\text{Ti}_3\text{C}_2\text{T}_x$ is mainly due to the protonation of oxygen functional groups at its surface,

which leads to change in the oxidation state of the surface titanium atoms. As the pseudocapacitive performance of the material is enhanced in H₂SO₄ aqueous electrolytes, following the previous studies, we used a 3 M H₂SO₄ solution as the electrolyte. Figure 4-7-a, b show the cyclic voltammetry (CV) curves of the electrodes fabricated using the largest and smallest MXene flakes, respectively. For both electrodes, at a low scan rate of 2 mVs⁻¹, a pair of anodic and cathodic peaks with small peak separations was observed, and as expected, the peaks became broader by increasing the scan rate. Similar CV curves were also observed for the electrodes fabricated using other flakes sizes (Fig 4-8).

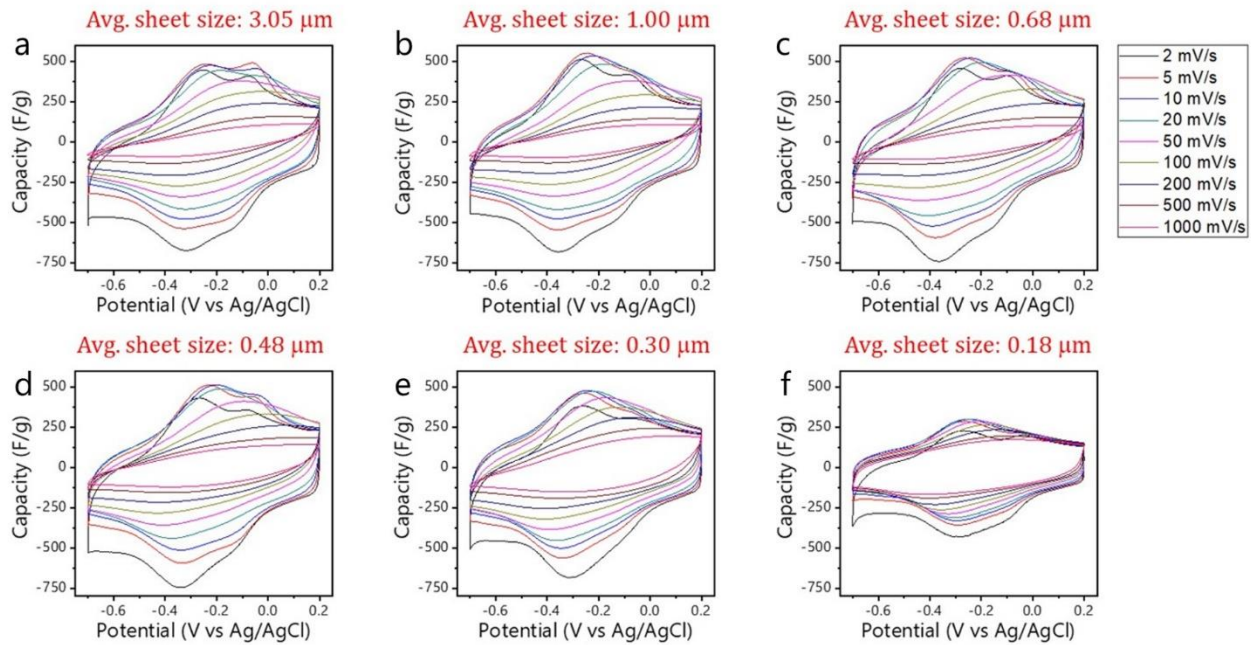


Figure 3-13: Cyclic voltammetry graphs for electrodes fabricated using Ti₃C₂T_x flakes with average sizes of a) 3.05 μm, (b) 1.00 μm, (c) 0.68 μm, (d) 0.48 μm, (e) 0.30 μm, and (f) 0.18 μm.

The effects of flake size on the performance of the MXene electrodes are best understood by looking at Fig. 4-7c which shows the gravimetric and volumetric capacitances of the electrodes

versus CV scan rate. At lower scan rates, electrodes fabricated using flakes with an average size of $\sim 0.48 \mu\text{m}$ or more (sonication time of less than 10 min) show comparable specific capacitances.

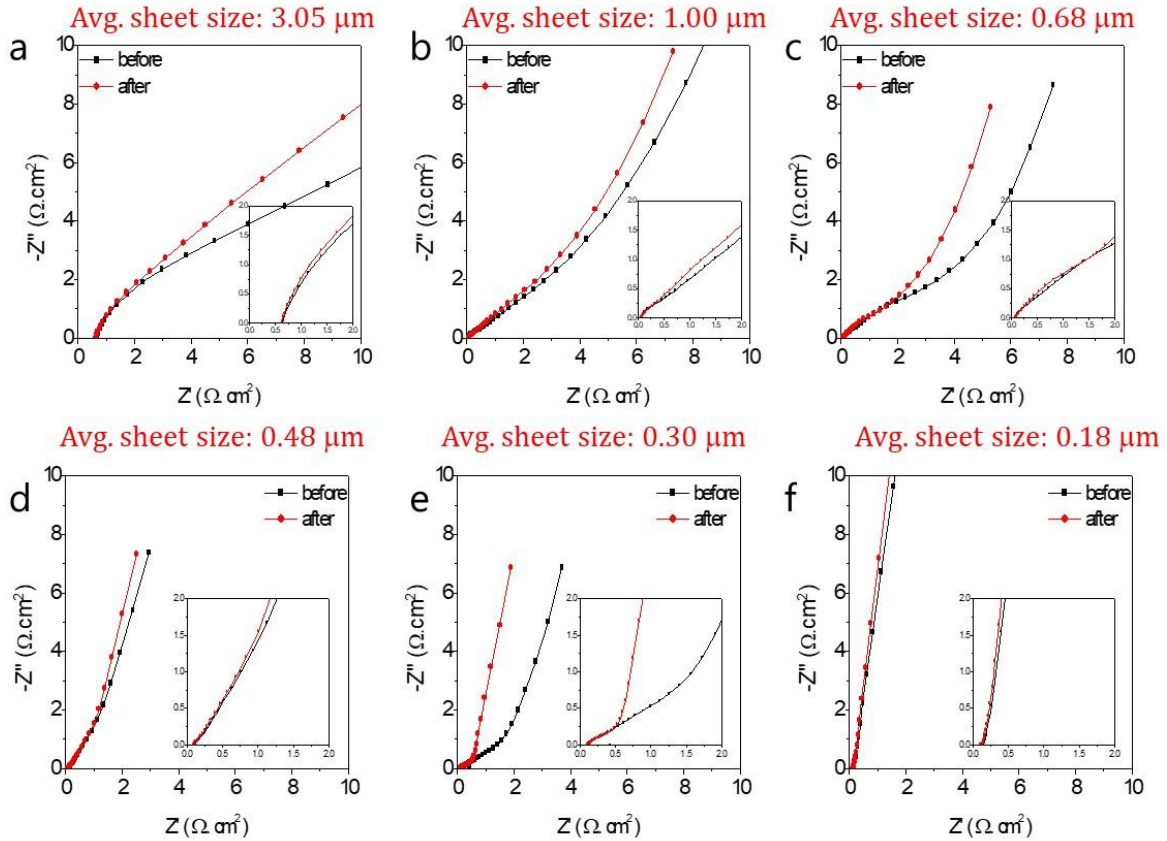


Figure 3-14: Electrochemical impedance spectroscopy graphs for electrodes fabricated using $\text{Ti}_3\text{C}_2\text{Tx}$ flakes with average sizes of (a) $3.05 \mu\text{m}$, (b) $1.00 \mu\text{m}$, (c) $0.68 \mu\text{m}$, (d) $0.48 \mu\text{m}$, (e) $0.30 \mu\text{m}$, and (f) $0.18 \mu\text{m}$.

The highest gravimetric and volumetric capacitance at a 2 mV s^{-1} scan rate was about 370 F g^{-1} and 1100 F cm^{-3} , respectively. However, the capacitance of the electrodes significantly drops as the flake sizes become smaller and the lowest specific capacitance was calculated for an electrode fabricated using MXene flakes with the smallest average size of $\sim 0.18 \mu\text{m}$ (specific capacitance of about 273 F g^{-1} and 819 F cm^{-3}). Two main reasons can be suggested for the

observed drop in the capacitance for the electrodes fabricated using very small flakes. First, as we hypothesized before, the lower capacitance can be related to the lower electronic conductivity of the films fabricated with smaller flakes (Fig. 4-10 shows the dependence of the conductivity of the electrodes on the flake sizes). Also, increasing the edge sites and the introduction of defects in the basal planes of the MXenes during sonication may reduce the active sites for the pseudocapacitive redox reactions and lead to the lower capacitance of the electrodes.(93) As shown in Figure 3c, at higher CV scan rates, the relation between the flake size and the capacitance of electrodes is reversed. At a very high scan rate of 1000 mV s^{-1} , an electrode fabricated using the smallest flakes shows the highest specific capacitances of 158 F g^{-1} and 474 F cm^{-3} . This indicates that at higher scan rates, the performance of the electrodes is largely influenced by the ion accessibility of the electrodes and their ion transport resistance.(14,16,95) This conclusion is supported by the results of electrochemical impedance spectroscopy (EIS) of the electrodes (Figure 4-7d and Figure 4-9) that show less ion transport resistance for electrodes fabricated using the smaller flakes. The main conclusion of the electrochemical studies summarized in Figure 4-8 is that the electrochemical performance of MXene electrodes is highly dependent on the size of the flakes used in the electrode fabrication. Therefore, for comparing the performance of various $\text{Ti}_3\text{C}_2\text{T}_x$ electrodes reported in the literature, the size of the flakes should always be considered.

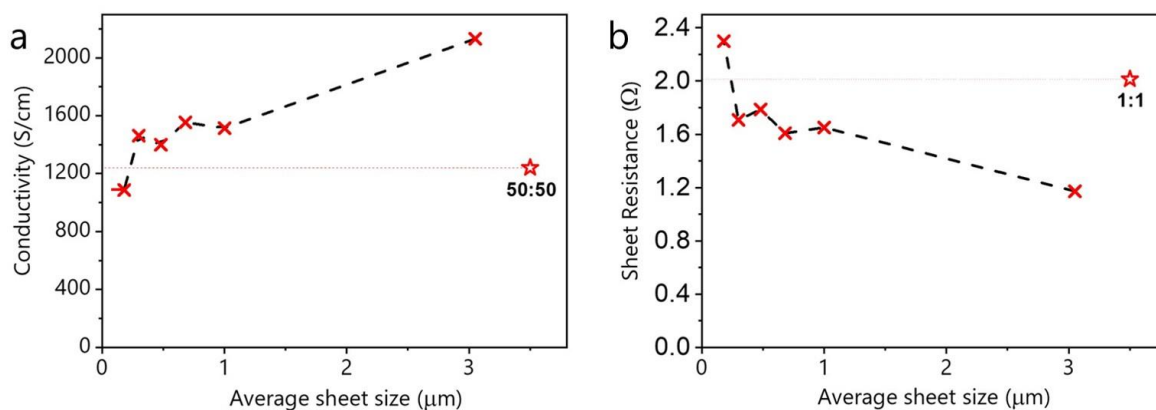


Figure 3-15: a) Sheet resistance and b) conductivity values of electrodes measured with four-probe measurement system.

After establishing the effect of flake size on their electrochemical performance, we examined how mixing the flakes of various sizes might affect the performance of the electrodes. MXene dispersion was prepared by mixing the smallest and the largest synthesized flakes in a 1:1 weight ratio and used to fabricate paper electrodes. Figure 3f is an AFM image of the $\text{Ti}_3\text{C}_2\text{T}_x$ flakes in the prepared mixed dispersion, showing both small and large flakes. The CV curves of the mixed electrode (Figure 4-6e) show the typical pseudocapacitive behavior seen for all tested electrodes, but the areas under the curves at higher scan rates were larger compared to those of the electrodes fabricated using only large or small flakes. The specific capacitance of the mixed electrodes (labeled as 1:1 electrode) is compared to other fabricated electrodes in Fig 4-7c. Interestingly, at low scan rates the specific capacitance of the mixed electrode is similar to electrodes fabricated using large flakes; however, as the scan rate increases, the 1:1 mixed electrode still shows high specific gravimetric and volumetric capacitances. At a high scan rate of 1000 mV s^{-1} , this electrode shows the highest capacitance among all tested electrodes (gravimetric

capacitance of 195 F g^{-1}), demonstrating the high electronic and ionic conductivity of the mixed electrodes. This was confirmed by EIS measurements (Nyquist plot of Figure 4-7d).

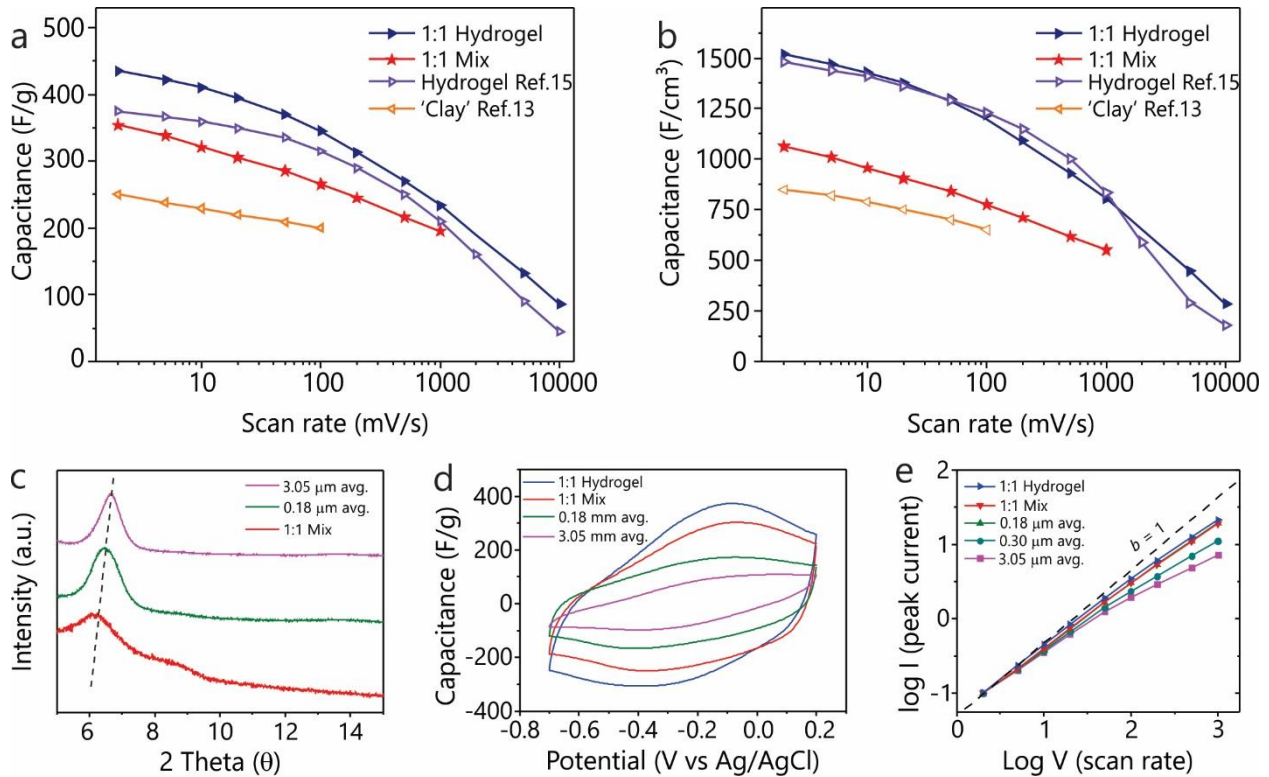


Figure 3-16: a) Gravimetric and b) volumetric capacitances of various $\text{Ti}_3\text{C}_2\text{T}_x$ electrodes versus CV scan rates. c) X-ray diffraction patterns of different $\text{Ti}_3\text{C}_2\text{T}_x$ electrodes. d) CV graphs of different $\text{Ti}_3\text{C}_2\text{T}_x$ electrodes at 1000 mV s^{-1} scan rate. e) Log (cathodic current peak) versus log (scan rate) used for calculation of b-values (94)

The almost vertical rise of the imaginary component of impedance indicates the highly capacitive performance of the mixed electrode and its low ionic transport resistance. Therefore, the mixed electrode benefits from a high electronic conductivity introduced by the large flakes and a high ionic conductivity due to small flakes. The latter is caused by the improved interlayer transport due to the smaller size of the flakes and the increased interlayer spacing of MXene flakes in the electrodes with small or mixed flakes sizes. Figure 4-11c compares the X-ray diffraction (XRD)

patterns of the electrodes fabricated using large, small, and mixed flake sizes. All XRD patterns show the characteristic (0002) peak of the MXene at low angles. However, compared to the electrodes with large flakes, for the electrode with small flakes, the peak has shifted by about 0.2° to smaller angles, indicating its slightly larger interlayer spacing. For the mixed electrode, however, the (0002) peak shifts to even lower angles and becomes broader, showing that this electrode has a larger interlayer spacing and a less ordered structure.(81,92)

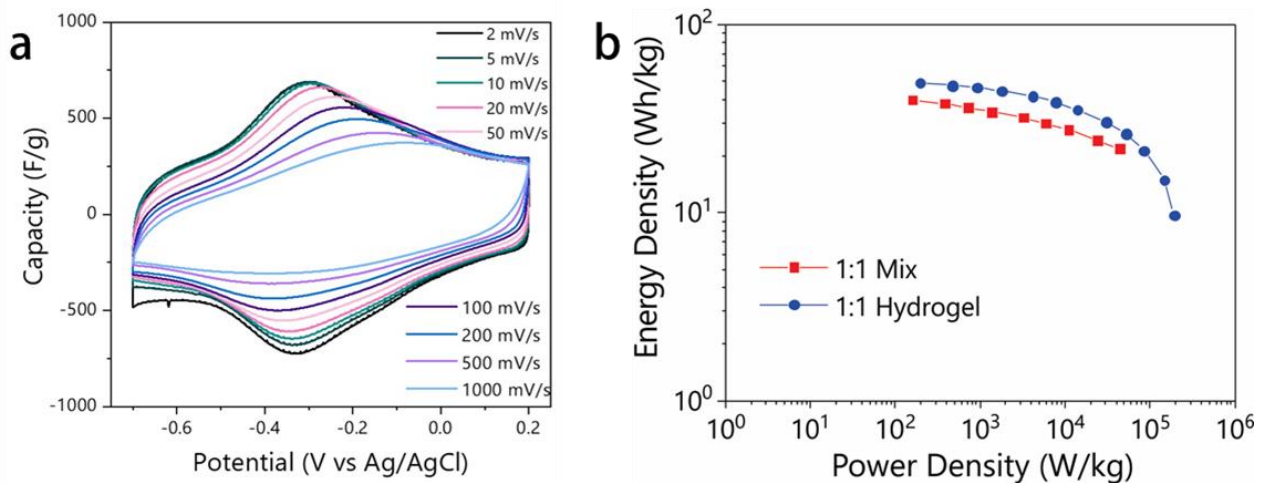


Figure 3-17: a) Cyclic voltammetry curves of the 1:1 Hydrogel electrodes b) Ragone plot for the 1:1 mixed and 1:1 hydrogel (The energy and power density are calculated for the electrodes from the results of the three-electrode tests and do not represent the energy and power density of a full cell)(94)

A very interesting strategy to improve the performance of MXene electrodes was recently reported that relies on assembling the $Ti_3C_2T_x$ flakes in hydrogel electrode structures.(14) This was achieved by exchanging the water trapped between the MXene layers (after their vacuum filtration and before drying) with an electrolyte. It was shown that the hydrogel electrodes have a drastically higher performance at very high scan rates compared to the conventional paper electrodes.(14) We used the same method to fabricate hydrogel electrodes using the 1:1 mixed

dispersions and studied their electrochemical properties. Figure 4-11a, b compare the performance of a 1:1 mixed hydrogel electrode with other $Ti_3C_2T_x$ electrodes fabricated in this study and the best performing electrodes reported in the literature. The 1:1 mixed hydrogel electrode shows the best performing electrodes reported in the literature. The 1:1 mixed hydrogel electrode shows the highest gravimetric and volumetric capacitances at all scan rates. At a low scan rate of 2 mV s^{-1} , a gravimetric capacitance of 435 F g^{-1} (volumetric capacitance of 1513 F cm^{-3}) was calculated for this electrode, and it also showed the highest specific capacitance at a very high scan rate of 10 V s^{-1} (86 F g^{-1} and 299 F cm^{-3}). Accordingly, the 1:1 mixed hydrogel electrode showed a very high-power density of 387 kW kg^{-1} at the energy density of 9.7 Wh kg^{-1} (as can be seen in the Ragone plot of Figure 4-12b). As shown in Figure 4-13, a hydrogel electrode fabricated using the 1:1 mixture retained 98% of its initial capacitance after 10 000 charge/discharge cycles. Figure 4d compares the CV curves of all fabricated electrodes at a high scan rate of 1 V s^{-1} , which clearly shows the highly capacitive performance of 1:1 mixed hydrogel electrode even at this high scan rate.

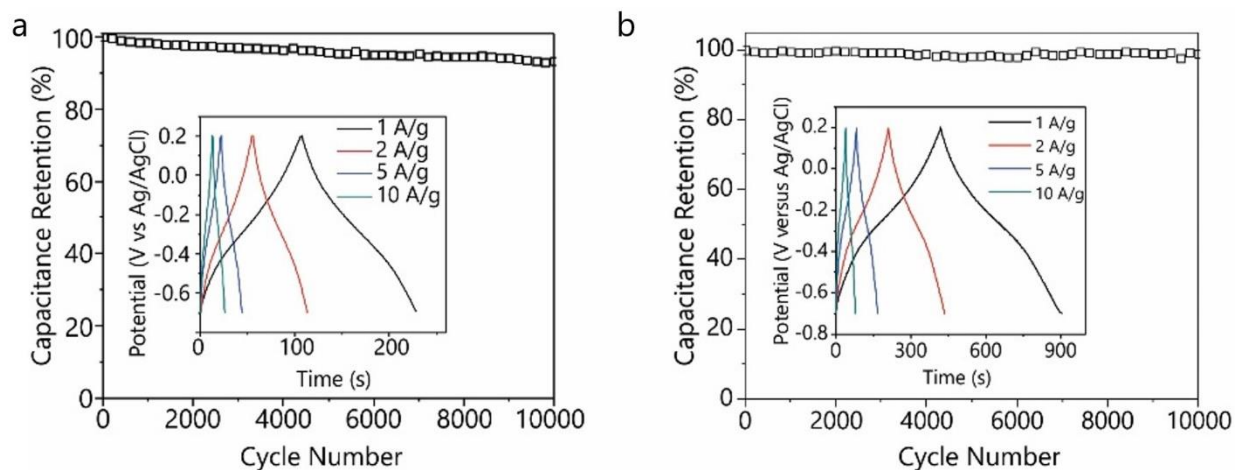


Figure 3-18: Cyclic performance and Charge–Discharge curves of (a) 1:1 mixture electrode and (b) 1:1 Hydrogel electrode(94)

The kinetics of the charge storage in various electrodes was studied by the analysis of the dependence of their peak CV currents on the scan rate following a previously reported method.^{29,30} In this method, a power law dependence of the peak current (i_p) on the scan rate (v) rate is assumed, where $i_p = av^b$ and a and b are adjustable values. The slope of the plot of $\log i_p$ versus $\log v$ (Figure 4e) equals b and provides important information about the kinetics of the charge storage. A b -value of 0.5 is the characteristic of a diffusion-limited process, and a b -value of 1 shows a capacitive storage mechanism.⁽⁹⁶⁾ As shown in Figure 4e, for the electrodes fabricated using the largest flakes (average size of $\sim 3 \mu\text{m}$) the slope of the curve (b -value) sharply decreases with increasing the scan rates, but the b -values of the electrodes fabricated using small flakes or 1:1 mixed flakes are close to 1 even at very high scan rates. The 1:1 hydrogel electrode shows the highest b -value at all scan rates, confirming its very high rate capability. As explained in the Supporting Information, this conclusion was confirmed by separating the contribution of the surface controlled capacitive processes and diffusion-limited process to the charge storage as shown in Figures 4-13 and 4-14.

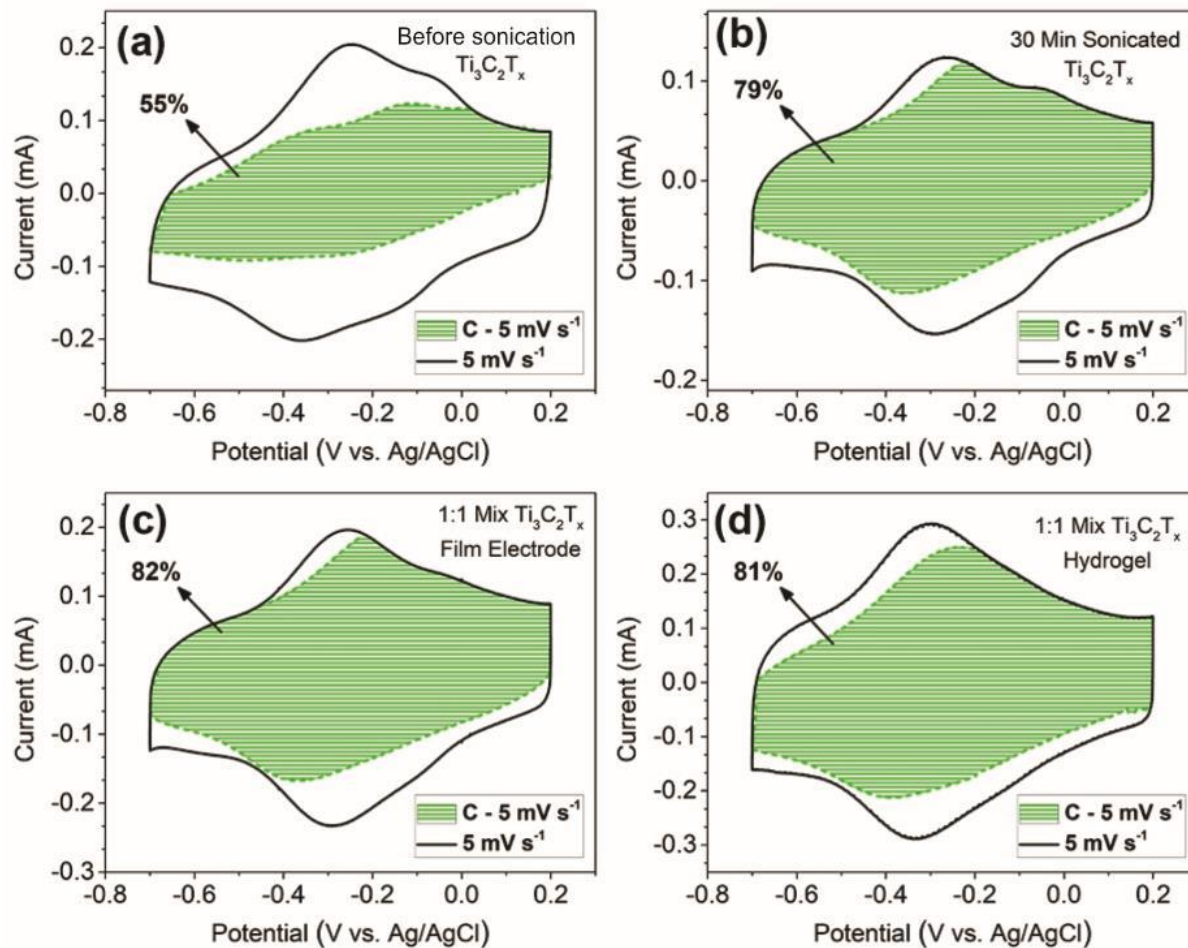


Figure 3-19: Capacitive (surface-controlled) charge storage contribution to the total CV current measured at 5 mVs⁻¹ for electrodes fabricated using (a) as-prepared large $Ti_3C_2T_x$ flakes before sonication, (b) flakes produced after 30 min of sonication, (c) 1:1 mix of large and small flakes, and (d) hydrogels fabricated using 1:1 mix of small and large flakes.(94)

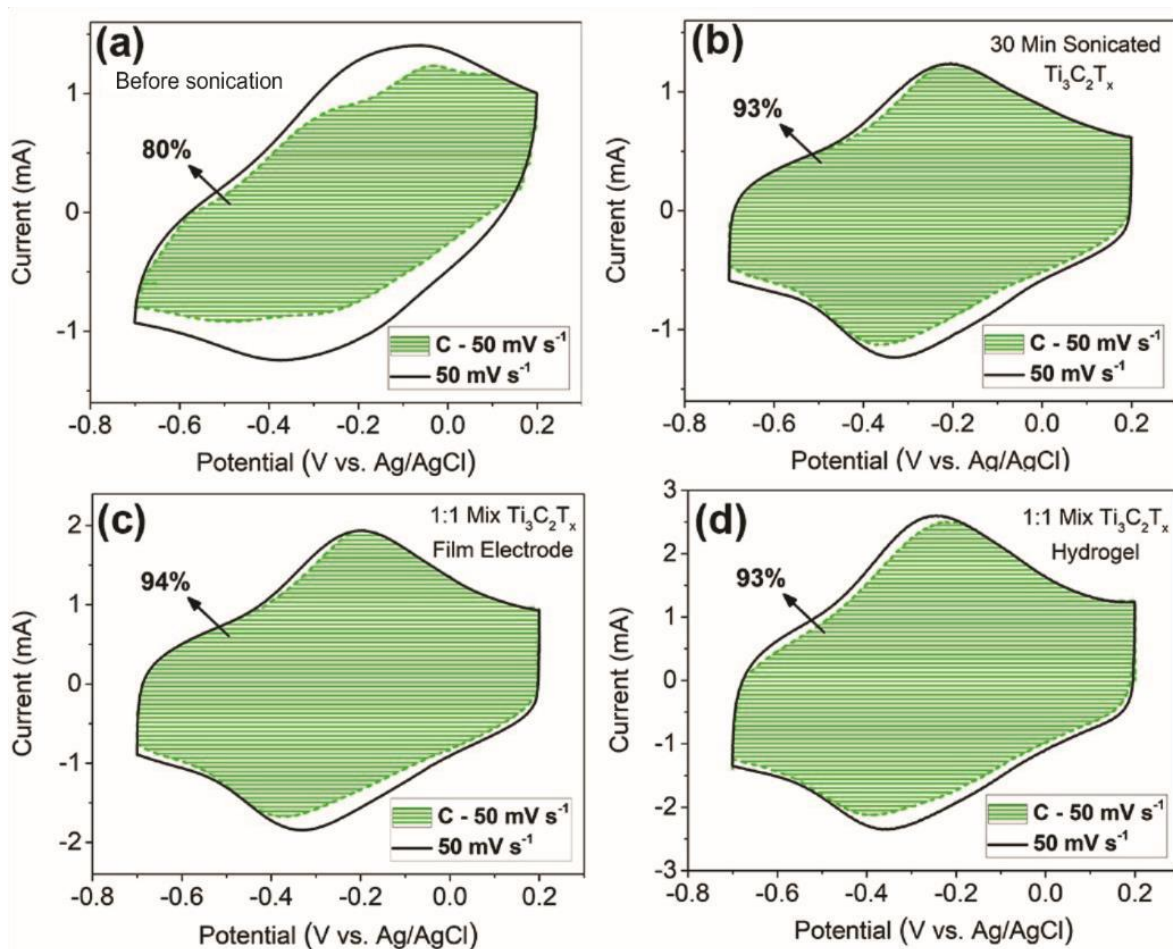


Figure 3-20: Capacitive (surface-controlled) charge storage contribution to the total CV current measured at 50 mVs⁻¹ for electrodes fabricated using (a) as-prepared large Ti₃C₂T_x flakes before sonication, (b) flakes produced after 30 min of sonication, (c) 1:1 mix of large and small flakes, and (d) hydrogels fabricated using 1:1 mix of small and large flakes.(94)

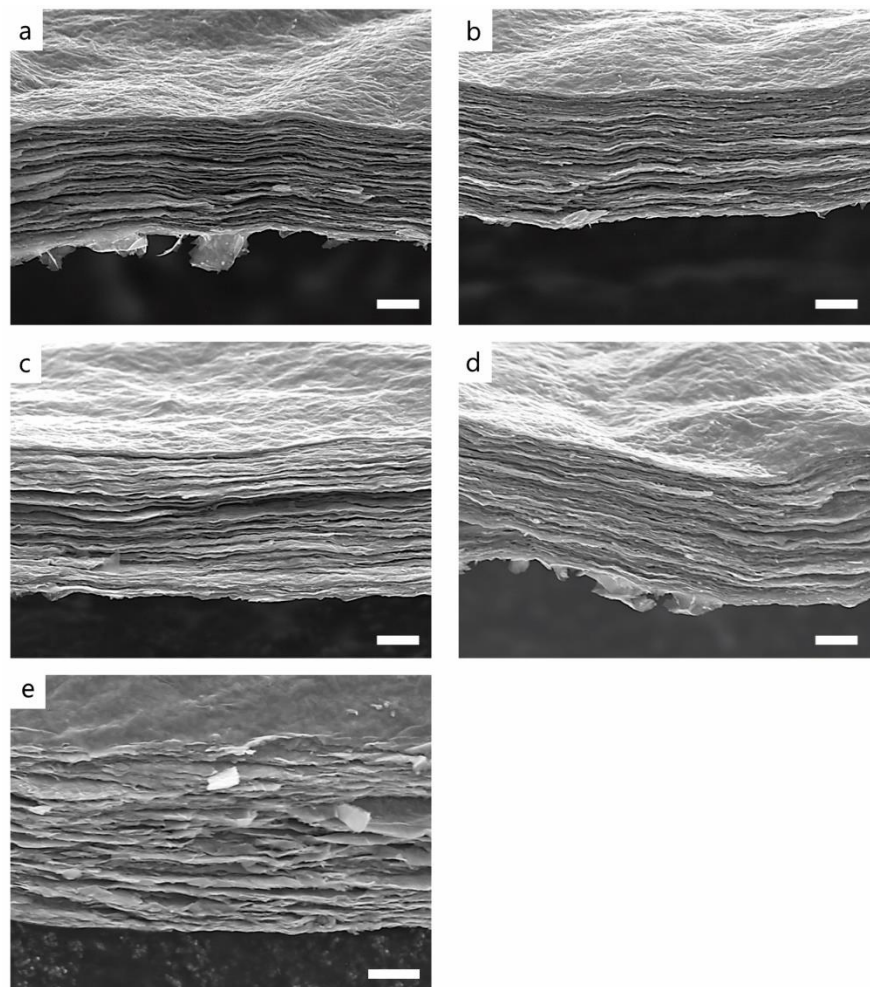


Figure 3-21: SEM images of different $Ti_3C_2T_x$ films showing electrodes thicknesses for the electrode fabricated with flakes of (a) $3.05 \mu m$ avg. size, (b) $1.00 \mu m$ avg. size, (c) $0.18 \mu m$ avg. size, (d) 1:1 mixture, (e) 1:1 hydrogel. (scale bar is $1 \mu m$) (94)

3.5 Conclusion

In summary, with this study we demonstrated for the first time that the size of the 2D flakes significantly affects the electrochemical performance of $Ti_3C_2T_x$ electrodes and by controlling the flake size, the performance of the electrodes can be improved. There is no reason to believe that an electrode fabricated by a 1:1 mixture of the large and small flakes has an optimum electrochemical performance, nor was it our intention to find the best flake size combination in

this study. However, the results presented in this dissertation demonstrate that high-performance MXene electrodes can be designed by a rational combination of various flake sizes. To avoid inconsistency in the reported electrochemical performance of MXenes, we suggest that all future reports on the electrochemical properties of these materials should include information about the size and size distribution of the flakes used in the fabrication of the electrodes.

Chapter 4: Effect of synthesis conditions on the mechanical properties of MXenes

This chapter will present the used methods to produce MXene sheets with different structure and discuss the obtained results regarding the mechanical properties of MXenes.

4.1 Introduction

Mechanical measurements of two-dimensional materials are proven to be a challenging task.⁽⁹⁷⁾ Since the thickness of 2D materials are in nanometer scale, direct indentation on these materials results in measuring the properties of the substrate underneath. For true measurement of two-dimensional materials several methods are proposed, such as suspending two dimensional materials over circular holes.⁽⁹⁷⁾ In 2008, Lee et al measured Young's modulus of mechanically exfoliated graphene sheets suspended over circular holes. Figure 4-17 shows their experimental set up as in the article.⁽⁸⁷⁾ Fig. 4-17-a features an SEM image showing single layer graphene flake covering holes etched into a Si/SiO₂ wafer, using e-beam lithography. Fig. 4-17-b and d shows AFM images before and after puncturing the graphene membrane over a hole whereas Fig. 4-17-c gives a schematic of the experimental set up. With this study, Young's modulus of graphene is found to be 1Tpa, making it strongest material ever measured.⁽⁸⁷⁾ The elastic moduli of different 2D materials such as different transitional metal dichalcogenides (MoS₂, WS₂, etc.) or hexagonal boron nitride (h-BN) are measured using the same method and found to be lower than the graphene.^(98–100) This method requires production of membranes which are 2D materials suspended over circular holes. Atomic Force Microscope is utilized as a unique tool capable of both locating the membranes and performing nanoindentation on the center of the membranes. It

is shown that graphene sheets can sustain up to 25% strains without breaking. This nanoindentation mechanism is further modeled into a mathematical equation where Young's modulus of the suspended 2D material can be calculated using the force applied by the AFM cantilever and the displacement of the tip during the indentation.(87,88) This equation is given as;

$$F = \sigma_o^{2D} \pi \delta + E^{2D} \frac{q^3 \delta^3}{r^2} \quad (1)$$

Where F is the applied force and δ is the displacement of the tip. Other variables include σ_o^{2D} as the pretension on the membrane, E^{2D} is the 2D Young's modulus of the material, r is the radius of the hole and q is a dimensionless constant where it can be written as;

$$q = 1/(1.05 - 0.15v - 0.16v^2) \quad (2)$$

v is the Poisson ratio for the material. It is shown that Eq.1 holds as long as tip radius is much smaller than hole radius, and the membranes do not slip during the indentation. Since Lee et al's paper this method is proven to be effective in measuring the mechanical properties of 2D materials.

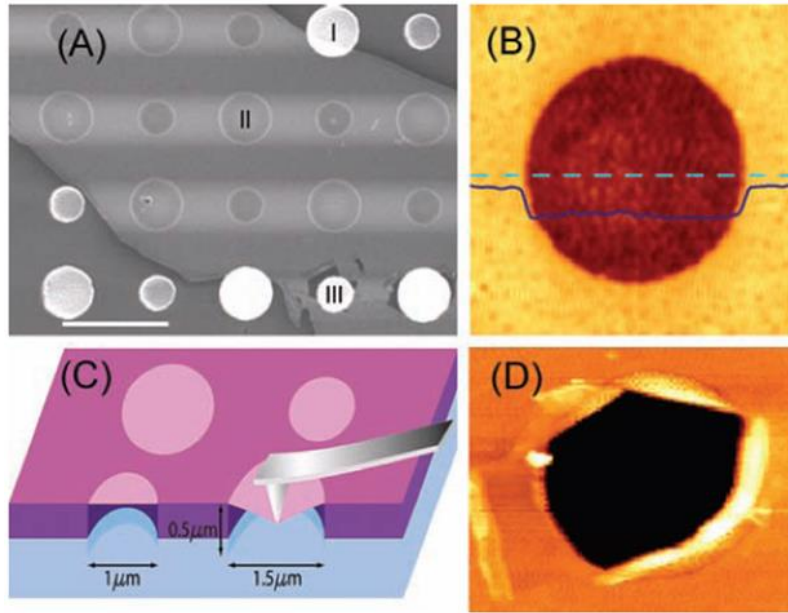


Figure 4-1: Experimental setup used in the measurement of mechanical properties of mechanically exfoliated graphene (87)

As proposed in the section 3.2 with the task 3, this section will address the preliminary results on mechanical measurements of $Ti_3C_2T_x$ MXene sheets. To achieve this goal, I have started the experiments with the synthesis and isolation of large-area $Ti_3C_2T_x$ MXene sheets similar as to explained in section 4.1.

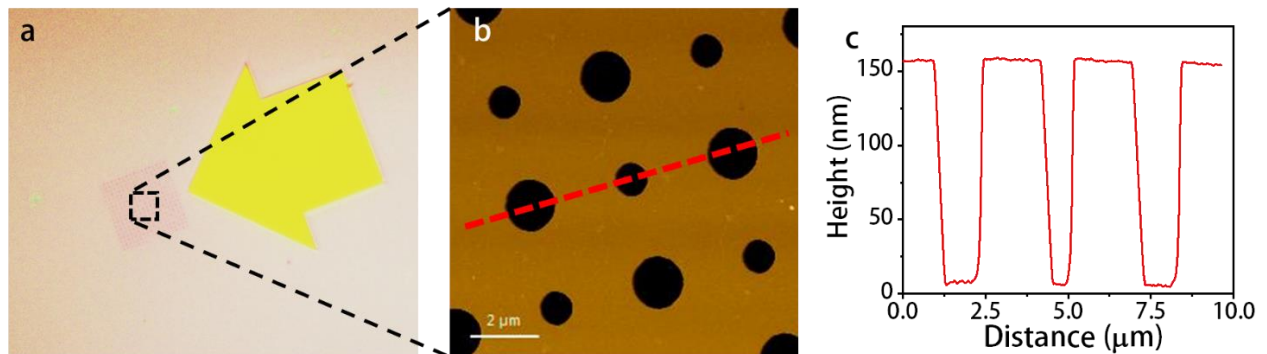


Figure 4-2: a) Optical microscope image of produced Si/SiO₂ wafers with holes b) AFM image and c) depth profiles of the produced holes

To produce holes on a substrate, Si wafers with 300 nm thermal oxide coating are chosen. Desired pattern of the holes is first designed in Advanced Design System (ADS, PathWave Design) software. Wafers are then coated with a polymer layer (Polymethyl methacrylate, PMMA) and loaded into e-beam lithography (EBL) system. EBL system is used to remove the PMMA layer as designed in the software. After holes are exposed on the wafer surface, an etching solution is prepared. Buffered Oxide Etchant (HF:NH₄F 1:7) solution is used to remove oxide layer from the wafer at about 10 nm per second rate. Etching was completed after 15 seconds and to remove PMMA layer wafer pieces were sonicated in acetone for 3 hours. After removal of PMMA layer wafer pieces have about 50x50 μm area covered with holes as shown in Fig. 4-18-a. Confirmation of the hole radius and depth was carried out via AFM and hole radius were found to be 1 μm and 1.5 μm whereas the depth is about 150 nm (Fig.4-18-b-c).

4.2 Assembly of MXene membranes

Next step in this study was to assembly of Ti₃C₂ membranes. Although the most common method to suspend 2D materials over holes in literature is direct mechanical exfoliation of the materials over the holes, mechanical exfoliation of MAX phases shown to be not possible. Several methods are carried out for the assembly of Ti₃C₂ membranes. Early attempts are made with drop casting and spin casting of the MXene solution directly over the holes. However, results show that assembly methods including liquid processing will not result in suspension of the sheets due to capillary forces. It was observed that during the drying process, MXene sheets get sucked into the holes resulting in breakage of the sheets as can be seen in Fig 4-19-a and b.

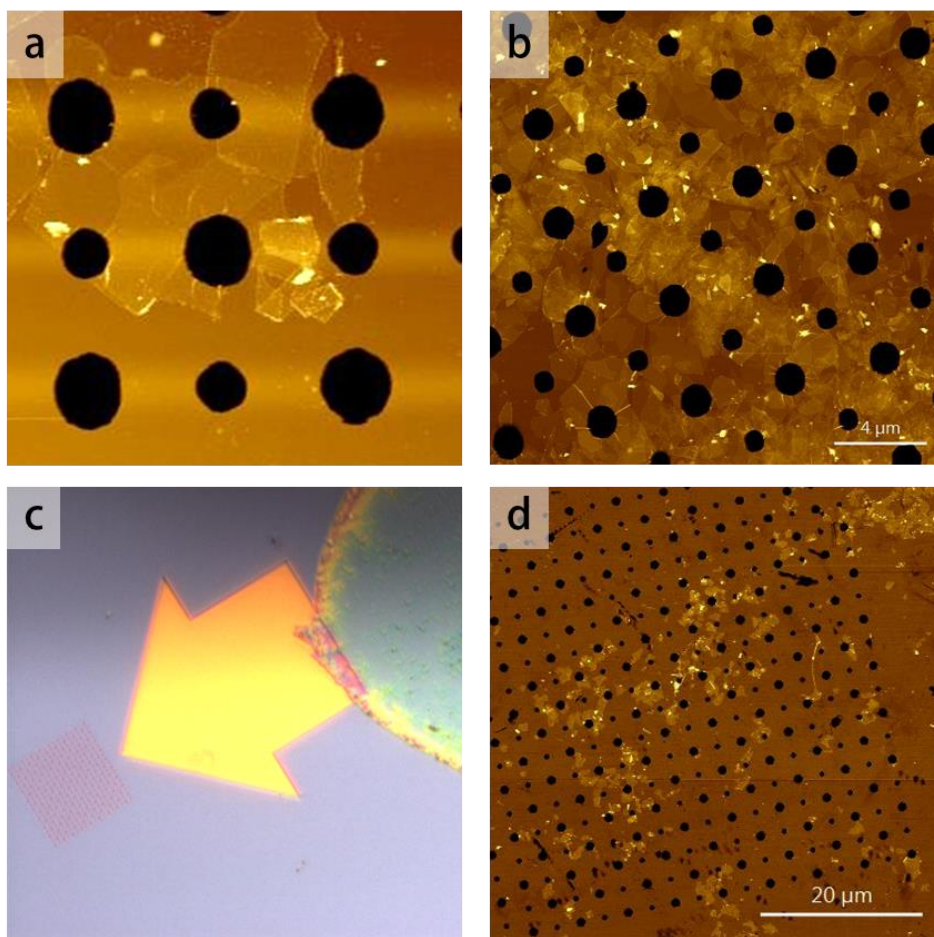


Figure 4-3: Ti₃C₂T_x sheets a) drop casted and b) spin casted over circular holes. c) Optical microscope and d) AFM images of drop casted and transferred Ti₃C₂T_x sheets

Based on these results dry assembly methods are carried out. First attempt was to use PDMS polymers as substrates from drop casting of MXene solutions. Drop casted sheets are dried on PDMS surface and then transferred over holes with bringing the polymer in contact with the wafer surface. Although the transfer of sheets is achieved, due to only a small area coverage of holes match of sheets and holes are not accomplished. Fig.4-19-c and d shows the mismatch of the transferred sheets and the patterned holes.

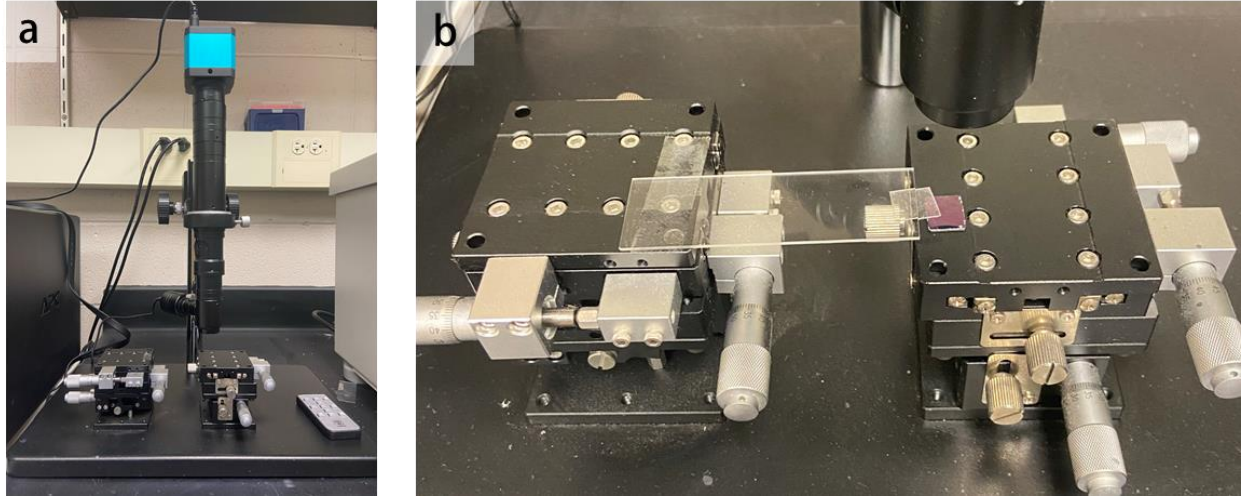


Figure 4-4: Photographs of optical microscope and micro-manipulators used in the transfer of specific $\text{Ti}_3\text{C}_2\text{T}_x$ sheets

In order to increase lateral precision of the transferring sheets experimental setup shown in Figure 4-20 is prepared. This setup includes an optical microscope and two micro-manipulators. MXene sheets on Si wafers were first located under optical microscope and characterized with AFM. After characterization, selected sheets are lifted off from the surface using PDMS under optical microscope. Same sheets are located on the PDMS and brought in contact with Si wafers with holes using optical microscope and micro-manipulators. AFM Characterization of the transferred $\text{Ti}_3\text{C}_2\text{T}_x$ sheets before and after the transfer can be seen in Fig. 4-21. Although precision in micron scale is achieved, it was shown that PDMS transfer of 2D materials are prone to breaking and wrinkling which makes nanoindentation impossible.

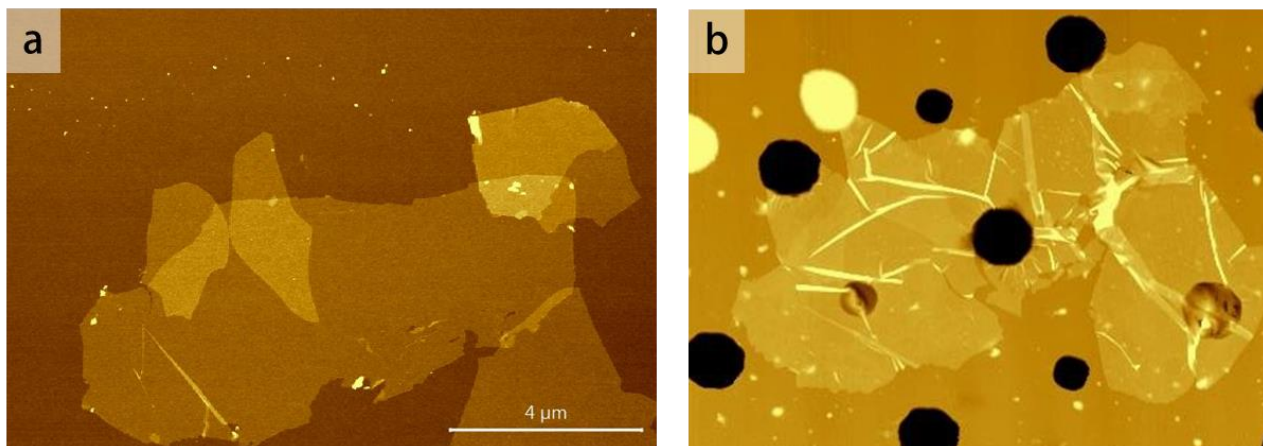


Figure 4-5: AFM images of $\text{Ti}_3\text{C}_2\text{T}_x$ sheets on Si/SiO₂ wafers; a) before and b) after transferring over to patterned wafers.

Based on these results I came up with a unique approach where MXene sheets can be self-assembled into large area single-layer films. Experimental setup is shown in Fig 4-22. In this method, 50 ml of a aqueous dilute MXene solution (0.1 mg/ml) is mixed with 2 ml of toluene. The mixture is stirred vigorously for 15 minutes and then poured onto 300 ml of DI water in a larger container. As expected, toluene does not mix with water and floats on the surface. Moreover, single-layer MXene film starts to form in the interface between toluene and water. When the mixture is left for about 30 minutes, all toluene evaporates and self-assembled MXene film floats on the surface of water. This floating MXene film can reach a few centimeters in lateral dimension. Also, films can be picked up by any substrate either with lifting from underneath the surface or any substrate that comes into contact with the water surface. In Fig.4-23-a optical microscope image of a Si wafer coated with single layer Ti_3C_2 film is shown. AFM characterization of the given film is also shown on 4-23-b. Furthermore, these films can be picked up with PDMS and transferred to different surfaces, such as our patterned wafers. Fig.4-23-c shows the $\text{Ti}_3\text{C}_2\text{T}_x$ sheets

suspended over holes prepared via this method. This method is proven to be an effective way of preparing MXene membranes over circular holes.

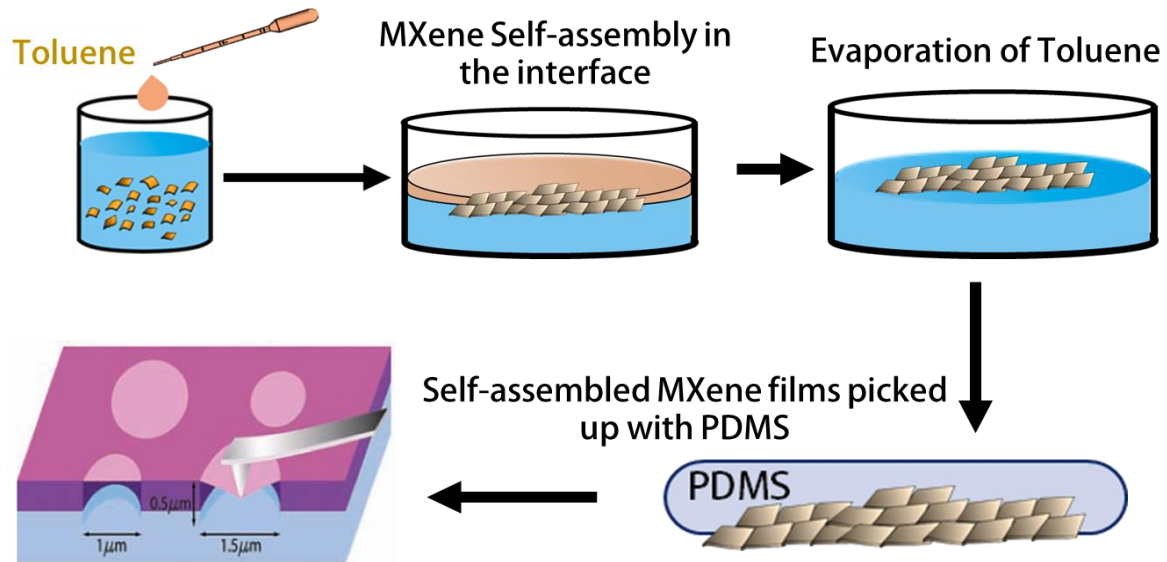


Figure 4-6: Schematic of proposed experimental setup for obtaining and transferring self-assembled $\text{Ti}_3\text{C}_2\text{T}_x$ MXene films

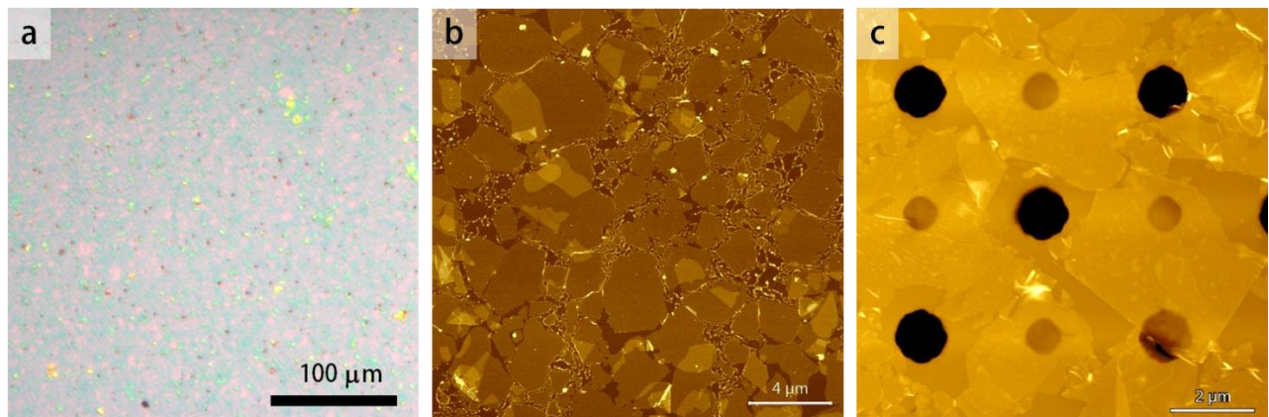


Figure 4-7: a) Optical microscope image of self-assembled $\text{Ti}_3\text{C}_2\text{T}_x$ films. AFM images of self-assembled $\text{Ti}_3\text{C}_2\text{T}_x$ films on Si/SiO₂ wafers b) directly picked up by non-patterned wafers, c) picked up with PDMS and transferred onto patterned wafers.

Since the method is proven to be effective preparing MXene membranes, prepared membranes are then used in nanoindentation measurements using AFM.

4.3 Effect of LiF:MAX molar ratio on the mechanical properties of single layer $\text{Ti}_3\text{C}_2\text{T}_x$ MXene sheets

To investigate the effect of the LiF concentration, and thus in situ HF concentration, on the mechanical properties of $\text{Ti}_3\text{C}_2\text{T}_x$ sheets, 3 different samples are produced with varying LiF:MAX phase molar ratios. This ratio is initially used as 7.5 M when Lipatov et al. reported the mechanical properties of $\text{Ti}_3\text{C}_2\text{T}_x$ sheets. Figure 4.10.a shows the experimental set up to study the mechanical properties of MXene sheets. As explained in the previous section, we initially assembled $\text{Ti}_3\text{C}_2\text{T}_x$ membranes with sheets produced with 7.5 M LiF. In Fig 4.10b-c, AFM analysis shows the assembled membranes. Thickness of the flakes is measured to be 3 nm, which is in agreement with previous studies, confirming the single layer nature of the MXene sheets. 25-30 nm depth of the membranes also show the interaction between the 2D material and walls of the holes.

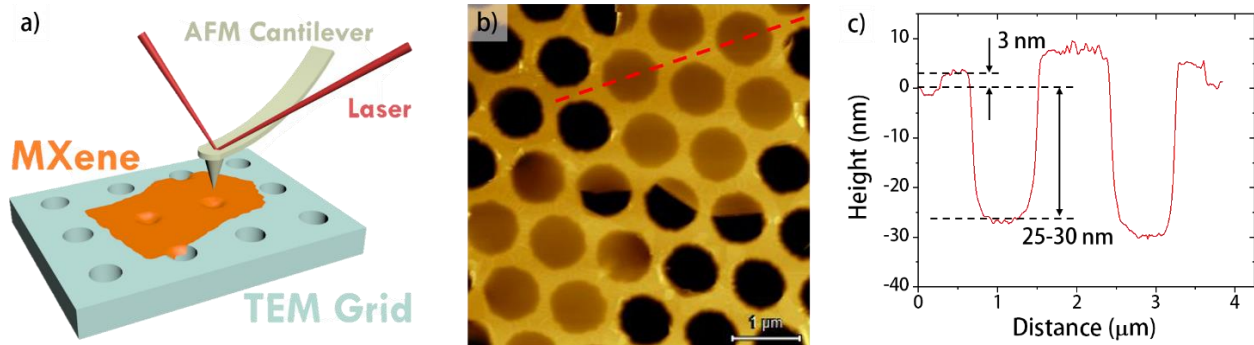


Figure 4-8: a) Schematic showing MXene sheet suspended over holes, b) AFM image showing two suspended $\text{Ti}_3\text{C}_2\text{T}_x$ sheets, c) Height profile of the red line marked in b, showing the thickness of the sheets and the depth of suspended sheets.

Prepared membranes are then used in nanoindentation experiments. Fig 4.11.a shows the Force-Distance (F/d) graphs obtained with nanoindentation experiments using an AFM. Each membrane is indented at least 3 times before fracturing and each indentation F/d data is used to calculate an in-plane Young's modulus (E^{2D}).

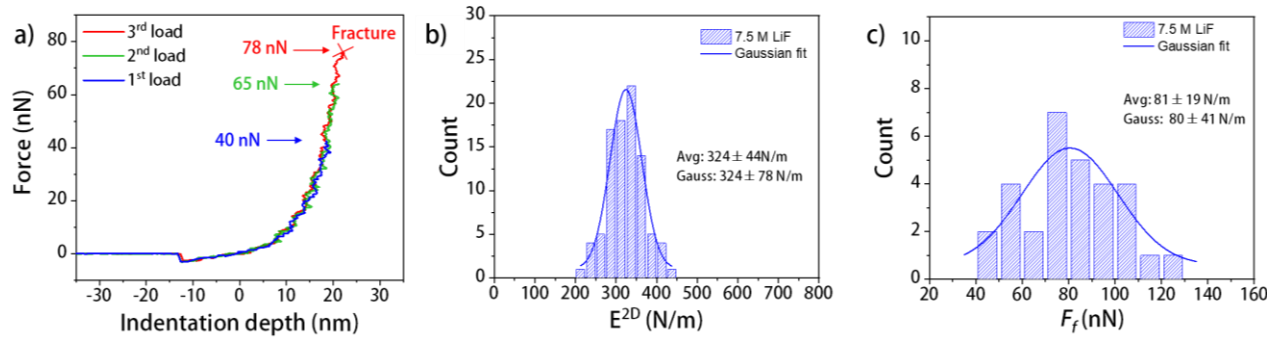


Figure 4-9: a) Force-Distance graph obtained with repeated nanoindentation experiments with increasing force values on suspended $Ti_3C_2T_x$ sheets produced with 7.5 M LiF:MAX molar ratio, b) Histogram graph showing the distribution of calculated E^{2D} values for the same sample, c) Histogram graph showing the distribution of the measured Fracture Force values for the same sample.

Fig. 4.11b shows the distribution of the calculated E^{2D} data from the nanoindentation experiments on 7.5 M LiF. Average of this data is found to be 324 ± 44 N/m for in-plane Young's modulus for this material. Lipatov et al. reported this property in 2018 as 326 ± 29 N/m, which confirms the validity of the experimental method used in this study.

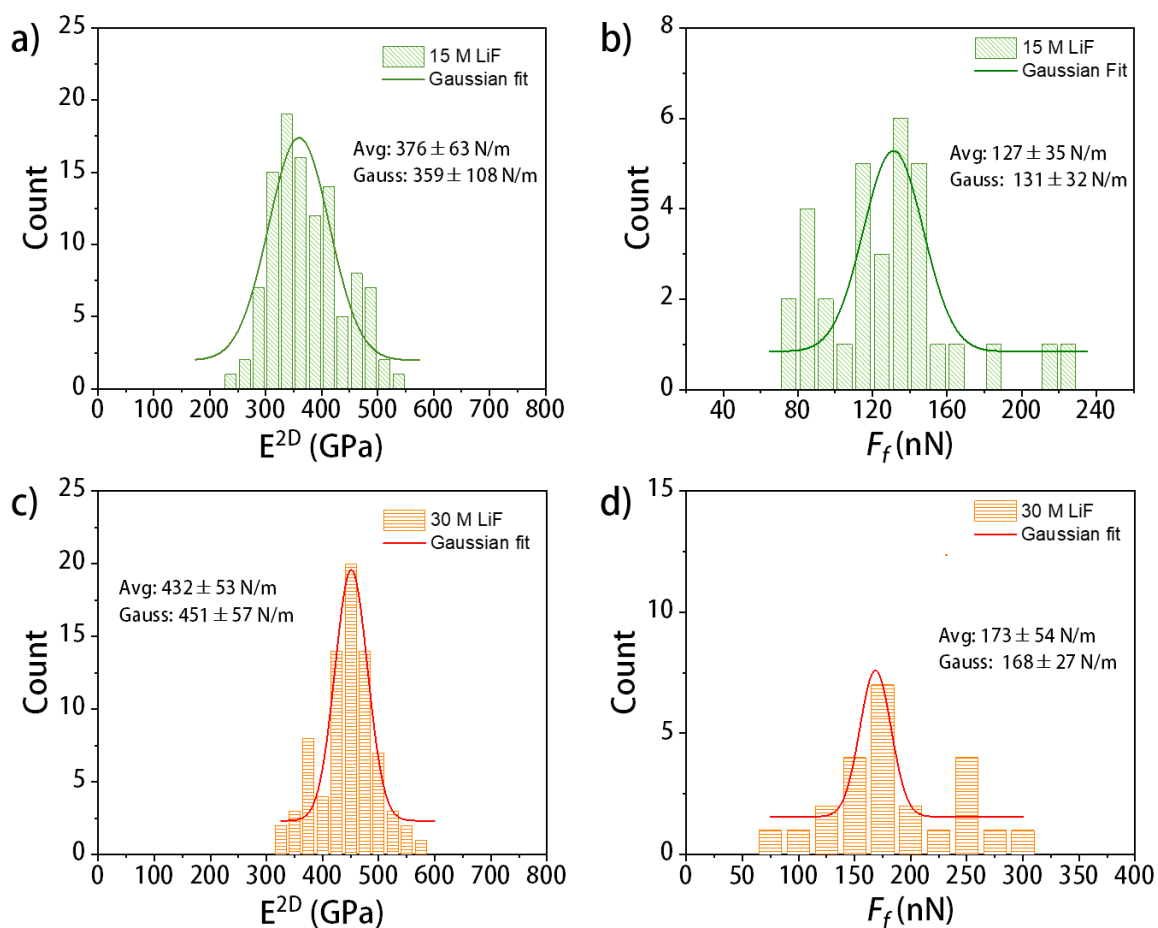


Figure 4-10: Histogram graphs showing the distribution of calculated E^{2D} values for the samples produced with a) 15 M and b) 30 M LiF:MAX molar ratio, c) Histogram graph showing the distribution of the measured Fracture Force values for the c) 15 M and d) 30 M LiF:MAX molar ratio

Figures 4.12 and 4.13 shows the data for $Ti_3C_2T_x$ membranes that were produced with increased LiF concentration. Surprisingly, increased LiF concentration which is predicted to be increasing the Ti vacancy defects on the surface, also improves the mechanical properties of the produced 2D sheets. E^{2D} value of 7.5M- $Ti_3C_2T_x$ increases from 324 ± 44 N/m to 376 ± 63 N/m with doubled LiF concentration of 15 M. $Ti_3C_2T_x$ sheets produced using 30 M LiF, have superior

mechanical properties compared to 7.5M and 15M LiF produced samples. E^{2D} of 30M- $Ti_3C_2T_x$ is calculated to be 432 ± 53 N/m. Young's modulus of these materials are also calculated using E^{2D} and thickness values of the materials. Thickness of $Ti_3C_2T_x$ is used as 0.98 nm in previous studies. Using this thickness value, in this study, calculated Young's modulus of 7.5M- $Ti_3C_2T_x$, 15M- $Ti_3C_2T_x$ and 30M- $Ti_3C_2T_x$ are 331 ± 53 GPa, 383 ± 63 GPa and 440 ± 53 GPa, respectively. Similarly, fracturing forces for each sample are also increased. These forces are found to be 81 ± 19 N/m, 127 ± 35 N/m and 173 ± 54 N/m for 7.5M- $Ti_3C_2T_x$, 15M- $Ti_3C_2T_x$ and 30M- $Ti_3C_2T_x$, respectively.

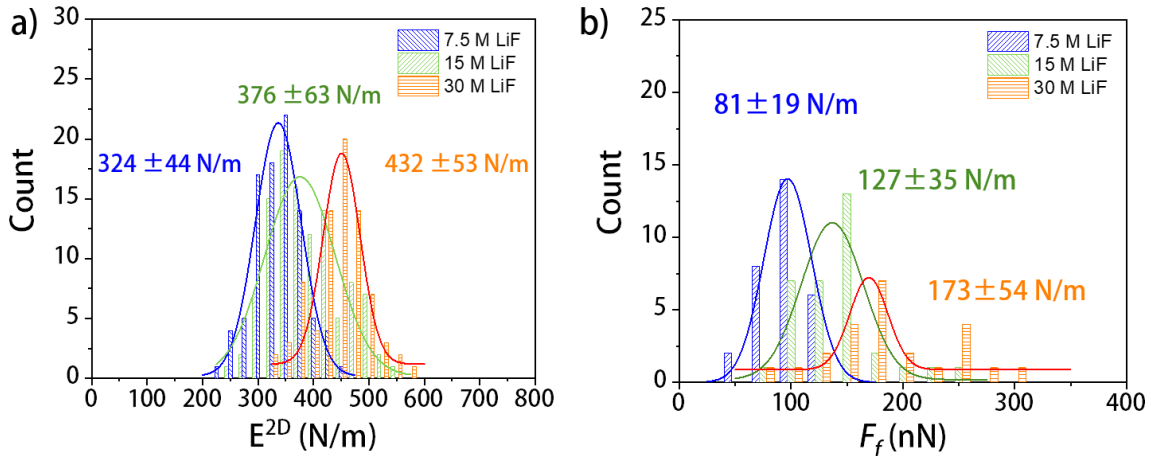


Figure 4-11: Histogram graphs comparing the distribution of calculated a) E^{2D} and b) Fracture Force values for 7.5 M, 15 M and 30 M LiF:MAX ratio samples

We hypothesize that removing Ti atoms from the MXene surface results in formation of titanium oxide structures on the surface. As the metallic Ti-Ti bonds convert to stronger, covalent Ti-O bonds, overall ratio of stronger covalent bonds to weaker metallic bonds also increases, and this results in a higher in-plane Young's modulus value. The improvement of fracturing force is also explained with more defective structure, similar to bulk materials, it is hypothesized that defects in the structure prevent the crack growth, resulting in a higher fracture force.

4.4 Mechanical Properties of $\text{Ti}_2\text{Mo}_2\text{C}_3$

In this section, previously explained experimental study is applied to a different MXene to discover its mechanical properties. Ordered double transition metal MXenes are first discovered in 2015. Similar to the published study, $\text{Ti}_2\text{Mo}_2\text{C}_3$ MXene is produced from its MAX phase counterpart, $\text{Ti}_2\text{Mo}_2\text{AlC}_3$. This MAX phase is also synthesized starting with elemental powders of Mo, Ti, Al and graphite. Molar ratio used for the mixing of powders is 2:2:1.3:2.7 for Mo/Ti/Al/C respectively. After ball mixing of 18 hours, powder mixture is heated to 1600 °C with a heating rate of 5 °C/min in alumina crucibles under constant Argon flow. After the heat treatment, compact MAX phase is initially milled using a TiN-coated milling bit and the powder is sieved through a 400-mesh sieve. Obtained powder is then used for MXene synthesis. For the synthesis, 1g of MAX phase is added to 10 ml of %51 aq. HF solution and mixed at 55 °C for 90 hours. The resulting mixture is washed with DI water several times using centrifuge until the pH of the supernatant is >6. To delaminate the MXene sheets, dilute (5%) aq. TMAOH solution is added to the etched powder and stirred for 30 minutes. After stirring, more DI water is added to the mixture and it is centrifuged at 3500 rpm for 30 minutes. First supernatant is discarded as it contains higher amount of TMAOH, second supernatant after the repeated washing is used to assemble MXene membranes, as it was explained in the previous sections.

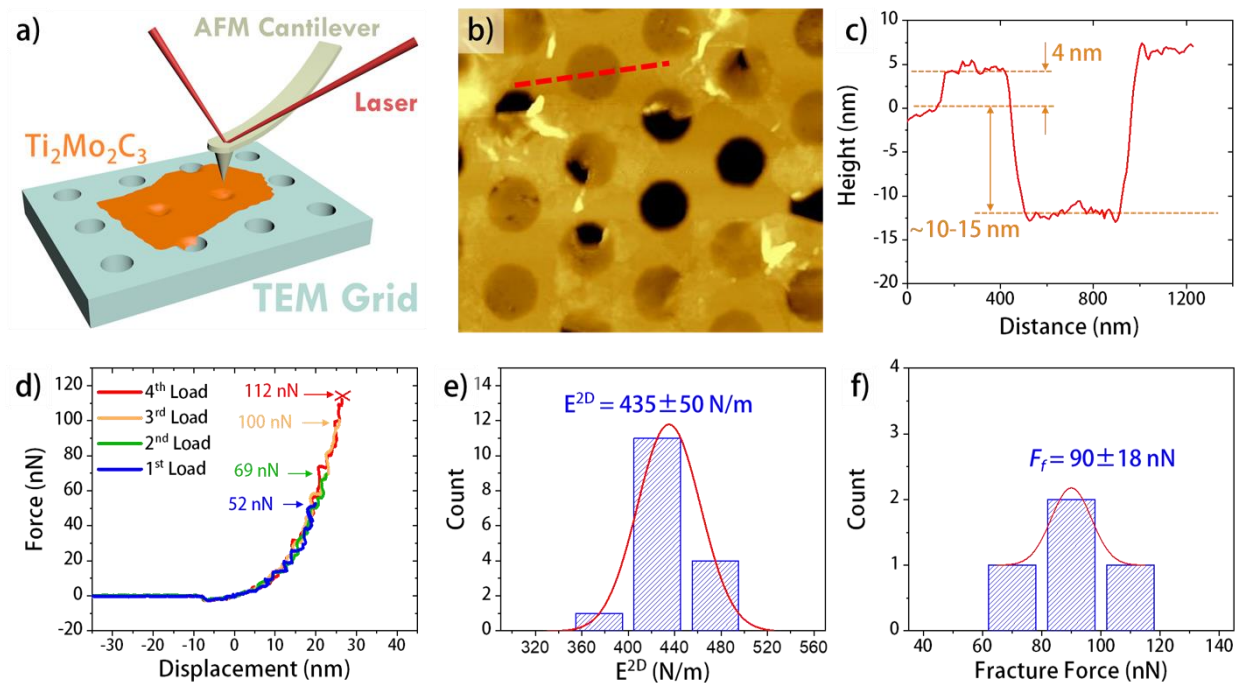


Figure 4-12: a) Schematic showing MXene sheet suspended over holes, b) AFM image showing suspended $\text{Ti}_2\text{Mo}_2\text{C}_3\text{T}_x$ sheets, c) Height profile of the red line marked in b, showing the thickness of the sheets and the depth of suspended sheets, d) Force-Distance graph obtained with repeated nanoindentation experiments with increasing force values on suspended $\text{Ti}_2\text{Mo}_2\text{C}_3\text{T}_x$ sheets b) Histogram graph showing the distribution of calculated E^{2D} values for the same sample, c) Histogram graph showing the distribution of the measured Fracture Force values for the same sample.

Fig 4.14 summarizes the mechanical properties of the single layer $\text{Ti}_2\text{Mo}_2\text{C}_3\text{T}_x$ MXene. 4 different single layer sheet is used for this analysis and each membrane is indented 3-4 times before fracturing. This study shows that single layer $\text{Ti}_2\text{Mo}_2\text{C}_3\text{T}_x$ MXene sheets have an in-plane Young's modulus value of 435 ± 50 N/m. Considering 413 MXene's 1.23 nm theoretical thickness, Young's modulus of this material is calculated to be 353 ± 50 GPa, marking the material's excellent mechanical properties. Fracture force of these sheets are also found to be 90 ± 18 nN.

4.5 Conclusion

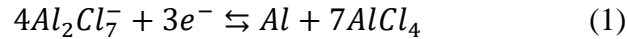
This study showed for the first time that by changing the synthesis conditions, mechanical properties of $\text{Ti}_3\text{C}_2\text{T}_x$ sheets can be improved. Young's modulus value of $\text{Ti}_3\text{C}_2\text{T}_x$ sheets reported in this study ranks the material among the strongest 2D materials ever measured. Also, the method explained here is applicable to different MXenes. This is showed by the measurement of mechanical properties of single layer $\text{Mo}_2\text{Ti}_2\text{C}_3$ MXene. This is an important step to discover superior mechanical properties of MXenes. Unique structure of these materials allows us to study the effect of different elements and number of atomic layers. Comparison of mechanical properties of MXenes such as Mo_2CT_x , Mo_2TiC_2 , Cr_2TiC_2 and $\text{Cr}_2\text{Ti}_2\text{C}_3$ with the $\text{Ti}_3\text{C}_2\text{T}_x$ and $\text{Mo}_2\text{Ti}_2\text{C}_3\text{T}_x$ MXenes reported in this work will present a unique opportunity to study the effect of bonding strength between different metals and carbon/nitrogen. These results have the potential to lead to production of 2D materials with superior and controlled mechanical properties and have utmost importance for the applications that require such unique mechanical properties.

Chapter 5: Development of a novel electrochemical etching method of MAX

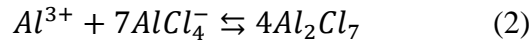
Phases using a battery system

5.1 Introduction

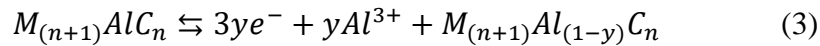
A new electrochemical etching method is introduced in this section. Two different MAX phases are used so far to test the capabilities of this etching method: Ti_3AlC_2 and Cr_2AlC . Although Ti_3AlC_2 has been reported as a precursor in various etching methods to the best of our knowledge Cr_2AlC was not able to be selectively etched to produce Cr_2CT_x MXenes. As introduced in the literature review, several ionic liquid electrolytes are able to deposit Al on different electrochemical setups. Electrochemical species that are active for deposition of Al are $AlCl_4^-$ and $Al_2Cl_7^-$ ions. Al deposition can be shown with the following equation;



This reaction is reversible where the reverse reaction is electrochemical dissolution of Al. These electrochemical species can also converse between each other which can be shown with the following equation;



Considering these we propose the electrochemical etching of MAX Phases can be shown with the following equation;



As it is crucial to control the concentration of the active electrochemical species, we chose to proceed with $\text{AlCl}_3/\text{Et}_3\text{NHCl}$ electrolyte. Fig. 4-25 shows Raman measurements demonstrating that changing the molar ratio of the reactants changes the concentration of electrochemical species present in the electrolyte. Furthermore, Et_3NHCl is a low-cost material which enables large amounts of electrolyte production with ease.(101,102) In Fig. 4-26-a it is demonstrated that in an electrochemical setup consisting Ta cathode, Al anode and $\text{AlCl}_3/\text{Et}_3\text{NHCl}$ electrolyte, Al deposition and Al stripping is reversible. Also, at voltage window of 0.1 V to 1.8 V it is demonstrated that Ta does not react with electrolyte and system is stable (Fig. 4-26-b). Addition of Ti_3AlC_2 MAX phase shows clear redox peaks in CV graphs which can attribute to reduction of Ti and Al in the MAX Phase.

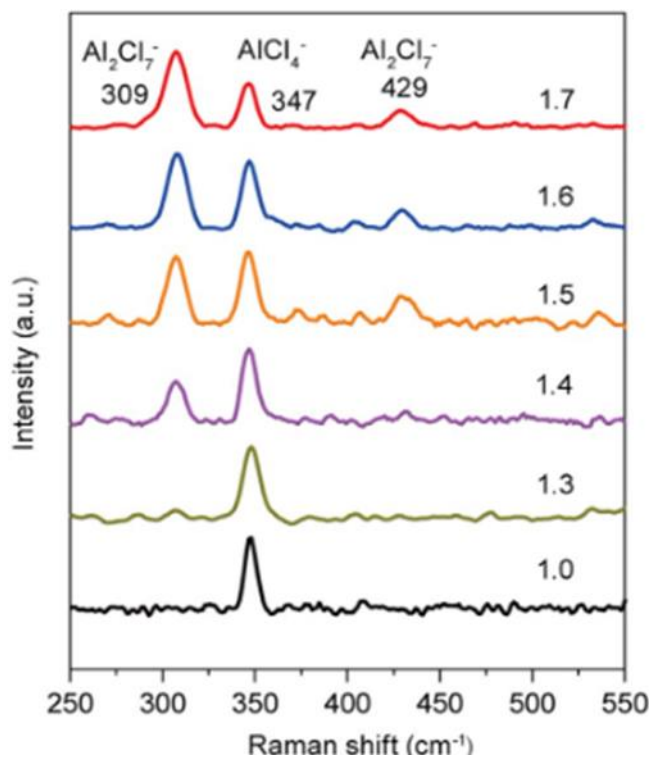


Figure 5-1: Raman measurements showing active electrochemical species in $\text{Et}_3\text{NHCl}/\text{AlCl}_3$ electrolytes with different molar ratios (101)

5.2 Experimental Setup

To be able to effectively load MAX phases into proposed electrochemical setup, MAX phase discs are produced with cold pressing of powders using a die with 0.25-inch diameter. Ta current collectors are then shaped to hold these discs in the given electrolyte. Digital images of the used electrochemical setup in this section is given in Fig 4-27.

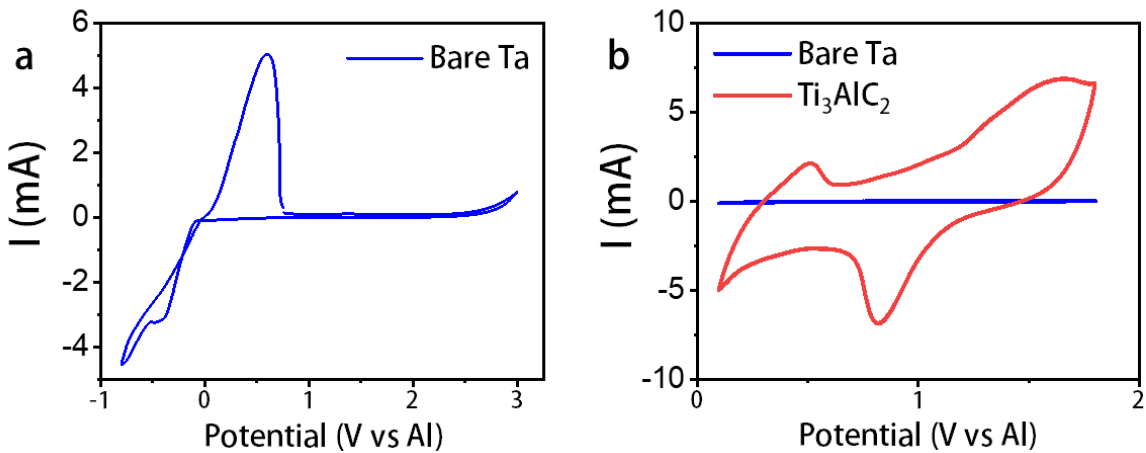


Figure 5-2: Cyclic Voltammetry graphs showing the interaction of $\text{Et}_3\text{NHCl}/\text{AlCl}_3$ electrolyte with Ta current collector, Ti_3AlC_2 MAX Phase cathode and Al anode; a) When the voltage window is set between -1 V to 3V b) when voltage window is set between 0.1-1.8 V

In such electrochemical etching system, there are several parameters that can affect etching rate, selectivity and efficiency of the etching such as ambient atmosphere, temperature, applied voltage (Constant voltage or alternating voltage, amplitude or frequency), active electrochemical species and the duration of the experiment. During my experiments I tried to find out the effect of each parameter on the etching process. For characterization of the etched MAX phase particles, several characterization techniques have been utilized such as SEM, XRD and AFM. Among these methods, in literature a practical tool for determining the selectivity of the etching has been the Energy Dispersive X-ray Spectroscopy (EDS). As shown in chapter 2, increase in the M/Al ratio (where M is Ti for Ti_3AlC_2 and Cr for Cr_2AlC) indicates that etching is selective. M/Al ratio of 312 MAX phases such as Ti_3AlC_2 is 3, and of 211 MAX phases such as Cr_2AlC is 2.

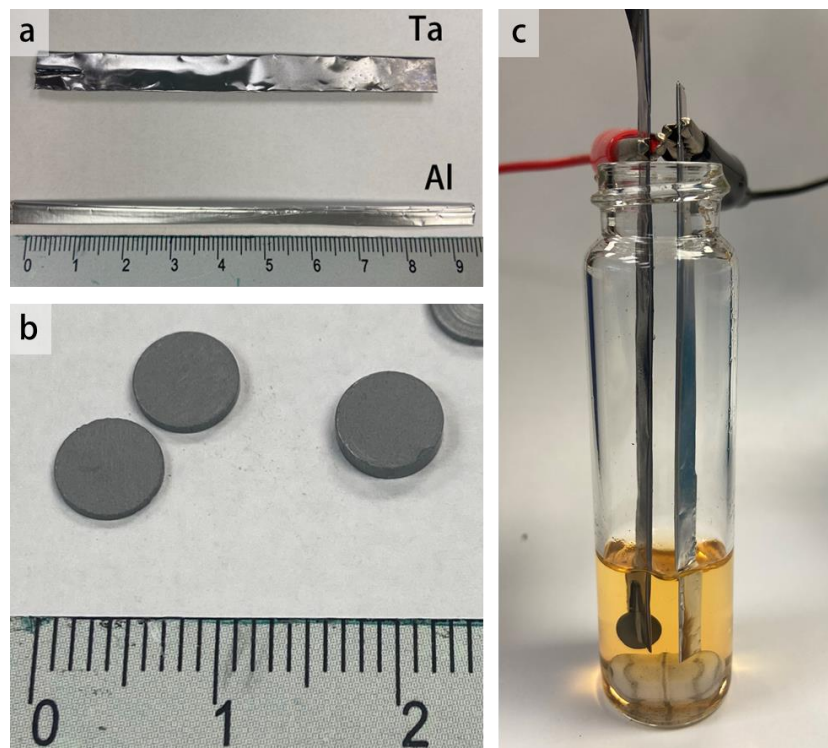


Figure 5-3: Electrochemical setup and its components used in the electrochemical etching

5.3 Electrochemical Etching of Ti_3AlC_2 and Cr_2AlC MAX Phases

First set of experiments are carried out using Ti_3AlC_2 MAX phase disc cathodes attached to Ta current collectors, $\text{AlCl}_3/\text{Et}_3\text{NHCl}$ (1.5 molar ratio) electrolyte and Al anodes. Firstly, experiments showed that used ionic liquid electrolyte is not stable under air and reacts with oxygen. Consumption of the electrolyte over time is observed and characterized reacted MAX phase particles showed presence of oxygen in the structure. Furthermore, Ti/Al ratio is found to be 1.5 which indicates stronger oxidation of Ti atoms rather than Al atoms. Based on these findings rest of the experiments are carried out under Argon atmosphere inside the glovebox.

Table 1: Different experimental parameters applied to Ti₃AlC₂ MAX Phase for electrochemical etching

MAX Phase	Electrolyte	Voltage	Ambient	Temperature	Duration	Ti/Al	Comments
Ti ₃ AlC ₂	AlCl ₃ /Et ₃ NHCl	Cons. 2V	Air	RT	24h	1.5	Some oxidized particles, Gray colored powder
Ti ₃ AlC ₂	AlCl ₃ /Et ₃ NHCl	Cons. 2V	Ar	RT	24h	3.2	Gray colored powder
Ti ₃ AlC ₂	AlCl ₃ /Et ₃ NHCl	1.8V-0V Sq. Pulse	Ar	RT	24h	3.5	Gray colored powder
Ti ₃ AlC ₂	AlCl ₃ /Et ₃ NHCl	1.8V-0V Sq. Pulse	Ar	75 C	72h	3.4	Dark gray colored powder
Ti ₃ AlC ₂	AlCl ₃ /Et ₃ NHCl	1.8V-0V Sq. Pulse	Ar	150 C	72h	5.9	Black colored powder
Ti ₃ AlC ₂	AlCl ₃ /Et ₃ NHCl	1V-0.5V Sq. Pulse	Ar	150 C	72h	3.9	Dark gray colored powder
Ti ₃ AlC ₂	AlCl ₃ /Et ₃ NHCl	1.4V-0V Sq. Pulse	Ar	150 C	72h	4.8	Dark gray colored powder

Next, the effect of the applied voltage type is studied. Applied voltage is changed between Constant 2V and square pulse of 45 seconds 1.8V and 15 seconds of 0 V for 24 hours. EDS Analysis of the etched particles suggests slightly better selectivity of the etching with 3.5 to 3.2 Ti/Al ratio with square pulse and constant voltage, respectively. Square pulse voltage application has also chosen for further experiments. However, EDS Analysis also showed strong presence of Al in the structure, meaning that etching rate is low. To further test the etching power of the electrochemical setup temperature is increased to 75 °C and 150 °C. Figure 4-28-a shows photographs of etched MAX phase powders. It can be clearly seen that powders etched at higher temperatures have darker color, indication of stronger etching. EDS Analysis of particles etched at 150 °C shows Ti/Al ratio of 5.9 which is almost the double of starting condition and indicating selective etching. In order to increase selectivity even more, experiments with different amplitudes

of applied square pulses are also carried out. However, amplitudes of 0.5 V and 1.4 V resulted in lower Ti/Al ratios of 3.9 and 4.8 respectively.

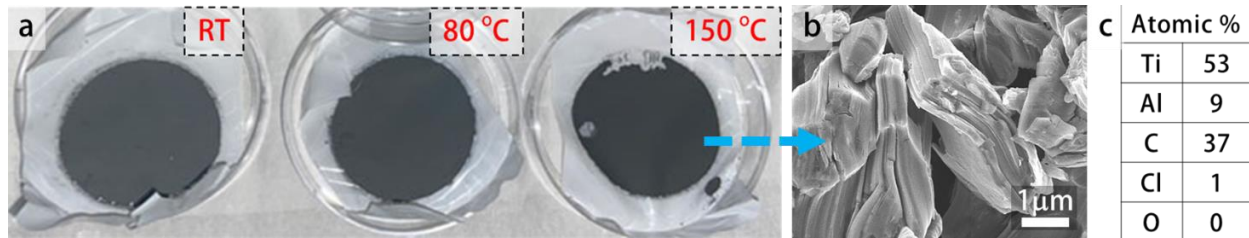


Figure 5-4: a) Digital images showing Ti_3AlC_2 powders obtained after etching at different temperatures. b) SEM image of etched Ti_3AlC_2 powders and c) EDS analysis showing atomic percentages within the etched particles

Based on these promising results, same parameters are also used for etching of Cr_2AlC MAX phase cathode discs. During this experiment, it was observed that etching reaction happens much faster with Cr_2AlC MAX phase as there was visible bubble forming on the cathode disc, and it disintegrated into the electrolyte only after 1 hour. Characterization of these etched particles revealed that some particles were over-etched, whereas some particles are not even reacted yet. This is expected since fast nature of the reaction allowed only particles on the outer part of the disc to react before crumbling into the electrolyte. Over-etching of Cr_2AlC particles was confirmed with EDS analysis. As shown in Fig 4-29-a, particles with almost no Cr or Al atoms were found. Nevertheless, same powder contains etched particles with high Cr/Al ratio of 6.7 (rather than 2 of the MAX Phase). These results clearly indicate milder etching conditions are required for this MAX phase and most likely that all MAX phases will need optimization of parameters based on their reactivity in this electrochemical setup.

Table 2: Different experimental parameters applied to Cr₂AlC MAX Phase for electrochemical etching

MAX Phase	Electrolyte	Voltage	Ambient	Temp.	Duration
Cr ₂ AlC	AlCl ₃ /Et ₃ NHCl	1.8V-0V Sq. Pulse	Ar	150 C	72h
Cr ₂ AlC	AlCl ₃ /Et ₃ NHCl	1.8V-0V Sq. Pulse	Ar	RT	72h
Cr ₂ AlC	AlCl ₃ /Et ₃ NHCl	1.8V-0V Sq. Pulse	Ar	75C	24h

Next, temperature is decreased to achieve milder etching conditions to RT and 75 °C. Experiments at RT even for 72 hours showed no indication of any etching. However, experiments at 75 C and 24 hours, showed a variety of etched particles. As shown in Fig. 4-29-b, some particles showed almost complete selective etching with Cr/Al ratio of 27.5. Yet, majority of the particles had lower Cr/Al ratio of 3.8 with still remaining Al in the structure.

To address the non-uniform etching among the MAX phase particles, a slurry of MAX phase powder is prepared with conductive carbon and binder polymer. 95% wt. Cr₂AlC powder is mixed with 5% wt. carbon black (Super-P) in 1 ml of aq. PVA solution. Resulted slurry is then casted on to carbon paper and placed into vacuum oven at 150 °C overnight for drying. Carbon paper with the MAX phase powders are then cut into strips to be used as cathodes in the electrochemical setup as shown in Fig. 4-30a. Goal of the making carbon paper electrodes was to expose more MAX phase particles to electrolyte at the same time, whereas in pressed disc electrodes reaction through the thickness of the electrode is diffusion limited.

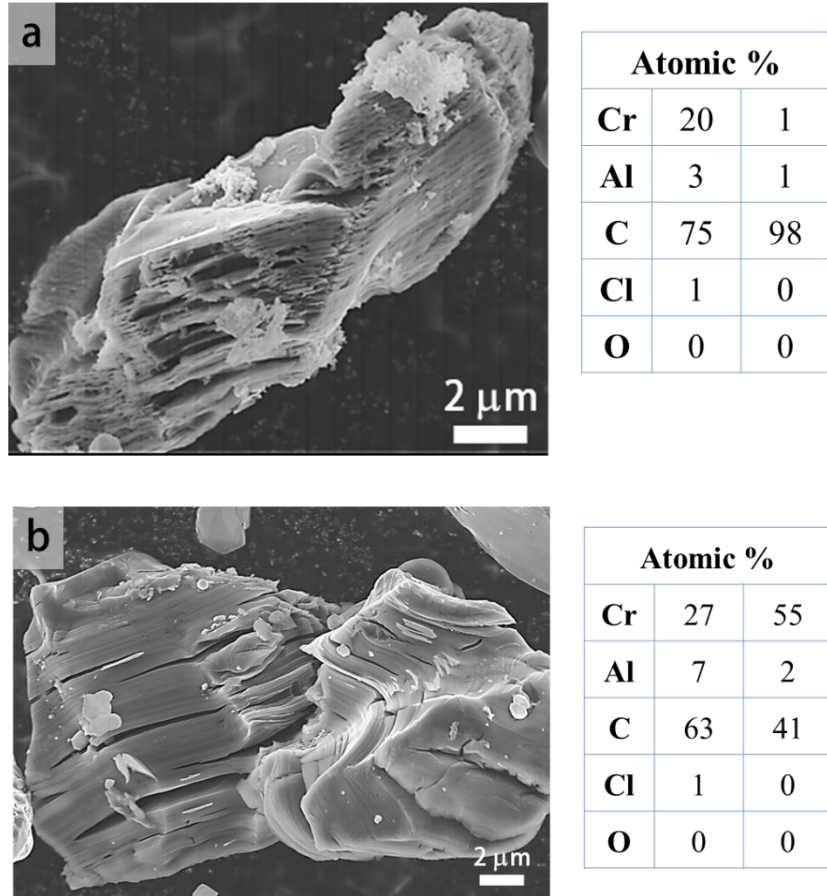


Figure 5-5: SEM images of electrochemically etched Cr₂AlC particles and corresponding EDS Analysis

For the experiments with carbon paper current collectors, initially a high temperature of 150 °C is chosen to complete the etching in a quick fashion. This experiment is then repeated to collect large amounts of etched MAX phase powder. Once the experiments are finished, electrodes are scraped off with a razor to gather the powders. Obtained powder is washed in HCl in IPA to dissolve side products that might be formed during etching such as Al or Cr salts. Using high-speed centrifuge etched powder is separated from the solution and transferred into Propylene carbonate (PC). A recent study showed that PC is an organic solvent with a large molecule that can intercalate between the etched MAX phase particles with the help of sonication and delaminate

MXene sheets to form stable MXene suspensions. Accordingly, processed powder in PC is sonicated under Ar atmosphere to prevent oxidation for 1 hour and centrifuged at 3500 rpm for 10 minutes.

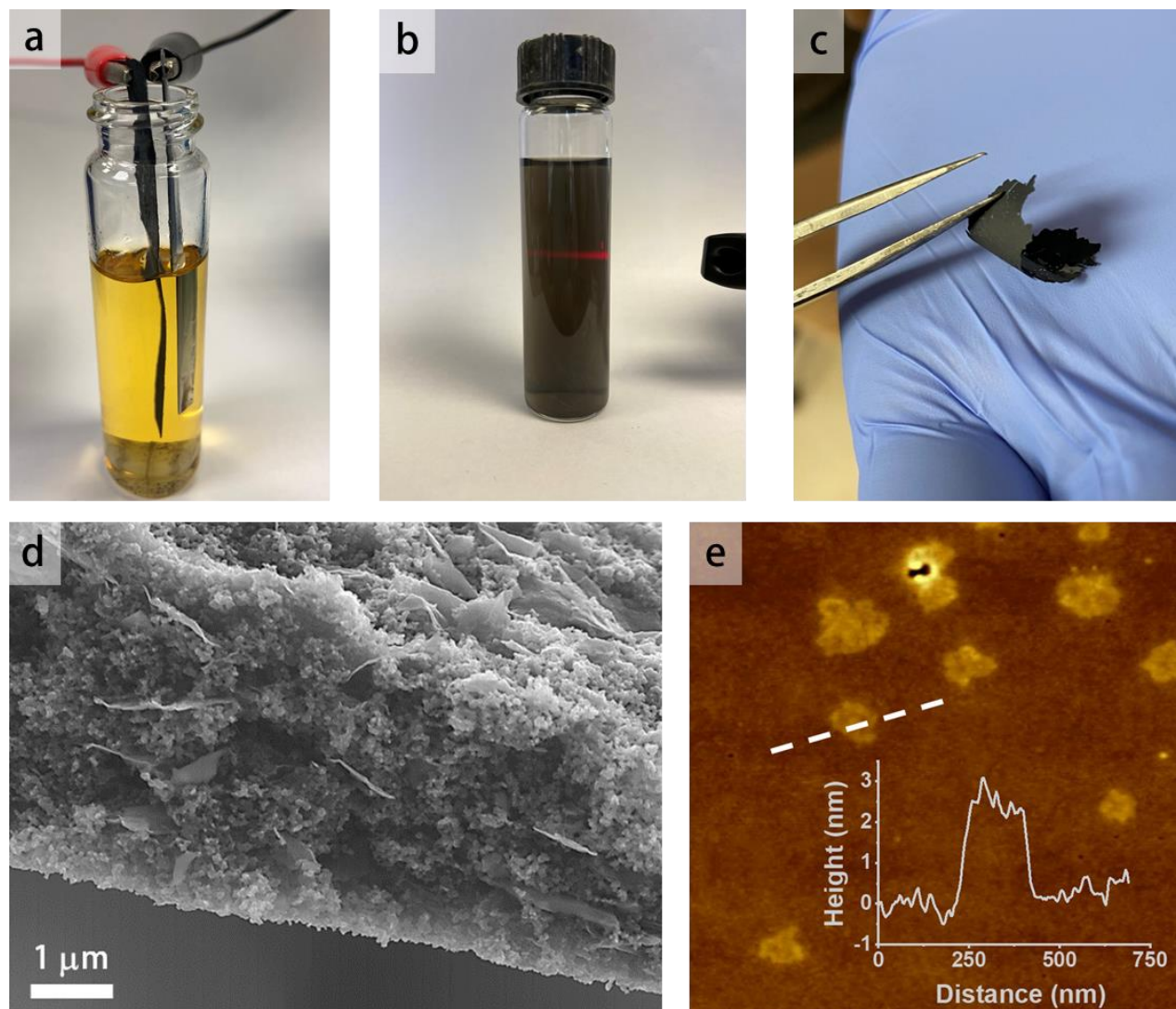


Figure 5-6: a) Electrochemical setup using Carbon paper as current collector for MAX phase cathodes b) Aqueous delaminated etched-Cr₂AlC and carbon black (CB) suspension c) Etched-Cr₂AlC-CB film obtained by vacuum-filtration of the solution shown. d) SEM image of the cross-section of obtained films. e) AFM image showing the thickness of Etched-Cr₂AlC sheets on Si/SiO₂ wafer surface.

As shown in Fig. 4-30b, a stable colloid solution is obtained. The solution is vacuum filtered and a flexible film similar to MXene papers is obtained, indicating existence of 2D materials. Accordingly, cross-section of the acquired film is examined under SEM. The film is shown to be consisting of spherical nanoparticles which are likely to be carbon black and sheet-like structures which are thought to be Cr_2CT_x MXene flakes. AFM Analysis is also carried out on the solution after it is drop casted on a Si wafer. Fig 4-30e, shows sheet-like structures with about 2 nm thickness and 250-500 nm lateral size.

5.4 Conclusion

These findings indicate that the method presented in this chapter might be capable of selectively etch different MAX phases including Cr_2AlC , which has not been reported to be selectively etched, to date. It is demonstrated that water-free, fluorine-free electrochemical etching of MAX phases is possible via this method. However, to confirm existence of MXene sheets, isolation of the sheets and structural characterization is mandatory. Although, completely and selectively etched particles are located with SEM, to be used as an efficient etching method, selectivity of the etching through the electrode must be improved. In this direction, results so far showed that parameters such as temperature and applied voltage are crucial for the selectivity of the etching. Based on the evidence presented in this section, we hypothesize that this method parameters can be optimized to achieve selective etching of different MAX phase particles. We also speculate that this etching method should result in MXene sheets with chlorine surface groups which are previously shown to be favorable in electrochemical applications. This study encourages to use etched MXene particles with this method in different electrochemical energy storage systems to demonstrate the effect of this new synthesis method on the performance.

Chapter 6: Outlook

Although MXene research started merely a decade ago, scientific community dedicated enormous amounts of resources to discover the potential of this 2D material family. Achieved results so far showed that MXenes are able to live up to expectations; especially in electrochemistry field MXenes delivered some of the best performances ever reported. Energy storage devices, a big part of the MXene research, are predicted to play a crucial part in the future of automotive industry, portable electronics and advanced micro and nano systems. Breakthroughs in MXene research will surely lead advancements in energy storage field as well. As an example, results reported in this study improve electrochemical properties of MXene electrodes up to 170% when used in aqueous supercapacitor systems and only by controlling the synthesis conditions. We showed here that synthesis conditions have a huge effect not only on the electrochemical, but also mechanical properties of MXenes. We showed for the first time that MXenes mechanical properties can be improved through their synthesis conditions and moreover, introduced a method that can lead to new studies. We know that understanding the characteristics of MXenes and its synthesis will have a direct impact on the future of its applications and there is still a lot to learn about MXenes. Theoretical calculations will guide experimental work and proof of concepts will pave the way through commercialization. In this perspective, noting the growing interest in MXenes, I believe that this study is now an essential source by means of exploring the fundamental properties of the material and providing different approaches for producing and assembling it for different applications. Consequently, the presented study will hopefully benefit to a large community of MXene researchers.

Chapter 7: References

1. Beidaghi M, Gogotsi Y. Capacitive energy storage in micro-scale devices: recent advances in design and fabrication of micro-supercapacitors. *Energy & Environmental Science*. 2014;7(3):867.
2. Yan J, Wang Q, Wei T, Fan Z. Recent Advances in Design and Fabrication of Electrochemical Supercapacitors with High Energy Densities. *Advanced Energy Materials*. 2014 Mar;4(4):1300816.
3. Lukatskaya MR, Mashtalir O, Ren CE, Dall'Agnese Y, Rozier P, Taberna PL, et al. Cation Intercalation and High Volumetric Capacitance of Two-Dimensional Titanium Carbide. *Science*. 2013 Sep 27;341(6153):1502–5.
4. Anasori B, Lukatskaya MR, Gogotsi Y. 2D metal carbides and nitrides (MXenes) for energy storage. *Nature Reviews Materials*. 2017 Jan 17;2(2):16098.
5. Naguib M, Mochalin VN, Barsoum MW, Gogotsi Y. ChemInform Abstract: 25th Anniversary Article: MXenes: A New Family of Two-Dimensional Materials. *ChemInform*. 2014 Apr 28;45(17):no-no.
6. Naguib M, Kurtoglu M, Presser V, Lu J, Niu J, Heon M, et al. Two-Dimensional Nanocrystals Produced by Exfoliation of Ti_3AlC_2 . *Advanced Materials*. 2011 Oct 4;23(37):4248–53.
7. Shahzad F, Alhabeab M, Hatter CB, Anasori B, Hong SM, Koo CM, et al. Electromagnetic interference shielding with 2D transition metal carbides (MXenes). *Science*. 2016;353(6304):1137–1140.
8. Srimuk P, Halim J, Lee J, Tao Q, Rosen J, Presser V. Two-Dimensional Molybdenum Carbide (MXene) with Divacancy Ordering for Brackish and Seawater Desalination via Cation and Anion Intercalation. *ACS Sustainable Chemistry & Engineering*. 2018 Mar 5;6(3):3739–47.
9. Li R, Zhang L, Shi L, Wang P. MXene Ti_3C_2 : An Effective 2D Light-to-Heat Conversion Material. *ACS Nano*. 2017 Apr 25;11(4):3752–9.
10. Zhang X, Zhang Z, Li J, Zhao X, Wu D, Zhou Z. Ti_2CO_2 MXene: a highly active and selective photocatalyst for CO_2 reduction. *Journal of Materials Chemistry A*. 2017;5(25):12899–903.

11. Zhao M-Q, Torelli M, Ren CE, Ghidui M, Ling Z, Anasori B, et al. 2D titanium carbide and transition metal oxides hybrid electrodes for Li-ion storage. *Nano Energy*. 2016 Dec;30:603–13.
12. Ghidui M, Lukatskaya MR, Zhao M-Q, Gogotsi Y, Barsoum MW. Conductive two-dimensional titanium carbide ‘clay’ with high volumetric capacitance. *Nature*. 2014 Dec;516(7529):78–81.
13. Levi MD, Lukatskaya MR, Sigalov S, Beidaghi M, Shpigel N, Daikhin L, et al. Solving the Capacitive Paradox of 2D MXene using Electrochemical Quartz-Crystal Admittance and In Situ Electronic Conductance Measurements. *Advanced Energy Materials*. 2015 Jan;5(1):1400815.
14. Lukatskaya MR, Kota S, Lin Z, Zhao M-Q, Shpigel N, Levi MD, et al. Ultra-high-rate pseudocapacitive energy storage in two-dimensional transition metal carbides. *Nature Energy*. 2017 Jul 10;2(8):17105.
15. Wang G, Zhang L, Zhang J. A review of electrode materials for electrochemical supercapacitors. *Chem Soc Rev*. 2012;41(2):797–828.
16. Lukatskaya MR, Bak S-M, Yu X, Yang X-Q, Barsoum MW, Gogotsi Y. Probing the Mechanism of High Capacitance in 2D Titanium Carbide Using In Situ X-Ray Absorption Spectroscopy. *Advanced Energy Materials*. 2015 Aug;5(15):1500589.
17. Naguib M, Mochalin VN, Barsoum MW, Gogotsi Y. 25th Anniversary Article: MXenes: A New Family of Two-Dimensional Materials. *Advanced Materials*. 2014 Feb;26(7):992–1005.
18. Alhabeab M, Maleski K, Anasori B, Lelyukh P, Clark L, Sin S, et al. Guidelines for Synthesis and Processing of Two-Dimensional Titanium Carbide ($Ti_3C_2T_x$ MXene). *Chemistry of Materials*. 2017 Sep 26;29(18):7633–44.
19. Peng Y-Y, Akuzum B, Kurra N, Zhao M-Q, Alhabeab M, Anasori B, et al. All-MXene (2D titanium carbide) solid-state microsupercapacitors for on-chip energy storage. *Energy & Environmental Science*. 2016;9(9):2847–54.
20. Novoselov KS. Electric Field Effect in Atomically Thin Carbon Films. *Science*. 2004 Oct 22;306(5696):666–9.
21. Bhimanapati GR, Lin Z, Meunier V, Jung Y, Cha J, Das S, et al. Recent Advances in Two-Dimensional Materials beyond Graphene. *ACS Nano*. 2015 Dec 22;9(12):11509–39.
22. Gogotsi Y, Anasori B. The Rise of MXenes. *ACS Nano*. 2019 Aug 27;13(8):8491–4.
23. Tan C, Cao X, Wu X-J, He Q, Yang J, Zhang X, et al. Recent Advances in Ultrathin Two-Dimensional Nanomaterials. *Chemical Reviews*. 2017 May 10;117(9):6225–331.

24. Novoselov KS, Mishchenko A, Carvalho A, Castro Neto AH. 2D materials and van der Waals heterostructures. *Science*. 2016 Jul 29;353(6298):aac9439.
25. Zhu J, Ha E, Zhao G, Zhou Y, Huang D, Yue G, et al. Recent advance in MXenes: A promising 2D material for catalysis, sensor and chemical adsorption. *Coordination Chemistry Reviews*. 2017 Dec;352:306–27.
26. Cao C, Sun Y, Filleter T. Characterizing mechanical behavior of atomically thin films: A review. *Journal of Materials Research*. 2014 Feb;29(03):338–47.
27. Miró P, Audiffred M, Heine T. An atlas of two-dimensional materials. *Chem Soc Rev*. 2014;43(18):6537–54.
28. Liu C, Li F, Ma L-P, Cheng H-M. Advanced Materials for Energy Storage. *Advanced Materials*. 2010 Feb 23;22(8):E28–62.
29. Wang T, Wang H, Kou Z, Liang W, Luo X, Verpoort F, et al. Xenes as an Emerging 2D Monoelemental Family: Fundamental Electrochemistry and Energy Applications. *Advanced Functional Materials*. 2020 Sep;30(36):2002885.
30. Novoselov KS, Jiang D, Schedin F, Booth TJ, Khotkevich VV, Morozov SV, et al. Two-dimensional atomic crystals. :3.
31. Geim AK, Novoselov KS. The rise of graphene. *Nature Materials*. 2007;6:183–91.
32. Wang QH, Kalantar-Zadeh K, Kis A, Coleman JN, Strano MS. Electronics and optoelectronics of two-dimensional transition metal dichalcogenides. *Nature Nanotechnology*. 2012 Nov;7(11):699–712.
33. Zavabeti A, Jannat A, Zhong L, Haidry AA, Yao Z, Ou JZ. Two-Dimensional Materials in Large-Areas: Synthesis, Properties and Applications. *Nano-Micro Letters* [Internet]. 2020 Feb [cited 2020 Nov 28];12(1). Available from: <http://link.springer.com/10.1007/s40820-020-0402-x>
34. Fang Q, Shen Y, Chen B. Synthesis, decoration and properties of three-dimensional graphene-based macrostructures: A review. *Chemical Engineering Journal*. 2015 Mar;264:753–71.
35. Nicolosi V, Chhowalla M, Kanatzidis MG, Strano MS, Coleman JN. Liquid Exfoliation of Layered Materials. *Science*. 2013 Jun 21;340(6139):1226419–1226419.
36. Coleman JN, Lotya M, O'Neill A, Bergin SD, King PJ, Khan U, et al. Two-Dimensional Nanosheets Produced by Liquid Exfoliation of Layered Materials. *Science*. 2011 Feb 4;331(6017):568–71.
37. Brukl C, Nowotny I, Benesovsky F. Die Kristallstrukturen von TiSi, Ti(Al,Si)₂ und Mo(Al,Si)₂. :8.

38. Radovic M, Barsoum MW. MAX phases: Bridging the gap between metals and ceramics. *MAX phases*. 92(3):8.
39. Naguib M, Mashtalir O, Carle J, Presser V, Lu J, Hultman L, et al. Two-Dimensional Transition Metal Carbides. *ACS Nano*. 2012 Feb 28;6(2):1322–31.
40. Eklund P, Beckers M, Jansson U, Högberg H, Hultman L. The $Mn_{n+1}AX_n$ phases: Materials science and thin-film processing. *Thin Solid Films*. 2010 Feb;518(8):1851–78.
41. Anasori B, Gogotsi Y. Introduction to 2D Transition Metal Carbides and Nitrides (MXenes). In: Anasori B, Gogotsi Y, editors. *2D Metal Carbides and Nitrides (MXenes): Structure, Properties and Applications* [Internet]. Cham: Springer International Publishing; 2019 [cited 2020 Nov 29]. p. 3–12. Available from: https://doi.org/10.1007/978-3-030-19026-2_1
42. Chaudhari NK, Jin H, Kim B, Baek DS, Joo SH, Lee K. MXene: an emerging two-dimensional material for future energy conversion and storage applications. *J Mater Chem A*. 2017 Dec 5;5(47):24564–79.
43. Feng A, Yu Y, Wang Y, Jiang F, Yu Y, Mi L, et al. Two-dimensional MXene Ti_3C_2 produced by exfoliation of Ti_3AlC_2 . *Materials & Design*. 2017 Jan;114:161–6.
44. Lipatov A, Alhabeab M, Lukatskaya MR, Boson A, Gogotsi Y, Sinitskii A. Effect of Synthesis on Quality, Electronic Properties and Environmental Stability of Individual Monolayer Ti_3C_2 MXene Flakes. *Advanced Electronic Materials*. 2016 Dec;2(12):1600255.
45. Xuan J, Wang Z, Chen Y, Liang D, Cheng L, Yang X, et al. Organic-Base-Driven Intercalation and Delamination for the Production of Functionalized Titanium Carbide Nanosheets with Superior Photothermal Therapeutic Performance. *Angewandte Chemie*. 2016 Nov 14;128(47):14789–94.
46. Li G, Tan L, zhang Y, Wu B, Li L. Highly Efficiently Delaminated Single-Layered MXene Nanosheets with Large Lateral Size. *Langmuir*. 2017 Sep 12;33(36):9000–6.
47. Li T, Yao L, Liu Q, Gu J, Luo R, Li J, et al. Fluorine-Free Synthesis of High-Purity $Ti_3C_2T_x$ (T=OH, O) via Alkali Treatment. *Angewandte Chemie International Edition*. 2018 May 22;57(21):6115–9.
48. Wang L, Zhang H, Wang B, Shen C, Zhang C, Hu Q, et al. Synthesis and electrochemical performance of $Ti_3C_2T_x$ with hydrothermal process. *Electronic Materials Letters*. 2016 Sep;12(5):702–10.
49. Xie X, Xue Y, Li L, Chen S, Nie Y, Ding W, et al. Surface Al leached Ti_3AlC_2 as a substitute for carbon for use as a catalyst support in a harsh corrosive electrochemical system. *Nanoscale*. 2014;6(19):11035–40.
50. Persson POÅ. MXene Surface Chemistry. In: Anasori B, Gogotsi Y, editors. *2D Metal Carbides and Nitrides (MXenes): Structure, Properties and Applications* [Internet]. Cham:

Springer International Publishing; 2019 [cited 2020 Nov 29]. p. 125–36. Available from: https://doi.org/10.1007/978-3-030-19026-2_8

51. Peng J, Chen X, Ong W-J, Zhao X, Li N. Surface and Heterointerface Engineering of 2D MXenes and Their Nanocomposites: Insights into Electro- and Photocatalysis. *Chem*. 2019 Jan;5(1):18–50.
52. Soundiraraju B, George BK. Two-Dimensional Titanium Nitride (Ti_2N) MXene: Synthesis, Characterization, and Potential Application as Surface-Enhanced Raman Scattering Substrate. *ACS Nano*. 2017 Sep 26;11(9):8892–900.
53. Li M, Lu J, Luo K, Li Y, Chang K, Chen K, et al. Element Replacement Approach by Reaction with Lewis Acidic Molten Salts to Synthesize Nanolaminated MAX Phases and MXenes. *Journal of the American Chemical Society*. 2019 Mar 20;141(11):4730–7.
54. Urbankowski P, Anasori B, Makaryan T, Er D, Kota S, Walsh PL, et al. Synthesis of two-dimensional titanium nitride Ti_4N_3 (MXene). *Nanoscale*. 2016;8(22):11385–91.
55. Kajiyama S, Szabova L, Iinuma H, Sugahara A, Gotoh K, Sodeyama K, et al. Enhanced Li-Ion Accessibility in MXene Titanium Carbide by Steric Chloride Termination. *Advanced Energy Materials*. 2017;7(9):1601873.
56. Lu J, Persson I, Lind H, Palisaitis J, Li M, Li Y, et al. Tin+1Cn MXenes with fully saturated and thermally stable Cl terminations. *Nanoscale Adv*. 2019 Sep 11;1(9):3680–5.
57. Pang S-Y, Wong Y-T, Yuan S, Liu Y, Tsang M-K, Yang Z, et al. Universal Strategy for HF-Free Facile and Rapid Synthesis of Two-dimensional MXenes as Multifunctional Energy Materials. *Journal of the American Chemical Society*. 2019 Jun 19;141(24):9610–6.
58. Sun W, Shah SA, Chen Y, Tan Z, Gao H, Habib T, et al. Electrochemical etching of Ti_2AlC to Ti_2CT_x (MXene) in low-concentration hydrochloric acid solution. *J Mater Chem A*. 2017;5(41):21663–8.
59. Lukatskaya MR, Halim J, Dyatkin B, Naguib M, Buranova YS, Barsoum MW, et al. Room-Temperature Carbide-Derived Carbon Synthesis by Electrochemical Etching of MAX Phases. *Angewandte Chemie International Edition*. 2014 May 5;53(19):4877–80.
60. Yang S, Zhang P, Wang F, Ricciardulli AG, Lohe MR, Blom PWM, et al. Fluoride-Free Synthesis of Two-Dimensional Titanium Carbide (MXene) Using A Binary Aqueous System. *Angewandte Chemie International Edition*. 2018;57(47):15491–5.
61. Zhao R, Wang M, Zhao D, Li H, Wang C, Yin L. Molecular-Level Heterostructures Assembled from Titanium Carbide MXene and Ni–Co–Al Layered Double-Hydroxide Nanosheets for All-Solid-State Flexible Asymmetric High-Energy Supercapacitors. *ACS Energy Letters*. 2018 Jan 12;3(1):132–40.

62. Anasori B, Xie Y, Beidaghi M, Lu J, Hosler BC, Hultman L, et al. Two-Dimensional, Ordered, Double Transition Metals Carbides (MXenes). *ACS Nano*. 2015 Oct 27;9(10):9507–16.
63. Rosen J, Dahlqvist M, Tao Q, Hultman L. In- and Out-of-Plane Ordered MAX Phases and Their MXene Derivatives. In: Anasori B, Gogotsi Y, editors. *2D Metal Carbides and Nitrides (MXenes): Structure, Properties and Applications* [Internet]. Cham: Springer International Publishing; 2019 [cited 2020 Nov 29]. p. 37–52. Available from: https://doi.org/10.1007/978-3-030-19026-2_3
64. Guo Z, Zhou J, Sun Z. New two-dimensional transition metal borides for Li ion batteries and electrocatalysis. *J Mater Chem A*. 2017 Nov 21;5(45):23530–5.
65. Qi S, Fan Y, Zhao L, Li W, Zhao M. Two-dimensional transition metal borides as highly efficient N₂ fixation catalysts. *Applied Surface Science*. 2021 Jan 15;536:147742.
66. Shao Y, Shao M, Kawazoe Y, Shi X, Pan H. Exploring new two-dimensional monolayers: pentagonal transition metal borides/carbides (penta-TMB/Cs). *J Mater Chem A*. 2018 Jun 5;6(22):10226–32.
67. Lei J-C, Zhang X, Zhou Z. Recent advances in MXene: Preparation, properties, and applications. *Frontiers of Physics*. 2015 Jun;10(3):276–86.
68. Frey NC, Price CC, Bandyopadhyay A, Kumar H, Shenoy VB. Predicted Magnetic Properties of MXenes. In: Anasori B, Gogotsi Y, editors. *2D Metal Carbides and Nitrides (MXenes): Structure, Properties and Applications* [Internet]. Cham: Springer International Publishing; 2019 [cited 2020 Nov 29]. p. 291–300. Available from: https://doi.org/10.1007/978-3-030-19026-2_15
69. Koo CM, Shahzad F, Iqbal A, Kim H. Electromagnetic Interference Shielding Using MXenes and Their Composites. In: Anasori B, Gogotsi Y, editors. *2D Metal Carbides and Nitrides (MXenes): Structure, Properties and Applications* [Internet]. Cham: Springer International Publishing; 2019 [cited 2020 Nov 29]. p. 399–416. Available from: https://doi.org/10.1007/978-3-030-19026-2_21
70. Fan W, Yan B, Wang Z, Wu L. Three-dimensional all-dielectric metamaterial solid immersion lens for subwavelength imaging at visible frequencies. *Science Advances*. 2016 Aug 12;2(8):e1600901–e1600901.
71. Johnson LR, Vojvodic A. Chemistry and Catalysis of MXenes. In: Anasori B, Gogotsi Y, editors. *2D Metal Carbides and Nitrides (MXenes): Structure, Properties and Applications* [Internet]. Cham: Springer International Publishing; 2019 [cited 2020 Nov 29]. p. 445–56. Available from: https://doi.org/10.1007/978-3-030-19026-2_23
72. Maleski K, Mochalin VN, Gogotsi Y. Dispersions of Two-Dimensional Titanium Carbide MXene in Organic Solvents. *Chemistry of Materials*. 2017 Feb 28;29(4):1632–40.

73. Yan J, Ren CE, Maleski K, Hatter CB, Anasori B, Urbankowski P, et al. Flexible MXene/Graphene Films for Ultrafast Supercapacitors with Outstanding Volumetric Capacitance. *Advanced Functional Materials*. 2017 Aug;27(30):1701264.
74. Demiroglu I, Peeters FM, Gülseren O, Çakır D, Sevik C. Alkali Metal Intercalation in MXene/Graphene Heterostructures: A New Platform for Ion Battery Applications. *The Journal of Physical Chemistry Letters*. 2019 Feb 21;10(4):727–34.
75. Li Y, Li Z, Shen PK. Simultaneous Formation of Ultrahigh Surface Area and Three-Dimensional Hierarchical Porous Graphene-Like Networks for Fast and Highly Stable Supercapacitors. *Advanced Materials*. 2013 May 7;25(17):2474–80.
76. Fu J, Yun J, Wu S, Li L, Yu L, Kim KH. Architecturally Robust Graphene-Encapsulated MXene Ti_2CT_x @Polyaniline Composite for High-Performance Pouch-Type Asymmetric Supercapacitor. *ACS Applied Materials & Interfaces*. 2018 Oct 10;10(40):34212–21.
77. Zhao M, Xie X, Ren CE, Makaryan T, Anasori B, Wang G, et al. Hollow MXene Spheres and 3D Macroporous MXene Frameworks for Na-Ion Storage. *Advanced Materials*. 2017 Oct;29(37):1702410.
78. VahidMohammadi A, Moncada J, Chen H, Kayali E, Orangi J, Carrero CA, et al. Thick and freestanding MXene/PANI pseudocapacitive electrodes with ultrahigh specific capacitance. *Journal of Materials Chemistry A*. 2018;6(44):22123–33.
79. Cai Y, Shen J, Ge G, Zhang Y, Jin W, Huang W, et al. Stretchable $Ti_3C_2T_x$ MXene/Carbon Nanotube Composite Based Strain Sensor with Ultrahigh Sensitivity and Tunable Sensing Range. *ACS Nano*. 2018 Jan 23;12(1):56–62.
80. Sun R, Zhang H-B, Liu J, Xie X, Yang R, Li Y, et al. Highly Conductive Transition Metal Carbide/Carbonitride(MXene)@polystyrene Nanocomposites Fabricated by Electrostatic Assembly for Highly Efficient Electromagnetic Interference Shielding. *Advanced Functional Materials*. 2017 Dec;27(45):1702807.
81. Zhao M-Q, Ren CE, Ling Z, Lukatskaya MR, Zhang C, Van Aken KL, et al. Flexible MXene/Carbon Nanotube Composite Paper with High Volumetric Capacitance. *Advanced Materials*. 2015 Jan;27(2):339–45.
82. Wang Q, Yan J, Wang Y, Wei T, Zhang M, Jing X, et al. Three-dimensional flower-like and hierarchical porous carbon materials as high-rate performance electrodes for supercapacitors. *Carbon*. 2014 Feb;67:119–27.
83. Jiao S, Zhou A, Wu M, Hu H. Kirigami Patterning of MXene/Bacterial Cellulose Composite Paper for All-Solid-State Stretchable Micro-Supercapacitor Arrays. *Advanced Science*. 2019 Jun;6(12):1900529.
84. Boota M, Anasori B, Voigt C, Zhao M-Q, Barsoum MW, Gogotsi Y. Pseudocapacitive Electrodes Produced by Oxidant-Free Polymerization of Pyrrole between the Layers of 2D Titanium Carbide (MXene). *Advanced Materials*. 2016 Feb;28(7):1517–22.

85. Sang X, Xie Y, Lin M-W, Alhabeb M, Van Aken KL, Gogotsi Y, et al. Atomic Defects in Monolayer Titanium Carbide ($Ti_3C_2T_x$) MXene. *ACS Nano*. 2016 Oct 25;10(10):9193–200.
86. Sang X, Naguib M, Alhabeb M, Unocic RR. Effect of Synthesis Methods on the Structure and Defects of Two-Dimensional MXenes. In: Anasori B, Gogotsi Y, editors. *2D Metal Carbides and Nitrides (MXenes): Structure, Properties and Applications* [Internet]. Cham: Springer International Publishing; 2019 [cited 2020 Nov 29]. p. 111–23. Available from: https://doi.org/10.1007/978-3-030-19026-2_7
87. Lee C, Wei X, Kysar JW, Hone J. Measurement of the Elastic Properties and Intrinsic Strength of Monolayer Graphene. *Science*. 2008 Jul 18;321(5887):385–8.
88. Lee G-H, Cooper RC, An SJ, Lee S, van der Zande A, Petrone N, et al. High-Strength Chemical-Vapor-Deposited Graphene and Grain Boundaries. *Science*. 2013 May 31;340(6136):1073–6.
89. Natu V, Pai R, Sokol M, Carey M, Kalra V, Barsoum MW. 2D $Ti_3C_2T_z$ MXene Synthesized by Water-free Etching of Ti_3AlC_2 in Polar Organic Solvents. *Chem*. 2020 Mar 12;6(3):616–30.
90. Li Z, Wang L, Sun D, Zhang Y, Liu B, Hu Q, et al. Synthesis and thermal stability of two-dimensional carbide MXene Ti_3C_2 . *Materials Science and Engineering: B*. 2015 Jan;191:33–40.
91. Meshkian R, Tao Q, Dahlgqvist M, Lu J, Hultman L, Rosen J. Theoretical stability and materials synthesis of a chemically ordered MAX phase, Mo_2ScAlC_2 , and its two-dimensional derivate Mo_2ScC_2 MXene. *Acta Materialia*. 2017 Feb;125:476–80.
92. Mashtalir O, Naguib M, Mochalin VN, Dall’Agnese Y, Heon M, Barsoum MW, et al. Intercalation and delamination of layered carbides and carbonitrides. *Nature Communications*. 2013 Apr 16;4:1716.
93. Kumar KS, Choudhary N, Jung Y, Thomas J. Recent Advances in Two-Dimensional Nanomaterials for Supercapacitor Electrode Applications. *ACS Energy Letters*. 2018 Feb 9;3(2):482–95.
94. Kayali E, VahidMohammadi A, Orangi J, Beidaghi M. Controlling the Dimensions of 2D MXenes for Ultrahigh-Rate Pseudocapacitive Energy Storage. *ACS Applied Materials & Interfaces*. 2018 Aug 8;10(31):25949–54.
95. Beidaghi M, Wang C. Micro-Supercapacitors Based on Interdigital Electrodes of Reduced Graphene Oxide and Carbon Nanotube Composites with Ultrahigh Power Handling Performance. *Advanced Functional Materials*. 2012 Nov 7;22(21):4501–10.
96. Augustyn V, Come J, Lowe MA, Kim JW, Taberna P-L, Tolbert SH, et al. High-rate electrochemical energy storage through Li^+ intercalation pseudocapacitance. *Nature Materials*. 2013 Jun;12(6):518–22.

97. Castellanos-Gomez A, Singh V, van der Zant HSJ, Steele GA. Mechanics of freely-suspended ultrathin layered materials: Mechanics of 2D materials. *Annalen der Physik*. 2015 Jan;527(1–2):27–44.
98. Suk JW, Piner RD, An J, Ruoff RS. Mechanical Properties of Monolayer Graphene Oxide. *ACS Nano*. 2010 Nov 23;4(11):6557–64.
99. Bertolazzi S, Brivio J, Kis A. Stretching and Breaking of Ultrathin MoS₂. *ACS Nano*. 2011 Dec 27;5(12):9703–9.
100. Zhang R, Koutsos V, Cheung R. Elastic properties of suspended multilayer WSe₂. *Applied Physics Letters*. 2016 Jan 25;108(4):042104.
101. Xu H, Bai T, Chen H, Guo F, Xi J, Huang T, et al. Low-cost AlCl₃/Et₃NHCl electrolyte for high-performance aluminum-ion battery. *Energy Storage Materials*. 2019 Feb 1;17:38–45.
102. Gao L, Wang L, Qi T, Li Y, Chu J, Qu J. Electrodeposition of Aluminum from AlCl₃/Et₃NHCl Ionic Liquids. *Acta Physico-Chimica Sinica*. 2008 Jun 1;24(6):939–44.